1-1-2016

System Frequency Support of Permanent Magnet Synchronous Generator-Based Wind Power Plant

Ziping Wu
University of Denver

System Frequency Support of Permanent Magnet Synchronous Generator-Based Wind Power Plant

Abstract

With ever-increasing penetration of wind power into modern electric grids all over the world, a trending replacement of conventional synchronous generators by large wind power plants will likely result in the poor overall frequency regulation performance. On the other hand, permanent magnet synchronous generator wind Turbine System (PMSG-WTG) with full power back to back converters tends to become one of the most promising wind turbine technologies thanks to various advantages. It possesses a significant amount of kinetic energy stored in the rotating mass of turbine blades, which can be utilized to enhance the total inertia of power system. Additionally, the deloaded operation and decoupled control of active and reactive power make it possible for PMSG-WTG to provide a fast frequency regulation through full-power converter.

First of all, a comprehensive and in-depth survey is conducted to analyze the motivations for incorporating the inertial response and frequency regulation of VSWT into the system frequency regulation. Besides, control classifications, fundamental control concepts and advanced control schemes implemented for auxiliary frequency support of individual WT or wind power plant are elaborated along with a comparison of the potential frequency regulation capabilities of four major types of WTs.

Secondly, a Controls Advanced Research Turbine2-Permanent Magnet Synchronous Generator wind turbine (CART2-PMSG) integrated model representing the typical configuration and operation characteristics of PMSG-WT is established in Matlab/Simulink,. Meanwhile, two different rotor-side converter control schemes, including rotor speed-based control and active power-based control, are integrated into this CART2-PMSG integrated model to perform Maximum Power Point Tracking (MPPT) operation over a wide range of wind speeds, respectively.

Thirdly, a novel comprehensive frequency regulation (CFR) control scheme is developed and implemented into the CART2-PMSG model based on rotor speed control. The proposed control scheme is achieved through the coordinated control between rotor speed and modified pitch angle in accordance with different specified wind speed modes. Fourth, an improved inertial control method based on the maximum power point tracking operation curve is introduced to boost the overall frequency support capability of PMSG-WTGs based on rotor speed control. Fifth, a novel control method based on the torque limit (TLC) is proposed for the purpose of maximizing the wind turbine (WT)'s inertial response. To avoid the SFD caused by the deloaded operation of WT, a small-scale battery energy storage system (BESS) model is established and implemented to eliminate this impact and meanwhile assist the restoration of wind turbine to MPPT mode by means of coordinated control strategy between BESS and PMSG-WTG.

Last but not the least, all three types of control strategies are implemented in the CART2-PMSG integrated model based on rotor speed control or active power control respectively to evaluate their impacts on the wind turbine's structural loads during the frequency regulation process. Simulation results demonstrate that all the proposed methods can enhance the overall frequency regulation performance while imposing very slight negative impact on the major mechanical components of the wind turbine.

Document Type

Dissertation

Degree Name

Ph.D.

SYSTEM FREQUENCY SUPPORT OF PERMANENT MAGNET SYNCHRONOUS GENERATOR-BASED WIND POWER PLANT

A DISSERTATION

PRESENTED TO

THE FACULTY OF THE DANIEL FELIX RITCHIE

SCHOOL OF ENGINEERING AND COMPUTER SCIENCE

UNIVERSITY OF DENVER

_____

IN PARTIAL FULFILLMENT

OF THE REQUIREMENTS FOR THE DEGREE

DOCTOR OF PHILOSOPHY

_____

by

ZIPING WU

MARCH 2016

ADVISOR: DAVID WENZHONG GAO

Author: Ziping Wu
Title: System Frequency Support of Permanent Magnet Synchronous Generator-based Wind Power Plant
Advisor: David Wenzhong Gao
Degree Date: March 2016

Abstract

With ever-increasing penetration of wind power into modern electric grids all over the world, a trending replacement of conventional synchronous generators by large wind power plants will likely result in the poor overall frequency regulation performance. On the other hand, permanent magnet synchronous generator wind Turbine System (PMSG-WTG) with full power back to back converters tends to become one of the most promising wind turbine technologies thanks to various advantages. It possesses a significant amount of kinetic energy stored in the rotating mass of turbine blades, which can be utilized to enhance the total inertia of power system. Additionally, the deloaded operation and decoupled control of active and reactive power make it possible for PMSG-WTG to provide a fast frequency regulation through full-power converter.

First of all, a comprehensive and in-depth survey is conducted to analyze the motivations for incorporating the inertial response and frequency regulation of VSWT into the system frequency regulation. Besides, control classifications, fundamental control concepts and advanced control schemes implemented for auxiliary frequency support of individual WT or wind power plant are elaborated along with a comparison of the potential frequency regulation capabilities of four major types of WTs.

Secondly, a Controls Advanced Research Turbine2-Permanent Magnet Synchronous Generator wind turbine (CART2-PMSG) integrated model representing the

typical configuration and operation characteristics of PMSG-WT is established in Matlab/Simulink,. Meanwhile, two different rotor-side converter control schemes, including rotor speed-based control and active power-based control, are integrated into this CART2-PMSG integrated model to perform Maximum Power Point Tracking (MPPT) operation over a wide range of wind speeds, respectively.

Thirdly, a novel comprehensive frequency regulation (CFR) control scheme is developed and implemented into the CART2-PMSG model based on rotor speed control. The proposed control scheme is achieved through the coordinated control between rotor speed and modified pitch angle in accordance with different specified wind speed modes. Fourth, an improved inertial control method based on the maximum power point tracking operation curve is introduced to boost the overall frequency support capability of PMSG-WTGs based on rotor speed control. Fifth, a novel control method based on the torque limit (TLC) is proposed for the purpose of maximizing the wind turbine (WT)'s inertial response. To avoid the SFD caused by the deloaded operation of WT, a small-scale battery energy storage system (BESS) model is established and implemented to eliminate this impact and meanwhile assist the restoration of wind turbine to MPPT mode by means of coordinated control strategy between BESS and PMSG-WTG.

Last but not the least, all three types of control strategies are implemented in the CART2-PMSG integrated model based on rotor speed control or active power control respectively to evaluate their impacts on the wind turbine’s structural loads during the frequency regulation process. Simulation results demonstrate that all the proposed methods can enhance the overall frequency regulation performance while imposing very slight negative impact on the major mechanical components of the wind turbine.

Acknowledgements

First of all, I would like to express my sincere appreciations to my academic supervisor, Dr. David Wenzhong Gao, for his guidance, inspiration and support during my Ph.D study at the University of Denver (DU). I am deeply grateful to him for his wisdom and expertise that assist me in accomplishing this dissertation.

Secondly, I would like to heartily extend my sincere gratitude to Dr. Eduard Muljadi, a principle engineer in NREL and an extinguished IEEE fellow, for his careful guidance and wonderful suggestions that takes my research to a higher level.

Thirdly, I am very grateful to Dr. Mohammad Matin, Dr. Jun Zhang and Dr. Duan Zhang for their valuable time to serve as my committee members as well as for their consistent support and advice about my research.

Next, I would like to thank Dr. Kimon Valavanis, the chair of Department of Electrical and Computer engineering for his durable support and assistance. Many special thanks go to other faculties and staffs in the Daniel Felix Ritchie School of engineering and computer science for their kind assistance and care during my study at DU. I also would like to thank all my great lab fellows at the Renewable Energy and Power Electronics Laboratory at DU for their support and valuable ideas they share with me.

Last but not the least, I am especially grateful to my great parents who provide me continued support and unconditioned assistance during my hardest time. Their love, trust and understanding enable me to accomplish my Ph.D study smoothly.

Table of Contents

List of Figures

List of Tables

Chapter 1 Introduction

1.1 Background and Motivation

Nowadays, a growing penetration of variable-speed wind turbine generators (VSWTGs) based on permanent magnet synchronous generators (PMSGs) and doubly-fed induction generators (DFIGs) may result in a decline in the system frequency regulation capability. That's due to VSWTG's decoupling interface between rotor speed and grid frequency via power converter as well as the declined inertia from conventional synchronous generators being gradually replaced or de-committed [1].

However, PMSGs inherently possesses a significant amount of kinetic energy stored in the rotating mass of their turbine blades and gearbox, and this can be employed to strengthen total inertia of a power system through fast and flexible power converter control. Moreover, fully decoupling the rotor speed from the grid frequency allows PMSGs to remain in stable operation and rapidly respond to grid frequency variations in any severe frequency event. Compared to DFIGs featured with identical power rating and inertial constant, PMSGs are capable of providing the larger inertial response and stronger frequency support thanks to their full power converter, which accommodates a wider range of rotor speed (0.4 p.u-1.2 p.u) in comparison with that of DFIG-WTG (0.7p.u. to 1.2p.u.) [2]-[3]. Therefore, it is valuable for the grid to take full advantage of the potential capability of PMSG-WTGs in supporting system frequency regulation.

From the perspective of secure power grid operation, Regional Transmission Organizations (RTOs) and Independent System Operator (ISOs) in many countries have come to realize the potential benefits of inertial response and frequency regulation provided by wind turbine (WT) in maintaining the dynamic active power balance between generation and demand. From the perspective of wind turbine manufacturers, the integration of auxiliary frequency control functions, consisting of de-loaded control, inertial response and primary droop control and automatic generation control (AGC) secondary control, can be simply realized by altering the existing control strategy of power converter and pitch angle control [4]-[5]. Besides, a large number of wind generators with frequency regulation functions are allowed to be integrated into power system, which yields extra profits by providing the ancillary service. With a great potential demand in power market, wind plant manufactures are also encouraged to further improve the VSWT's auxiliary frequency control customized for specific power system. On the other hand, especially when the wind power needs to be dispatched down in case of low load demand and high wind speed condition or according to other operation constrains, a certain amount of untapped wind power can be harnessed as spinning reserve to assist in the system frequency regulation under the subsequent severe disturbances [4]. Therefore, a win-win solution can be achieved by implementing the frequency control into PMSG-WTG for the mutual benefits of wind power plants and electrical power grid.

In most current literatures, auxiliary frequency controllers are proposed as add-on functions for DFIG-WTG. Therein, the inertial control utilizes the kinetic energy in the rotating mass of wind turbine (WT) to provide the temporary frequency response [6]-[8].

The de-loaded control enables the wind turbine to run in the de-loaded mode so as to reserve partial wind power for the primary and secondary frequency regulations [9]-[13]. The droop control emulates the primary frequency response of conventional synchronous generators [6],[10],[14]-[15]. A secondary frequency controller in a supervisory wind farm control system can respond to an AGC signal or the power flow adjustment from the transmission system operator [11]-[13]. As for the comprehensive control based on the above controllers, a coordinated frequency regulation scheme is presented for DFIG-WTG operating under different wind speeds in [16]. The frequency response capability of the full converter variable speed wind turbine generator in the Maximum Point Power Tracking (MPPT) mode is investigated under different constant wind speed conditions in [15]. Overall, the vast majority of current researches are centered on the DFIG-WTG frequency regulation capabilities due to its current higher market share [2],[6],[9],[11]-[14],[16]. Very a few published papers or documents emphasize the comprehensive frequency regulation capacity of PMSG based on rotor speed-based control under different wind speeds or enhanced inertial response based on active power-based control when operating in MPPT mode, especially with respect to the potential impact of frequency regulation on the mechanical components of wind turbines.

Therefore, the research presented herein intends to address the major issues as to maximize the performance of PMSG-WTG for short-term and long-term frequency regulations in accordance with its specific operation characteristics and control structure. Meanwhile, the impact of frequency support on the WT's mechanical stress and structural load should be carefully observed when enabling PMSG-WTG to perform the proposed frequency regulations.

1.2 Research Objectives

The objective of this research is to provide fundamental knowledge about the frequency regulation by VSWTGs and advanced controller design that enables PMSG-WTGs based on rotor speed control or active power control to provide the optimal frequency support. This dissertation work is mainly focused on the development and implementation of the enhanced inertial response and primary frequency regulation, which is suitable for PMSG-WTGs in terms of de-loaded operation and MPPT mode respectively. Specific objectives and procedures of research project are illustrated in Figure 1.1:

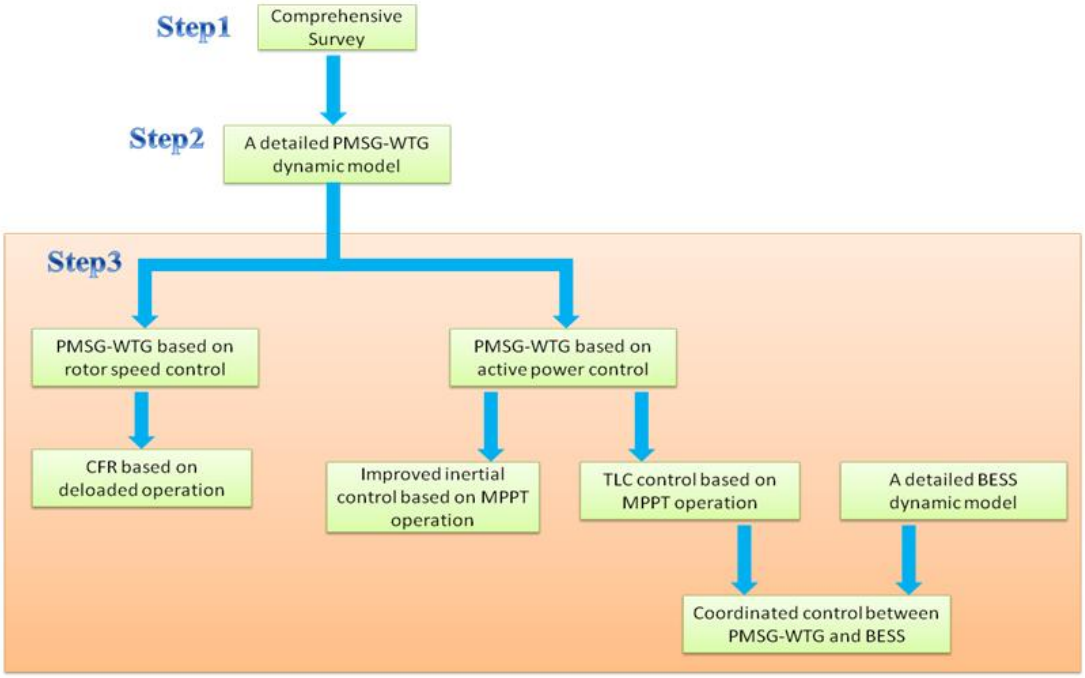

Figure 1.1 Schematic of research project plan

The first objective of this project is to conduct a comprehensive and in-depth survey on the inertial response and auxiliary frequency regulation provided by various types of wind generations.

The second objective of this project is to design and develop a detailed PMSG-WTG model with aerodynamic and mechanical components represented by the FAST-based CART2 model. The purpose of this work aims to construct a reliable simulation platform that is able to accurately represent the physical characteristics and dynamic performance of real PMSG-WTG over different wind speeds, so that the development and validation of the proposed frequency control schemes can be carried out by investigating their impacts on the power grid and wind turbine simultaneously.

The third objective of this project is to develop a novel comprehensive frequency regulation (CFR) scheme for PMSG-WTGs based on rotor speed control by combining rotor speed control with modified pitch angle control. The implementation of this control strategy is based on the de-loaded operation of PMSG-WTG over a wide range of wind speeds.

The fourth objective of this project is to develop an improved inertial control to enable the PMSG-WTG based on rotor-speed control to improve the overall frequency support in case of large supply-demand imbalances. The implementation of this control strategy is based on MPPT operation without additional power reserve required. If necessary, Battery Energy Storage System (BESS) can be employed to coordinated with the PMSG-WTG to accomplish the temporary frequency support.

1.3 Contributions

The main contributions of this project are listed as follows:

1) To come up with a novel comprehensive frequency control (CFR) scheme, which is suitable for PMSG based on rotor-speed control to achieve both constant

inertial response and variable droop frequency regulation by coordinating the rotor speed control and pitch angle control. Moreover, a complete operation of PMSG is categorized into the low, medium and high wind speed modes according to the deloaded margin level and rotor speed limit. By implementing the proposed CFR scheme, the rotor-speed-control oriented PMSG-WTG is enabled to optimally participate in the short-term and long-term frequency regulation over a full range of wind speeds.

2) To present an improved inertial control method based on the maximum power point tracking operation curve to enhance the overall frequency support capability of power control-based PMSG-WTGs when they are operating in MPPT mode. In the meanwhile, the possible secondary frequency drop (SFD) can be mitigated in case of severe frequency disturbance.

3) To make the same PMSG-WTG perform much stronger inertial response, a follow-up control method based on the torque limit (TLC) is proposed to signifcantly enhance the temporary frequency support within the mechanical constraint. To avoid its subsequent Secondary SFD issue resulting from WT's inertial energy recovery, a small-scale BESS is employed to eliminate this impact and meanwhile assist the wind turbine in restoring the rotor speed to MPPT mode through the proposed coordinated control strategy of BESS and PMSG-WTG.

4) Last but not the least, all three types of control strategies are implemented in the CART2-PMSG integrated model based on rotor speed control or active power control to study their impacts on the wind turbine’s structural loads during the inertial response process.

1.4 Outline of Dissertation

The remaining parts of this dissertation presents a detailed study of three control methods discussed previously, in addition to a comprehensive survey of frequency regulation by wind farm plants.

Chapter 2 presents a complete literature review on the frequency response by wind power plants. It specifically describes the control concepts, theories and principles of prevailing frequency regulation apart from the frequency regulation performance comparison among four major types of WTG. Furthermore, this review also provide a overview of the latest industry development and applications, ongoing domestic and international research activities as well as updated grid codes associated with the VSWT's emerging frequency regulation technologies. Finally, authors provide a comprehensive insights and analysis into several critical issues with respect to the participation of VSWTs in the grid frequency regulation from perspectives of system operation, control, protection as well as power market.

Chapter 3 presents a detailed CART2-PMSG wind turbine model equipped with two different control strategies, consisting of rotor speed-based control and active power-based control. Based on a series of simulation tests, it is proved the proposed CART2-PMSG integral model can accurately represent the steady-state and dynamic characteristics of real wind turbine in terms of both mechanical and electrical aspects when both control strategies are implemented in the rotor-side converter, respectively.

Chapter 4 presents a novel comprehensive frequency regulation (CFR) scheme fit for PMSG-WTGs based on rotor speed control by combining rotor speed control with

modified pitch angle control. It is concluded that the CFR can enable PMSG-WTG to contribute to the active power regulation and promote the overall frequency regulation performance in case of frequency disturbance.

Chapter 5 presents an improved inertial control method based on the maximum power point tracking operation curve to enhance the overall frequency support capability of PMSG-WTGs in the case of large supply-demand imbalances. Simulation results demonstrate that the improved inertial control enables the PMSG-WTG to enhance the transient frequency regulation performance even in the low wind power penetration condition, whereas the proper deloaded value can avoid the SFD throughout the rotor speed recovery process.

Chapter 6 presents a coordinated control strategy of BESS and PMSG-WTG to improve the overall frequency characteristics. A novel control method based on the torque limit (TLC) is proposed to maximize the PMSG-WTG's inertial response. To avoid the undesirable secondary frequency drop (SFD), a small-scale BESS model is utilized to support the wind turbine to recover to the MPPT state by using the proposed coordinated control scheme.

Chapter 7 provides a conclusion of the presented research work and several recommendations for the future work.

Chapter 2 Literature Review on the Frequency Response by Wind Power Plants in the Power Grid

This work conducts a comprehensive survey on the inertial response and auxiliary frequency regulation provided by various types of wind generations. It specifically describes, analyzes and illustrates the prevailing frequency regulation controls of VSWT from the perspectives of fundamental frequency regulation concepts, control principles and coordinated control strategies. Besides, a concrete comparison on the potential performance of four popular types of wind power plants is illustrated with respect to system frequency regulation capability including their benefits and drawbacks.

2.1 Wind Turbine Ancillary Functions

In principle, grid frequency response can be divided into four regulation stages in the time scales: inertial response, primary frequency response, secondary frequency response and tertiary frequency response as shown in Figure 2.1 [17]. Until now, active power control strategies applied in the rotor side converter of VSWT involve torque control, active power control and rotor speed control in order to realize the MPPT operation mode [18],[20]-[24]. To equip VSWT with emulated frequency regulation functions, supplementary frequency controllers should be carefully designed and integrated into both converter power control loop and pitch angle control loop to

manipulate the corresponding set points like torque, active power or rotor speed according to specific frequency regulation requirement[10], [19] ,[25]-[29].

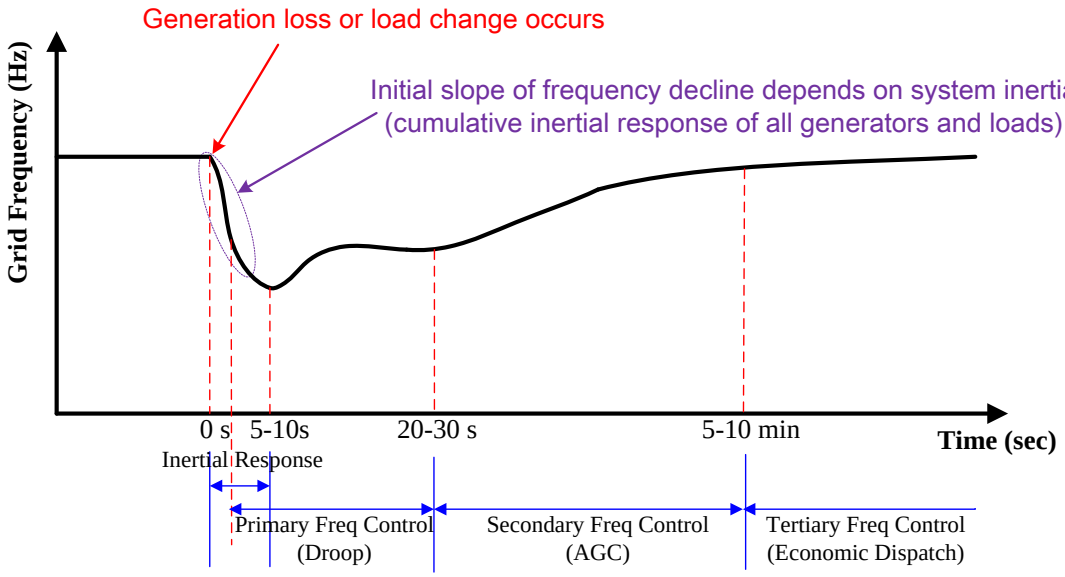

Figure 2.1 Schematic diagram of comprehensive frequency control following a large generation loss or a sudden load change (Figure derived from Pouyan Pourbeik of EPRI)

2.1.1 Inertial Control

In a power system, inertial response is an immediate response to severe frequency excursion within seconds due to the sudden and large power supply-demand imbalance. The system frequency changes at a certain rate initially determined by the cumulative inertia of all spinning generations (synchronous generators) and the composite load damping (motor, pumps and *et al*) [30]-[32]. The additional energy stored in rotating mass of both wind turbine and generator can be extracted and then released into the power grid via grid-side converter to arrest the rate of change of frequency (ROCOF). For instance, the typical value of wind turbine inertia is approximately 3.5s [33]. The total moment of inertia of a 2 MW-scale VSWT is approximately six times than that of the conventional generator [14].

Once the inertial energy is totally released up at the moment of frequency nadir, the energy extracted from the rotating mass needs to be recovered from the available wind power in order to restore the WT rotor speed and kinetic energy to their pre-disturbance value. In this sense, the inertial control is essentially "the energy neutral process" although the total amount of recovery energy can be greater than that of inertial response due to the WT mechanical and electrical losses during this process [34]. The duration of the natural recovery depends on the turbine mechanical dynamics and normally sustains several tens of seconds. A short-term dip may occur to the active power output during the recovery process for a portion of wind energy is utilized to restore the kinetic energy. Thus, a large aggregated energy recovery of wind farms will result in a secondary system frequency drop at some 10 to 15 seconds (even lower than the first frequency nadir) following the initial generation loss [14],[7]-[8],[35]-[44]. With respect to the inertial recovery process, three main parameters that determine its behavior include starting time to reduce active power, generation reduction amount as percentage of WT rated power (or actual power output level) as well as total duration for generation reduction [7]. The acceleration period of the WT rotor speed is set to be longer than the deceleration period by changing the rate of power ramp so as to relieve the pressure brought about by restoring process on the rest of the system [3]- [4].

According to the equation (1), the amount of kinetic energy ΔE for the inertial response of a single wind turbine is mainly determined by the initial rotor speed ω_0, rotor speed variation $(\Delta\omega = \omega_0 - \omega_1\,, \Delta\omega > 0)[\mathrm{rad/s}]$, the moment of inertia of wind turbine J [kg·m2] and inertia response duration (t_0-t_1) [s] [63],[45].

$$\Delta E_{inertial} = \int_{t0}^{t1} \Delta P_{inertial}(t)dt = \frac{1}{2}J(\omega_0^2 - \omega_1^2) = \frac{1}{2}J(2\omega_0\Delta\omega - \Delta\omega^2 \text{ [Joule]} \quad (2.1)$$

Furthermore, the inertial response capability of a wind power plants is dependent on the wind power penetration level, the number of WTs capable of providing inertial response, initial operation mode of a single WT under full load or partial load as well as individual WT physical characteristics, including the upper and lower limits of rotor speed, over-loading capability of power converter and generator, auxiliary controller parameters, maximum rate of change of power $(\frac{dP}{dt})_{max}$ as well as reserve margin level [39]-[40], [45]-[50]. To alleviate mechanical stresses on WT drive trains and extend its lifetime, the $(\frac{dP}{dt})_{max}$ should not exceed 0.45 p.u./s according to several manufacturers' datasheets [45]. A certain reserve margin can supply power headroom for VSWT to perform enhanced inertial response, and also eliminate or reduce the impact resulting from inertial response recovery [7][50]. Under low wind speed condition where WTG operates just above the minimum rotor speed, kinetic energy available for inertial response is quite limited due to stalling prevention and a relatively long response restoration follows. In between medium and high wind conditions where WTG operates at MPPT conditions, adequate kinetic energy is available to provide inertial response, so as to shorten the recovery period and mitigate the decline in rotor speed. Under high wind speed condition that rotor speed is maintained at the rated value due to pitch angle control, kinetic energy cannot be released until rotor speed drops below the rated. The inertia response is finite since the total power output of a single WT cannot exceed the specified overloaded value (eg.1.1p.u.) due to the capacity limits of power converter [34].

Inertial response dominates initial frequency variation following a frequency disturbance, so it plays an essential role in determining the sensitivity of system frequency to power imbalance. In the meantime, emulated inertia control can obviously improve the system small signal stability since the system damping effect of the dominant oscillation mode can be further reinforced [51]. In general, the greater the rotor speed from WT declines, the higher the transient active power surge becomes following the disturbance and the more positive effect will result in the frequency excursion, despite more time is needed to arrive at another steady state condition [36]. With the WT's contribution to system inertia, ROCOF (rate of change of frequency) and frequency nadir (the lowest point of frequency) can be improved to eliminate the possibility of load shedding triggered by UFLS (under frequency load shedding) protection scheme, and thus improve the system reliability during large loss-of-supply events [52]. Meanwhile, another benefit of enhanced inertia response of VSWT is to decrease the times of peak power output from the conventional generators, which picks up the load at their slow rates after the frequency disturbance.

However, the industrial design of inertia response must respect the WTG's component constrains consisting of converter and generator electrical ratings as well as mechanical loadings, such as turbulence management, drive-train and tower loads. Until now, three typical sorts of inertial control have been proposed to equip VSWT with emulated inertial response, which can be mainly categorized into Natural Inertial Control, Constant Inertial Control and Virtual Inertia Control [6],[26],[14], [7],[35]-[42].

A. Natural inertia control

Natural inertial control is proposed to generate an WT incremental active power following a severe frequency decline, which magnitude is in proportion to ROCOF $\frac{df}{dt}$ to emulate a synchronous inertia-alike response [43]. Currently, there are two main types of natural inertial controllers consisting of a one shot $\frac{df}{dt}$ controller and a continuously acting $\frac{df}{dt}$ controller [16],[44].

The one shot $\frac{df}{dt}$ controller is proposed to deliver an initial power surge in proportion to the ROCOF once the frequency event occurs. A certain amount of kinetic energy featured with a defined ramp rate and decay period is immediately injected into grid from the inception of frequency drop. This control scheme can be implemented by applying a lookup table with the initial $\frac{df}{dt}$ value as X-coordinate and the corresponding active power increment as Y-coordinate. As is shown in Figure 2.2, the full active power output can be achieved within 200ms and then declines exponentially over a specified duration of T_S. A short power recovery period of 0.95 p.u. or above of nominal power is allowed but restricted to avoid the risk of subsequent frequency disturbance because other generation is offline or load unexpectedly rises [44].

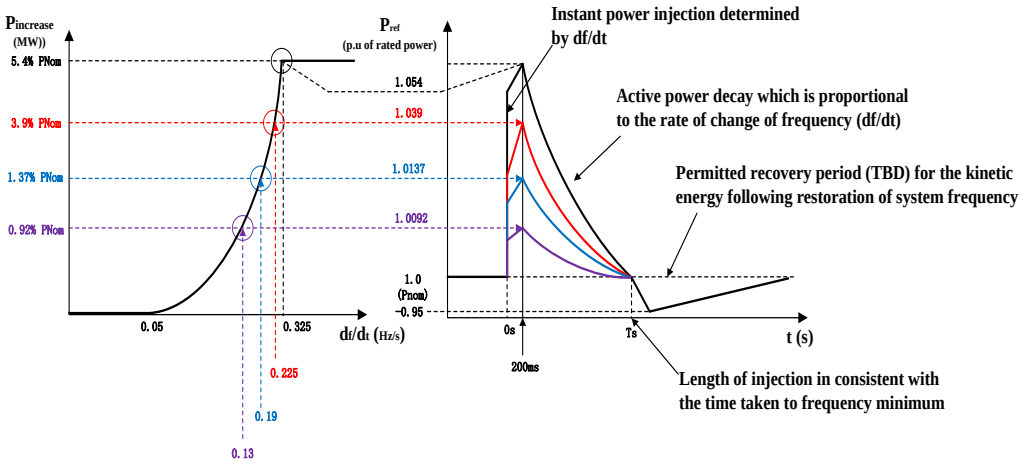

Figure 2.2 Control strategy of one shot $\frac{\mathbf{df}}{\mathbf{dt}}$ controller

The continuously acting $\frac{df}{dt}$ controller is developed with a continuously acting $\frac{df}{dt}$ controller, which works through the entire disturbance to regulate the additional active power injection based on ROCOF . As to this control method, the per unit inertial power ΔP_{in} and per unit inertial torque $\Delta\tau_{in}$ generated by inertial controller are expressed as

$$\Delta P_{in} = K_{inertial} \times \overline{w_s} \times \frac{d\overline{w_s}}{d_t} \tag{2.2}$$

$$\Delta\tau_{in} = K_{inertial} \times \frac{d\overline{w_s}}{d_t} \tag{2.3}$$

where, $K_{inertial}$ is the gain of the inertial controller, $\overline{w_s}$ is the per-unit synchronous generator speed. $K_{inertial}$ is analogous to the equivalent moment of inertia. ΔP_{in} corresponds to the part of the rotor kinetic energy extracted for the additional active power injection. Usually, the $\frac{d\overline{w_s}}{d_t}$ can be superseded by $\frac{df_{sys}}{d_t}$ so that the WT inertial response magnitude is directly proportional to the ROCOF. Using traditional method, $K_{inertial}$ is simplified as twice total inertia constant H of the wind turbine [35],[53]. However, to make PMSG-WT supply the appropriate inertial response, the $K_{inertial}$ value of PMSG-WT is tuned for the purpose of preventing the wind turbine from rotor speed

stalling [16]. A low pass filter is added after derivative function block to minimize the interference from measurement noise. Moreover, the natural inertia control is also named as delta power control because of the shape of inertial power output resembling “delta” throughout the overall response process. Figure 2.3 presents the control block diagram of natural inertia response. The performance of WT's natural inertia response can be enhanced by either increasing the auxiliary controller gain K or relaxing the limit on the rate of change of electrical power output [45].

Last but not least, it is noted that the $\frac{df}{dt}$ is inherently a noise amplifying process, which likely cause unpredictability of emulated inertial response. So, a proper filtering is required to eliminate this noise. However, the inertial controller relying on the $\frac{df}{dt}$ is triggered equally by the pseudo generation tripping like switching incidents [46] .

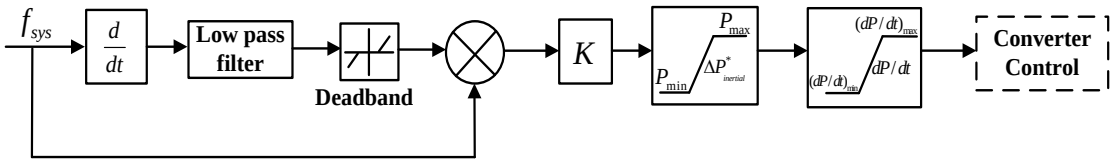

Figure 2.3 Control block diagram of the continuously acting $\frac{\mathbf{df}}{\mathbf{dt}}$ controller

B. Constant inertial control

Constant inertial response is defined as a certain amount of constant active power, which is released from kinetic energy sustaining for up to ten seconds under various wind speed conditions [3],[42],[54][54]. Compared with natural inertial response, the inertial power using this control can be tuned in different shapes in accordance with its magnitude and duration and also its response is much faster without relying on the measurement of ROCOF. This control method can significantly uplift the frequency nadir and mitigate the impact of kinetic energy recovery by tuning a desirable and steady

additional power injected into the grid, being carried out without relying on the instantaneous system frequency [43]. The effect of constant inertia response is usually dependent on several factors including overproduction step amount, duration time, ramp rate limit for power descending and ascending stages, wind speed (namely, present wind power output) as well as the inertia constant HWT.

One control method is proposed to generate the constant inertial response by modifying the rotor speed set point throughout the frequency event. The constant inertial power is derived from

$$P_{in}t = \frac{1}{2}J\omega_{ro}^2 - \frac{1}{2}J\omega_{rt}^2 \tag{2.4}$$

where, t is the duration for constant inertial power, ω_{r0} is the initial rotor speed and ω_{rt} is the rotor speed at the end of inertial response. Therefore, the reference value of rotor speed is available as:

$$\omega_{ref} = \omega_{rt} = \sqrt{\omega_{r0}^2 - 2\frac{P_{in}}{J}t} \tag{2.5}$$

By substituting inertial constant $J = \frac{2HS}{\omega_{base}^2}$ into (2.5) and defining $\omega_{p.u.} = \frac{\omega}{\omega_{base}}$ as per-unit rotor speed plus $P_{in\_p.u.} = \frac{P_{in}}{S}$ as per-unit inertial power, the per-unit rotor speed reference is rewritten in the per-unit form:

$$\omega_{rt\_p.u.} = \sqrt{\omega_{ro\_p.u.}^2 - \frac{P_{in\_p.u.}}{H}t} \tag{2.6}$$

The control block diagram of constant inertial response is depicted in Figure 2.4.

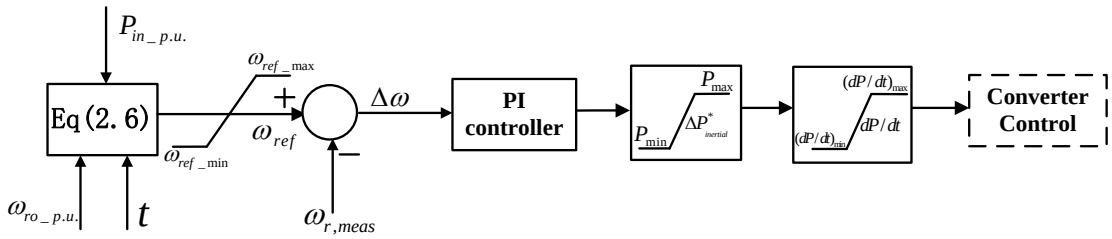

Figure 2.4 Control block diagram of the constant inertial response based on rotor speed regulation

The other method to carry out the constant inertial control is proposed in [31] to increase the actual power reference by adding Temporary Over-Production (TOP) value ΔP_{op} on top of the pre-event active power reference P_{e0} in case of frequency disturbance. The ΔP_{op} is derived from the kinetic energy stored in the WT rotating masses. Thus, the generated electrical power output P_e is defined as:

$$P_e = P_{e0} + \Delta P,\ \Delta P = \Delta P_{op} \text{ or } \Delta P_{Up} \tag{2.7}$$

During the normal operation, VSWT runs on the MPPT point according to the actual wind speed. In the event of frequency, a constant over-production in a quantity ΔP_{op} is achieved by quickly altering the active power set point through power converter, so that the rotor speed maintains deceleration as a result of the increasing imbalance in mechanical and electromechanical torque. Until the rotor speed reaches ω_{min}, the overproduction process will be over and then the active power set point will be adjusted to enable the electrical power output below the mechanical power input by a constant quantity P_{acc}. During this underproduction period, the rotor speed is accelerated and returned to previous MPPT point for the given wind speed or another operation point corresponding to the new wind speed. In Figure 2.5, the basic principle of this control mechanism is illustrated. Note that the value of P_{acc} can be constant or variable, depending on the specific strategy selected during the underproduction period. By

increasing the P_{acc}, the underproduction period is shorten and meanwhile the wind turbine rotor speed can be restored to the optimal operating point more rapidly. Assumed a bigger VSWT inertia constant, the overproduction and associated recovery periods are much longer due to larger kinetic energy stored.

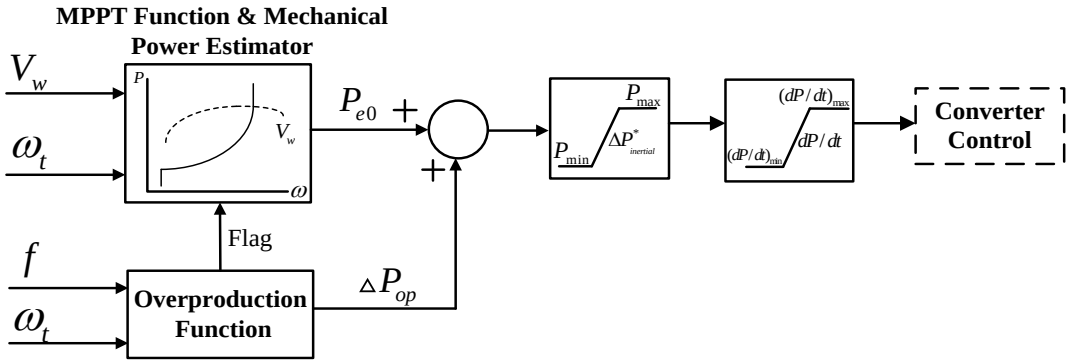

Figure 2.5 Control block diagram of the constant inertial response based on active power control

However, the extra active power production using this TOP method is always followed by an acceleration process, which more likely results in negative effect on the system frequency due to reduced power output of VSWT. Thus, an Improved Primary Frequency Response (IPFR) technique based on TOP method is proposed in [2] to avoid the acceleration phase and reduce the frequency deviation by combing de-loaded approach with TOP control. This IPFR response is mainly determined by over-production step magnitude, duration and wind speed condition. IPFR method can allow VSWT to enhance the overall system inertia response without under-production stage.

C. Virtual inertial control

Recently, another novel inertial control strategy named virtual inertia control (VIC) is presented to utilize the “hidden inertia” of the turbine blades to provide a fast dynamic frequency support. One method is to adjust the active power output of DFIG based on the system frequency deviation in order for contribution to the system inertia

response. This type of regulation can be implemented by means of shifting operating point from the MPPT power tracking cure toward the VIC power tracking curve to compensate for the mismatch in the power supply and demand and then rotor speed gradually recovers to initial MPPT point [55]. The upper and lower limits of VIC power curve are defined as P_{VIC_max} and P_{VIC_min} respectively to ensure the DFIG to operate in a steady state under various wind speed conditions. The coefficient KVIC is a function of frequency deviation:

$$K_{VIC} = \frac{\omega_{ro}^3}{(\omega_{ro}+2\pi\lambda\Delta f)^3} k_{opt} \tag{2.8}$$

where, $\lambda = \frac{\Delta\omega_r}{\Delta\omega_e} = \frac{\omega_{r1}-\omega_{r0}}{\omega_{e1}-\omega_{e0}}$, k_{opt} is optimal curve coefficient. Assuming that the rotor speed of DFIG varies from ω_{r0} to ω_{r1} so its kinetic energy to be released acts as the equivalent amount of kinetic energy from a synchronous generator with rotor speed varying from ω_{e0} to ω_{e1}. A washed out block is utilized to eliminate the steady-state dc component of the frequency error. The corresponding control block diagram is illustrated in Figure 2.6.

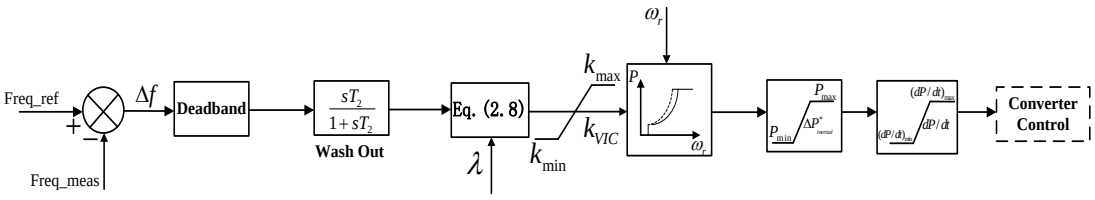

Figure 2.6 Control block diagram of VIC

An optimal controller for VIC is proposed in [42] to emulate the inertial response with the purpose of enhancing the frequency regulation in a diesel dominant system. The optimal virtual inertia factor K_{VIC} can be identified using deterministic linear quadratic regulator (LQR) method.

2.1.2 Primary Frequency Control

Primary frequency control is the automatic governor response in proportion to the frequency deviation from scheduled value. It belongs to a local automatic control without communication required between generator and dispatch center. This response, also named as governor droop control or frequency responsive reserve, is typically provided by conventional generators with governor control to regulate the power output in terms of the frequency deviation and droop settings [53], [11]-[13],[56]-[60]. The primary frequency regulation by WT resembles that of convention generators. It is usually activated within a few tens of seconds and can sustains for up to 15 min (usually completed within 12s-14s [30]) when grid frequency deviation exceeds an allowable limit [59]. This dominates the steady-state frequency deviation after inertial response until secondary frequency control (AGC) takes over for zero-error frequency regulation.

Unlike inertial response, the power generation needs to be curtailed aforehand by de-loaded control for wind power plant to actively respond to the under-frequency disturbance. The abilities of WT primary frequency regulation are evaluated from the following perspectives: delay time, ramping speed, magnitude and response speed [61]-[62]. Furthermore, the wind turbine can perform better in the primary frequency regulation under medium to high wind speed since more kinetic energy is combined to boost active power output [3].

A. Droop control/governor frequency control

To emulate the governor response of conventional generators for primary frequency regulation, droop control is implemented in VSWT to correlate variation in

grid frequency with a corresponding change in the fast active power output through converter controller. As shown in Figure 2.7, it responds to large deviation in grid frequency by increasing/decreasing power output in frequency events. The relationship between the active power change and frequency deviation can be expressed in $\Delta P_{droop}^{VSWT} = K_{droop}(f - f_0)$,where f_0 is the nominal frequency. The parameter K_{droop} is the inverse of speed adjustment rate R as follows.

$$R = \frac{\Delta f}{\Delta P} = \frac{1}{K_{droop}} \tag{2.9}$$

The value of R usually lies within the range from 3% to 5% for conventional generators. Large positive values of $K_{droop} = \frac{1}{R}$ can provide a more desirable effect in reducing the steady-state frequency deviation without obvious influence on the small signal stability of power system [40],[51]. As shown in Figure 2.7, a high pass filter is required after the frequency deviation to ensure a permanent small frequency deviation cannot affect the overall control system accuracy [5]. The frequency deadband is used to avoid the unnecessary primary response launch during normal operation [63].

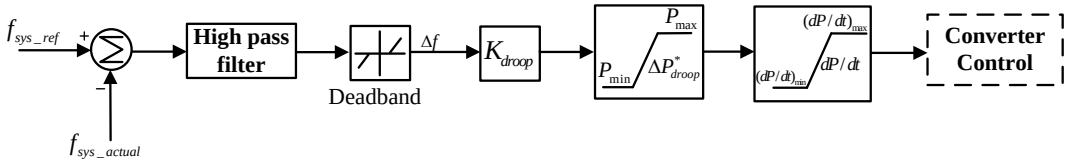

Figure 2.7 Control block diagram of droop response

1) Droop curve parameters:

As depicted in Figure 2.8, there are several important parameters to determine the droop curve behavior, including droop slopes (up\down), dead-band and ramp rate. These parameters need to be appropriately selected to ensure that the droop response is able to perform within the available reserve margin when unacceptable system frequency

deviation is detected [63],[17]-[46],[64]. Moreover, a droop curve with a suitable dead band can prevent the droop controller from persistent activation in response to any small frequency fluctuation. An Integral of Squared Error (ISE) is proposed in [65] to tune the DFIG controller parameters optimally to improve its frequency regulation capability. Note that symmetric droops are not required at all to realize the primary frequency regulation. According to different regulation ranges and stages of frequency deviation, the active power reference can be calculated using following equations:

$$P_{ref} = \begin{cases} P_{MPPT} & \Delta f \le f_{\min} - f_{DB\_lower} \\ P_{deloaded} + \dfrac{1}{R_1} \times \Delta f & f_{\min} - f_{DB\_lower} < \Delta f \le 0 \\ P_{deloaded} - \dfrac{1}{R_2} \times \Delta f & 0 < \Delta f \le f_{switch} - f_{DB\_upper} \\ P_{deloaded} - \dfrac{1}{R_3} \times \Delta f & f_{switch} - f_{DB\_upper} < \Delta f \le f_{\max} - f_{DB\_upper} \end{cases} \tag{2.10}$$

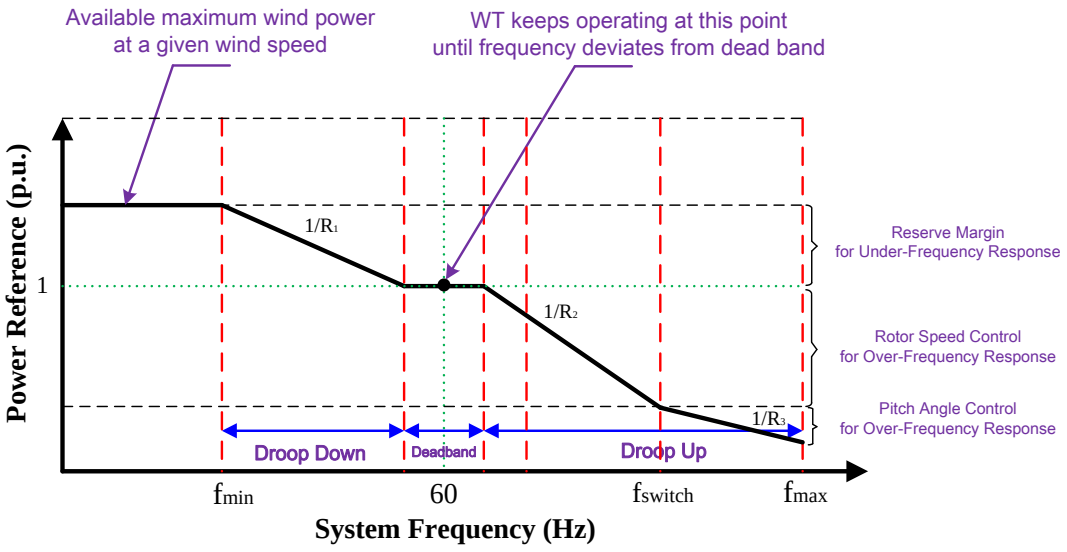

Figure 2.8 Frequency-power characteristics of basic droop control

In case the frequency declines above deadband f_{DB_lower}, active power reference of WT can be adjusted based on droop-down control until increasing to P_{MPPT} at given

wind speed. On the other hand, provided the frequency rises above the deadband f_{DB_upper}, active power reference is increased by raising up the rotor speed along with the de-loading tracking curve. If frequency keeps rising until the f_{switch} is reached, the rotor speed cannot continue to increase due to its upper limit. At this moment, the pitch angle controller is activated to further reduce the WT active power output by increasing the pitch angle β. During this process, the rotor speed remains constant at the maximum value. It is worth noting that the slope value of R3 mainly depends on the allowable variation range of β [28].

2) Static Droop and Dynamic Droop Controls

Static droop Control is similar to traditional governor control, which is used to provide additional active power based on the grid frequency deviation. Static droop curve represents a primary frequency response from WTG by converting measured grid frequency variation to an expected percentage of the rated power of the turbine [61]. Static droop control features a droop curve with a fixed slope and pre-defined dead band. Through simulation tests in [17]-[46], this control can assist in arresting system frequency decline and minimize the steady-state frequency deviation as well.

Dynamic droop control indicates that the slope and dead-band of droop curve can be tuned in real-time manner according to the ROCOF value, de-loaded level and variable wind speed conditions. Using this control method, a possible tradeoff between frequency regulation performance and resulting impacts on the structural and component loads is attained. A study in [17] demonstrates that dynamic droop curves can effectively enhance the primary response without dramatically adding the induced structural loads to

turbine components, such as shaft and tower. Compared with an aggressive static droop curve, the frequency nadir, steady-state frequency and frequency recovery process can also be improved by implementing dynamic droop control. On the other side, there is no sufficient reserve for WTGs operating especially under low wind speed to provide the primary frequency response. So, a static low droop setting will lead to WT operation instability. Meanwhile, a static high droop also induces a noticeable oscillation during the frequency recovery due to its overly fast droop response [50]. To achieve a tradeoff, a variable droop control is utilized to optimize the power shared among deloaded WTs during low wind speeds so as to enhance the overall primary frequency contribution of individual WTs based on their available power reserves corresponding to different wind speeds [66]. Another similar variable speed-droop mechanism is proposed in [53] for DFIG wind farm to change their droop coefficients based on the variable power reserve so that the number of unit output reversals and Root Mean Square (RMS) of frequency deviation are significantly decreased.

Besides, non-symmetric droop characteristic is proposed in wind power plants as well [17],[62]. The positive and negative droop coefficients, frequency dead bands and reserve margin can be properly determined to optimize the primary frequency response of aggregated WTGs.

B. Deloaded Control

To enable VSWT to participate in the primary, secondary and tertiary frequency control, VSWT needs to be operated in the sub-optimal mode through the de-loaded control. So, an adequate spinning reserve margin\headroom is established to deliver the additional active power in the frequency event.

Nowadays, the common primary reserve is achieved through either "Balance" type control that reserves the power output at a scheduled constant amount (namely, a constant percentage of rated power) [25],[53] or "Delta" type control that reserves a fixed proportion of available maximum aerodynamic power regardless of wind speeds [40], [67], [68]. Another de-loading approach is "De-rating" type that restricts maximum available wind power at a specific level only when wind speed goes beyond the rated value [63]. These three types of de-loaded operations for frequency regulation are mathematically described as follows [63]:

1) Balance type:

$$P_{ref} = \begin{cases} 0, & P_{Avail} \le \Delta P_{Reserve} \\ P_{Avail} - \Delta P_{Reserve}, & P_{Avail} \le P_{Rated} \\ P_{rated} - \Delta P_{Reserve}, & P_{Avail} > P_{Rated} \end{cases} \tag{2.11}$$

$$\Delta P_{Reserve} \in [0.0, \dots, \Delta P_{MAX}]$$

2) Delta type:

$$P_{ref} = \begin{cases} (1 - K_{Reserve}) \bullet P_{Avail}, & P_{Avail} \le P_{Rated} \\ (1 - K_{Reserve}) \bullet P_{Rated}, & P_{Avail} > P_{Rated} \end{cases} \tag{2.12}$$

$$K_{Reserve} \in [0.0, \dots, 1.0]$$

3) De-rating type:

$$P_{ref} = \begin{cases} P_{Rated} - \Delta P_{Derating}, & \Delta P_{Derating} \le P_{Rated} \\ P_{Rated}, & \Delta P_{Derating} > P_{Rated} \end{cases} \tag{2.13}$$

$$\Delta P_{Derating} \in [0.0, \dots, P_{Rated}]$$

Where, P_{ref} is the active power reference for individual wind turbine generator, P_{Rated} is the rated power of wind turbine generator, $\Delta P_{Reserve}$ is a fixed amount of active power for spinning reserve operation over a full scope wind speeds, P_{Avail} is the total amount of available wind power at the given wind speed, $K_{Reserve}$ is a fixed percentage of spinning reserve from the available wind power. $P_{Derating}$ is the de-rating amount of available wind power when wind speed goes beyond the rated value. Compared with the balanced type, the delta is higher energy efficient due to the long-term power reserve guaranteed regardless of wind velocities. So, a massive cost on the energy loses is saved without excessively compromising the wind power production. It is shown in [69] that offshore wind farms with state-of-the-art technology is capable of maintaining a 5% of the rated power as reserve sustaining for up to 89% of the event duration under varying wind speed conditions. Usually, VSWTs are de-loaded by 5% to 20% below the MPPT operation condition to ensure the sufficient reserve margin for primary frequency regulation [44]. On the other side, a certain amount of spinning reserve margin can enable the inertial control to perform a better function during the initial frequency regulation since the temporary active power injection is much larger [3]. In contrast, short-term rapid change in wind plants output can be effectively mitigated using balance type so as to enhance the certainty of wind power production and minimize the variability in power system operation and dispatch [4],[25],[40],[16],[66],[70]. Note that the reserve margin level are dependent on prevailing wind speeds, prediction errors and allowable upper limit of the VSWT's rotor speed [45],[66]. One dynamic reserve

allocation approach is presented in [9] to distribute the total wind farm reserve according to individual wind velocities of each wind turbine.

Lastly but not least, the investment on conventional reserve can be decreased with the de-loaded control implemented. That's due to its frequency response is much faster and more accurate by means of power converter control [9]. Thus, de-loaded control plays an essential role in supporting long-term frequency regulation from the perspectives of system dynamics and economics.

C. Pitch Angle Control

The original objective of pitch angle control in WT is to prevent the power output of generator from overloading or rotor speed from overspeed [23]. To provide a supplementary frequency regulation, the pitch control needs to be modified in terms of various wind conditions. Moreover, the primary frequency response can be effectively supplied under the high and medium wind speeds although the rotor speed is maintained as the maximum rotor speed. Meanwhile, the initial pitch angle β_0 is regulated to keep a certain power reserve. Due to the servo time constant of the pitch controller, the response of pitch control appears to be slower than that of over-rotor speed control through power electronic converter. As illustrated in Figure 2.9, two types of modified control approaches are integrated into the pitch angle controller according to different control objectives [3] .

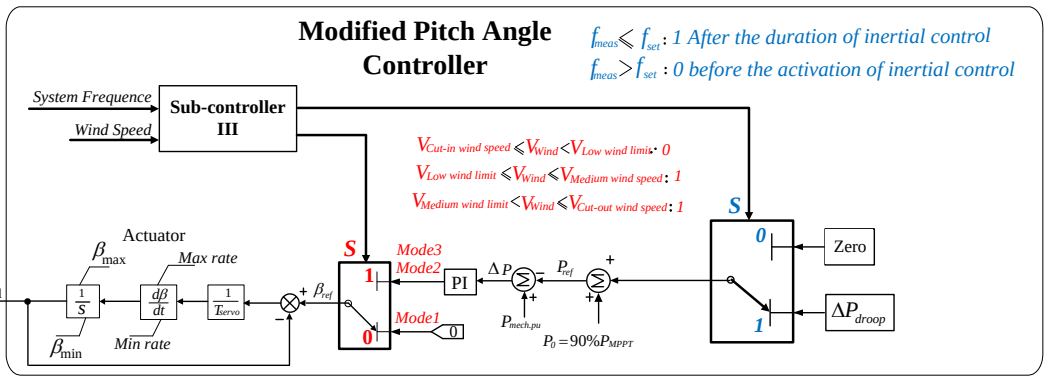

(a) Modified pitch angle control based on the active power regulation.

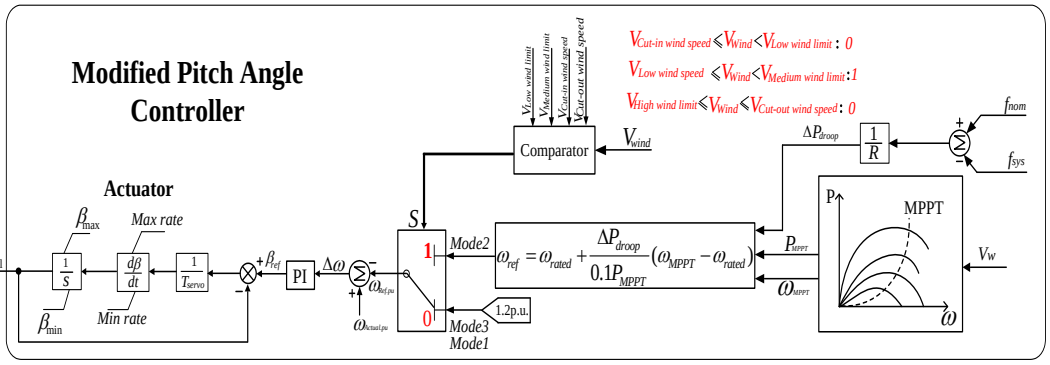

(b) Modified pitch angle control based on the rotor speed regulation.

Figure 2.9 Schematic diagram of modified pitch angle control strategy

D. Rotor Speed Control

In accordance with a PMSG-WT sub-optimum power extraction curve in Figure 2.10, the WTG output is deloaded by shifting the operation point toward the left or right side of the maximum power point tracking curve during low-to-medium wind speed without hitting the rotor speed upper limit. The WTG output can be adjusted between P_{deload} and P_{max} by altering its rotor speed between ω_{deload} and ω_{max} [3],[16]. The operating power reference (P_{ref}) of the deloaded WTG under the given rotor speed can be acquired using a simplified linear equation (2.14) or referring to a predefined look-up table in [66].

$$P_{ref} = P_{del} + (P_{max} - P_{del}) \left[\frac{\omega_{r,del} - \omega_{r,meas}}{\omega_{r,del} - \omega_{r,max}} \right] \quad (2.14)$$

where, P_{max} is maximum power [p.u.]; P_{del} is deloaded power [p.u.]; $\omega_{r,max}$ is DFIG rotor speed corresponding to P_{max} [p.u.]; $\omega_{r,del}$ is rotor speed at P_{del} [p.u.]; $\omega_{r,meas}$ is measured rotor speed [p.u.].

The left sub-optimal operation point is unstable because it is more likely to cause the wind turbine to stall under the frequency event. The wind turbine is bound to operate along the right sub-optimal curve in order to maintain a stable operation when providing the frequency response over a full scope wind speeds. Another benefit of right sub-optimal operation is to enable VSWT to contribute the combined reserved active power and more kinetic energy stored in a faster rotating mass to frequency response when operating point moves from the de-loaded state to the maximum power state. Moreover, it can minimize the tear and wear losses of pitch angle during the process of system frequency regulation.

Considering that the possible rotor speed ω required for de-loading operation exceeds the rotor speed ω_{max} maximum under medium and high wind speeds, three types of wind speed modes is determined in terms of control objectives and secure operation constraints: low wind speed mode where the de-loading operation is carried out merely by rotor speed control, medium wind speed mode where the de-loading operation is conducted by combined pitch angle control and rotor speed control as well as high wind speed mode where the modified pitch angle control needs to be adopted for the de-loaded operation [19],[16],[5]. It is noted that limited kinetic energy is available for inertial response under high wind speed condition due to constant rotor speed and rated power condition [33] .

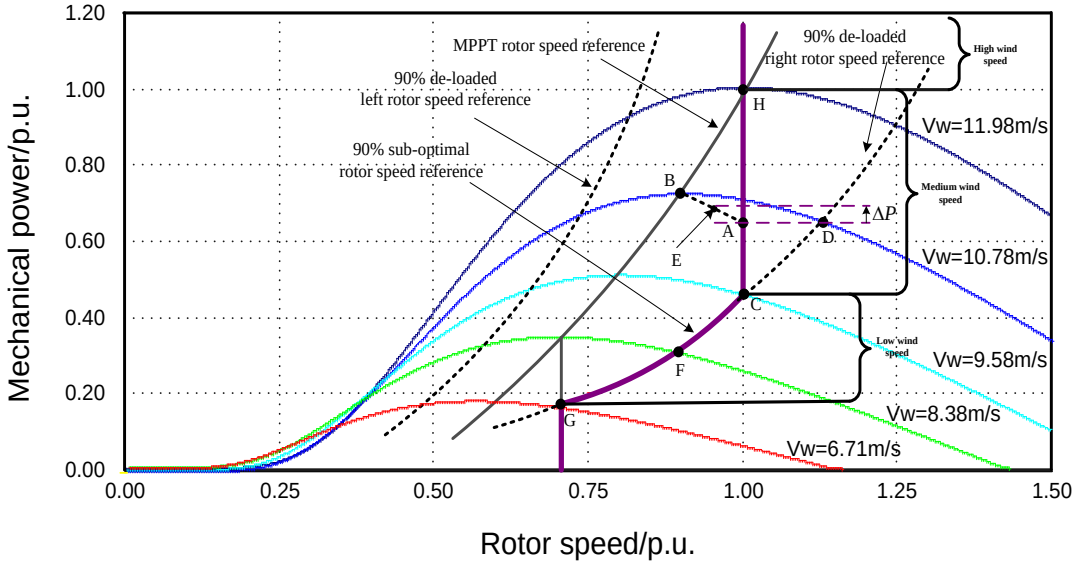

Figure 2.10 90% PMSG-WT sub-optimal operation curve

2.1.3 Secondary Frequency Control /AGC

Secondary frequency control, also called Automatic Generation Control (AGC) or Load Frequency Control (LFC), is implemented during both emergency events and normal condition [9]-[53]. The secondary frequency control starts within several tens of seconds and sustains for up to several tens of minutes [59]. This control is a minute by minute continuous response to allocate the load change among individual WTs with the purpose of maintaining both the system frequency deviation and the tie line power flow deviation as zero [47]. In figure 11, a simplified frequency control model is applied to validate the dynamic characteristics of each generation participating in the AGC regulation [71]. The AGC set-point of each WT depends on the PI controller parameters and participation factors (PFs). The optimal method to decide PFs is developed by taking into account the up/down ramp rate, operating reserves, dispatch limit and generating cost [72].

A secondary frequency controller based on a Supervisory Wind Farm Control System (SWFCS) fully utilize secondary frequency reserve to respond the command from the system operator including AGC demand (power set-point) and power flow adjustment [53],[13],[9]. Another novel control system is proposed in [73] to enable wind turbine to change the active power reference in accordance with AGC or set-point power command so as to meet the system operators' requirement. In [72], a coordinated AGC control strategy between WTs and combined heat and power plants (CHPs) is proposed to mitigate the real-time power imbalance by down-regulating the wind power production when CHPs are unable to track the required response. Due to the fast ramp rate of WTs, area control error (ACE) can be greatly reduced so as to make the system frequency more reliable and secure.

2.1.4 Tertiary Frequency Control

Compared with other frequency controls mentioned above, tertiary frequency control is a much slower power balance control with the long decision time step from the order of minutes to hours, which is activated only after the secondary control is completed [59],[62],[74]. This control method comprises dispatching actions commanded by the system operator to fulfill the reserve deployment and restoration for the WT's tertiary frequency control that enables unit commitment, economic dispatch and optimal power flow according to marketing signals or other system requirements [27]. As shown in Figure 2.11, the actual operation reference value of conventional generators and wind farms equal to the sum of AGC and economic dispatch set points. Economic dispatch usually updates this operating set point every 1-5 min while AGC does the same every

0.1-1 sec [75]. Nowadays, there are two types of power markets associated with tertiary frequency control, including intraday real-time market with every minute economic dispatch and day-ahead market with every day economic-unit commitment [32].

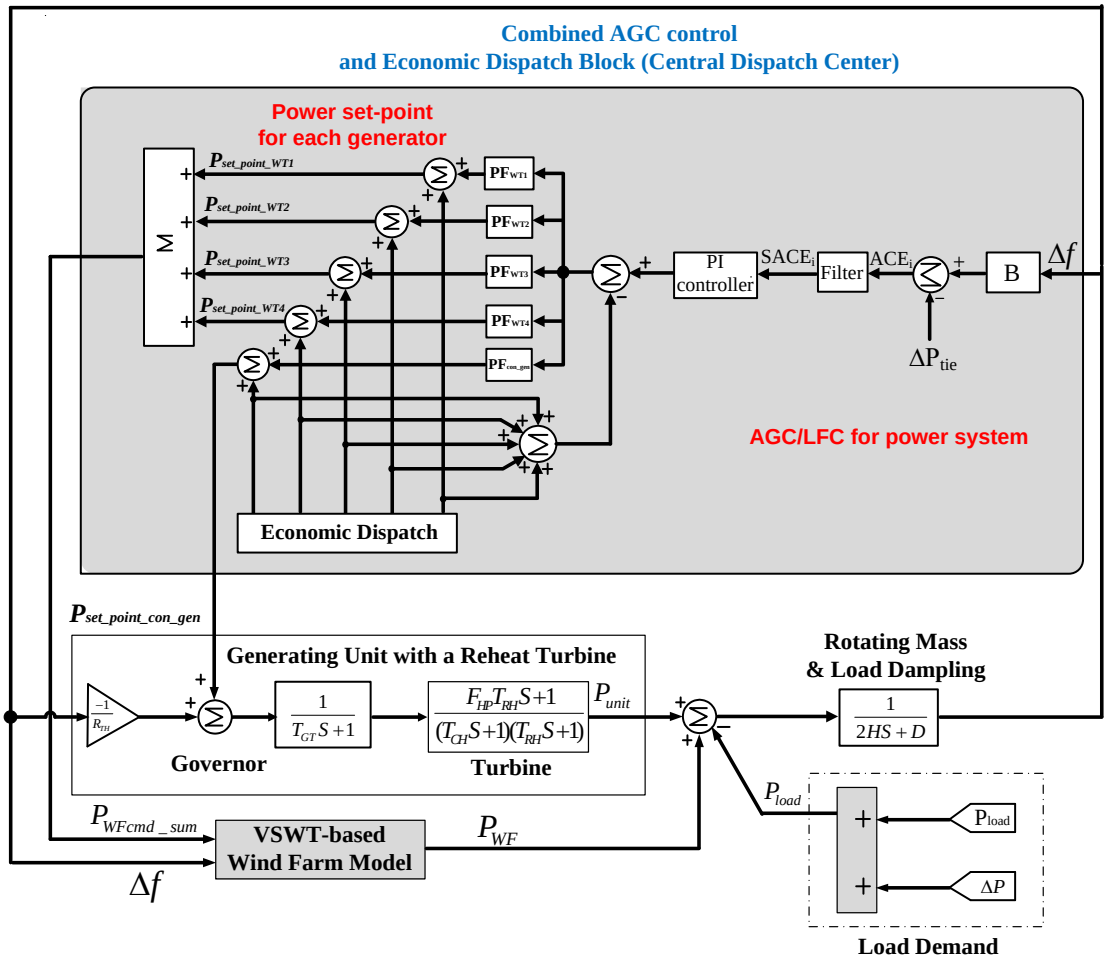

Figure 2.11 Schematic diagram of load-frequency control loop

2.1.5 Coordinated Frequency Control

Considering the initial operation condition, frequency fault magnitude and duration, a combined inertial response, primary frequency control and secondary frequency control by VSWT can enhance the overall frequency regulation capability of power system and alleviate the burden of frequency regulation on conventional units once

large frequency contingency occurs [3],[45],[16],[62]. The basic process of coordinated down-frequency regulation can be described as below: during the first transient process of frequency drop event, inertial response plays a key role in reducing ROCOF and increasing the frequency nadir point. Once deadband is hit for more than a specified delay time, the primary frequency response further enhance the frequency regulation capability by using a droop control until the frequency settles into another steady state, so that the nadir is greatly lifted and smoothly restored within an acceptable limit. Lastly, AGC control is activated to achieve the zero-error frequency regulation through PI controller. According to different control strategies, the coordinated frequency controllers can be designed as shown in Figure 2.12.

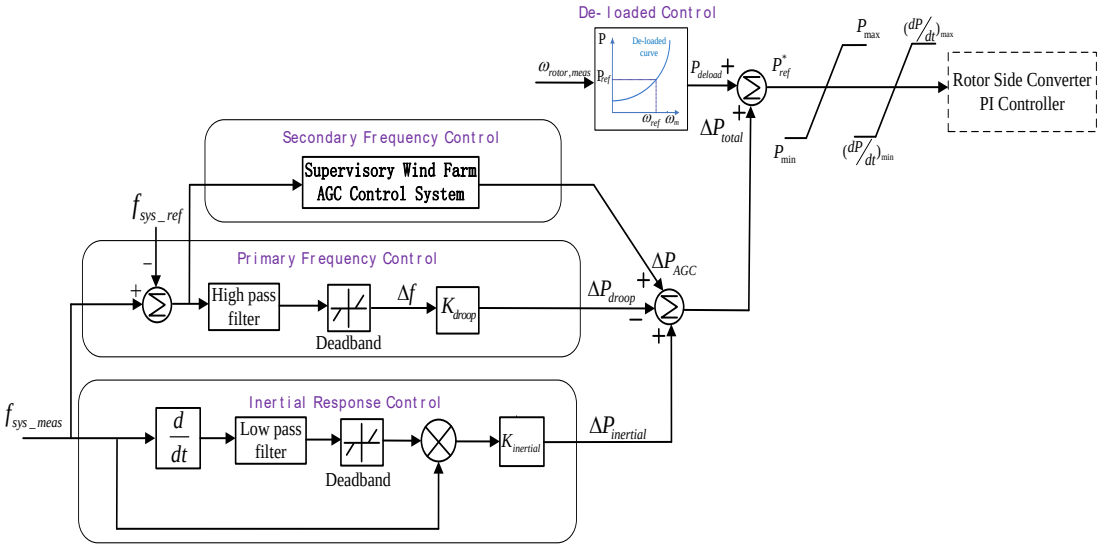

(a) Coordinated frequency control based on active power control

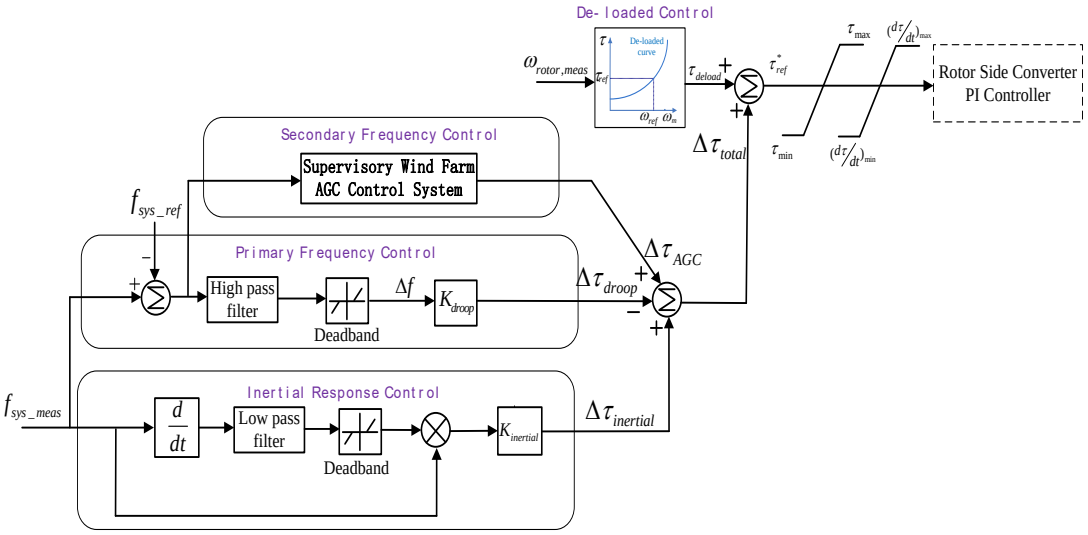

(b) Coordinated frequency control based on torque control

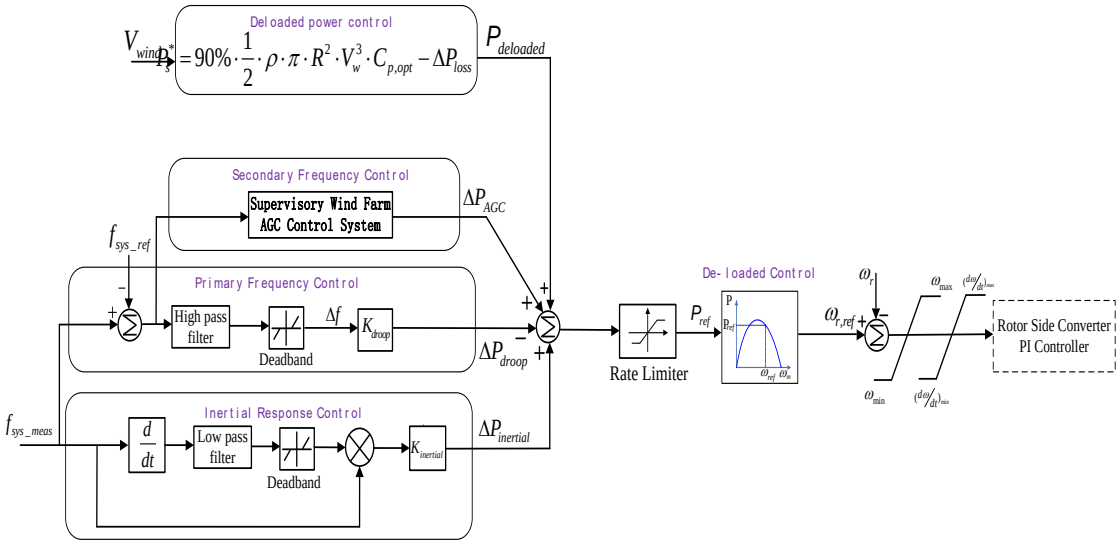

(c) Coordinated frequency control based on rotor speed control

Figure 2.12 Coordinated frequency control strategy for VSWT

Several coordinated control strategies based on pitch angle control and rotor speed control are subsequently proposed to improve VSWT's frequency regulation capability, enhance the system damping and mitigate the power oscillation. Without de-loaded control, a temporary up-regulated and down-regulated frequency support can be provided by VSWTs through an adaptively combined pitch angle and rotor speed control

over different wind speeds [76]. The work in [25],[53] considers a K deviation method for DFIG-WTG to perform frequency regulation in real-time variance tracking mode. The study in [16] proposes a novel coordinated frequency regulation strategy for DFIG-based WT according to low, medium and high wind speed conditions. In [3], a coordinated frequency control scheme appropriate for PMSG-WT is designed by synthesizing the constant inertial control, over-rotor speed control and pitch angle control under a full range of wind speed. The work in [19] is focused on the combined pitch angle and rotor speed control to achieve the frequency regulation throughout the frequency event. A coordinated control strategy in [11]-[12] employs a direct control on the electromagnetic torque and rotor speed of DFIG-based wind turbine to allow for additional active power control based on operator's request under the varying wind conditions. In [70], a Kinetic/Inertia, Proportional gain & Enhanced Pitch (KIPEP)-control is presented to support the primary and secondary frequency regulation and smooth out the wind power output in the short-term frame as well.

2.2 Performance of Various Speed Wind Turbine Generations on Frequency Regulation

A WTG possesses a certain amount of kinetic energy stored in the rotating mass which can be utilized to provide a short-term frequency support in the event of power imbalance. In general, wind turbine can be divided into two main groups: fixed-speed WTs (FSWT) and variable-speed WTs (VSWT). Each group has its own benefits and drawbacks in terms of their contributions to the system frequency support. The FSWT inherently can provide a certain inertial response to minimize the ROCOF, so integration

of these types cannot obviously mitigate the system inertia. In contrast, VSWTs cannot naturally supply any inertial power into the electrical grid due to partially or fully decoupling between generator rotor speed and grid frequency through power converter. However, modern VSWT is able to provide the emulated inertial response and frequency regulations by equipping with supplementary control loops on the converter controller and pitch angle controller. Furthermore, it is emphasized in several literatures that VSWTs are capable of providing superior inertial response to conventional generators due to their faster power response, a wider variation range of rotor speed and larger inertia constant [5],[7],[15],[26],[33],[77]. In addition, another novel type of VSWT based on the electromagnetic coupler (WT-EMC) is studied with respect to its frequency contribution through the emulated inertial response and droop frequency regulation over a full scope wind speed conditions [29].

2.2.1 Type 1 and Types 2 FSWTs

Thanks to a direct coupling between the rotational rotor speed and system frequency, Type 1 Induction Generator with Fixed Speed and type 2 Wound-rotor Induction Generator with Adjustable External Rotor Resistance-Variable Slip can contribute to the system frequency by providing the limited inertial response. For type 1, inertial response is a passive process in which the kinetic energy stored in the generator, gearbox and wind blades is intrinsically released or absorbed as system frequency decreases or increases. Commercial fixed speed wind turbines (FSWT) with rated above 1 MW possesses 3-5s inertial constant H [77]. The stored energy in each FSWT is basically unrelated with wind speed, and the aggregated kinetic energy of wind farm

increases with the number of turbines online [71]. Generally, the larger kinetic energy stored in type 1 wind turbine will be released in the form of extra inertial power as the initial rate of change of frequency (ROCOF) decline faster. However, it is difficult to tune the inertial response to meet the system requirement without supplementary controller adopted. So, inertial response from type 1 WTGs is limited and uncontrollable. Type 2 WTGs maintain the power output at the rated value despite a abrupt frequency drop occurs because the external rotor resistance regulates the power output at all times according to the target value. Therefore, type 2 hardly makes any contribution to the system inertial response [67],[23].

However, it is noted that both types can allocate a constant amount or a constant proportion of available aerodynamic power as reserve margin by pitch angle controller. In this way, they are capable of delivering the surplus power into the grid based on primary droop control, so as to improve the frequency regulation capability even if productivity loss of wind power results.

2.2.2 Type 3 and Type 4 VSWTs

Type 3 Double Fed Induction Generators (DFIG) with Variable Speed and type 4 Direct Drive Permanent Magnet Synchronous Generator with Variable Speed and Full Converter System (PMSG) inherently cannot provide any inertia response. However, they are capable of achieving a fast, flexible and accurate active power regulation through power electronic converter. Compared with type 1 and type 2 FSWTs, the rotor speed of VSWT can operate at the lower rotor speed to release the kinetic energy for inertial response according to the specific operation mode. Meanwhile, due to variation in

regional wind profiles, their kinetic energy available from VSWTs always changes significantly in magnitude [77]. These two types of VSWTs act like a fly-wheel device to mitigate the power fluctuations resulting from variable wind conditions, which can be stored as kinetic energy in the rotating mass. In contrast with FSWTs, inertial response of VSWTs is an active process in which the system frequency or ROCOF is monitored and measured in real time, so that their response can be tuned by setting proper control parameters to enhance the system comprehensive frequency regulation capabilities. To better arrest the frequency decline, a certain headroom for inertial power release is required for VSWTs to provide more active power within the maximum power capability of converter and generator[14]-[15],[19],[16], [77].

Due to asynchronous operation, speed variation of type 3 is much larger than system frequency variation [77]. The rotor speed of type 3 WTGs can be controlled between 0.67p.u-1.33p.u through modern power converter technology [66]. Thus, the emulated inertia of type 3 is as large as several times of its inherent inertia by using inertial control loop. The partial-scale power converter (20%-30% of full rating) utilized in the rotor circuit of type 3 imposes certain limitation on the de-loaded level, maximum inertial response as well as the rotational speed variation range (within ±20%-±30% of synchronous speed) [2]. Compared to type 3 with the same rated power capability and inertia constant H, type 4 is capable of providing greater frequency regulation capabilities and stronger inertia response due to its wider operating range of rotor speed and a full power converter employed [77].

2.3 Conclusion and Discussion

In this chapter, the motivation for incorporating the inertial response and frequency regulation of VSWT into the system frequency regulation is summarized. Moreover, the classifications, fundamental concepts and control schemes implemented for auxiliary frequency control of individual WT and wind farm are clarified in detail. Also, the potential frequency regulation capabilities of four main types of WTs are discussed.

Chapter 3 Modeling and Simulation of a CART2-PMSG Integrated Model

According to basic operation characteristics and key physical parameters of Controls Advanced Research Turbine (CART2) Test Bed, a 600kW CART2-PMSG integrated model is developed as a simulation platform using MATLAB/Simulink in attempt to investigate the impact of the proposed inertial response and primary frequency regulation on the wind turbine's structural and component loads. In the meanwhile, the frequency regulation performance can be fully evaluated by means of CART2-PMSG-based wind farm model in case of one generator trip.

A complete CART2-PMSG wind turbine system mainly consists of CART2 aerodynamic model, a permanent magnet synchronous generator (PMSG) and a full-scale average voltage-sourced converter (VSC). Each component of the entire model is established in Simulink based on its mathematical equations. This control scheme can achieve the maximum power operation and active/reactive power decoupling control: generator-side converter can control the generator rotor speed or its active power to fulfill the MPPT operation while grid-side converter can maintain the dc-link capacitor voltage constant as well as the reactive power exchanged with grid at the specified value. Lastly, validity of established model equipped with corresponding control strategy for MPPT operation is assessed through simulation study considering the step-change of wind speed and real wind speed conditions respectively.

3.1 CART2 Test Bed

The Controls Advanced Research Turbine (CART2) is a two-bladed, teetered, upwind, active-yaw, variable-speed wind turbine located at the National Wind Technology Center (NWTC) of the National Renewable Energy Laboratory (NREL). Currently, two types of generators are available in CART: a wound field synchronous generator for CART3 and a squirrel-cage induction generator for CART2. These two sets of system serves as a test bed for various aspects of advanced control schemes for medium- to large-scale machines. For the real CART2 machine, it is a gearbox-operated wind turbine equipped with squirrel cage induction generator and connected through a full-scale power converter to the power grid [80]. Each blade can be independently pitched through its own electromechanical servo system. These make it possible to control the torque from minus rating ($-\tau_{\text{rated}}$, motoring) to plus rating ($+\tau_{\text{rated}}$, generating) at an acceptable range of the rotor speed by power electronics, which are utilized to command the specified generator torque. In the meanwhile, the full-span blade pitch controls the rotor speed. Figure 3.1 illustrates four operation regions where wind power generator safely and efficiently operate according to different wind speed conditions. The rated electrical power is 600 kW at a low-speed shaft speed of 48.32 rpm, and it is maintained in Region 3 using a conventional variable-speed approach as shown in Figure 3.1

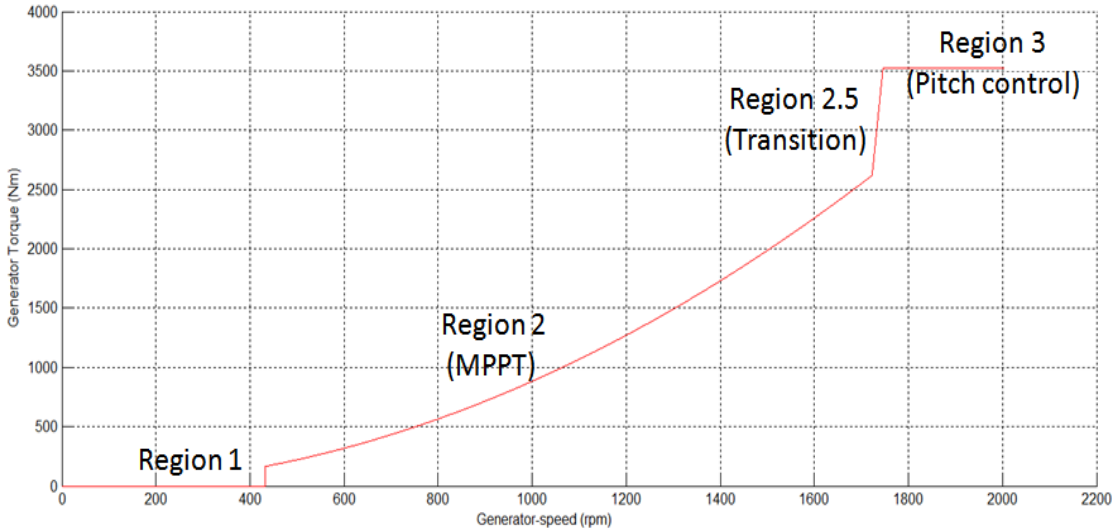

Figure 3.1 Variable-speed turbine operating regions of the CART2 model

In addition, the machine is installed with a full complement of instruments that gather meteorological data at four heights. Blade-root flap and edge-strain gages, tower-bending gages as well as LSS and high-seed shaft (HSS) torque transducers gather load data [80]. Accelerometers in the nacelle measure the tower's fore-aft (f-a) and side-side (s-s) motion. Absolute position encoders gather data on pitch, yaw, teeter, LSS, and HSS positions with a sample of 100 Hz. The custom-built control system collects these data and controls the turbine at a control loop cycle rate of 100 Hz [80].

3.2 CART2 Simulink Model

To simulate the characteristics of the CART2 test bed before the field test is carried out, a CART2 model is developed in MATLAB/Simulink based on the Fatigue, Aerodynamics, Structures, and Turbulence (FAST) module [81]. In Figure 3.2, CART2 model incorporates a simplified generator model, yaw controller, and pitch angle controller. Figure 3.3 shows a typical relationship among FAST, the generator model, pitch controller, and yaw controller. Figure 3.1 illustrates four regions wherein the wind

power generator safely and efficiently operates under different wind speed conditions. In Region 1, the wind turbine stays in a stall state due to the low wind speed. In Region 2, the wind turbine runs in MPPT mode when the tip speed ratio (TSR) is maintained constant at the optimal value to maximize the wind energy capture through the generator torque control. At the same time, the blade pitch is held constant at its run-pitch value (-1 degree). In Region 2.5, the rotor speed starts at a value lower than the rated value and gradually reaches the rated torque at the rated speed or slightly below it for the sake of safety margin. In this way, a smooth transition is achieved from Region 2 to Region 3. In Region 3, the generator torque remains constant at the rated value, and the pitch angle controller is activated under the high wind speed condition to restrict the rotor speed below the rated value [23],[81]. Since the Region 2.5 is not operation area that this work intends to focus on, it is neglected and will be discussed in the future research. Therefore, there is no transition zone between region 2 and region 3 for the CART2-PMSG model used herein, which means that active power output of CART2-PMSG is kept as rated value corresponding to the nominal rotor speed without pitch angle control involved.

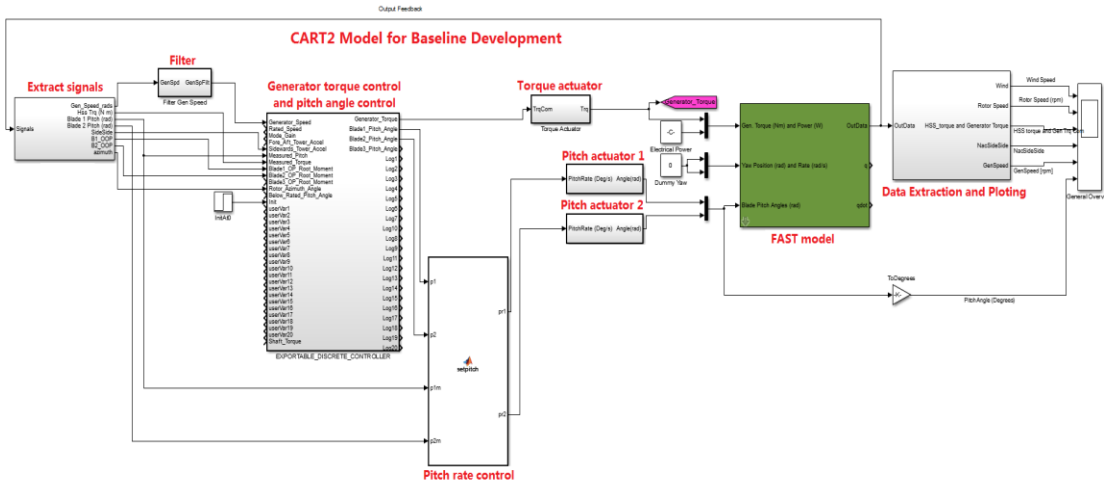

Figure 3.2 The configuration of CART2 simulink model

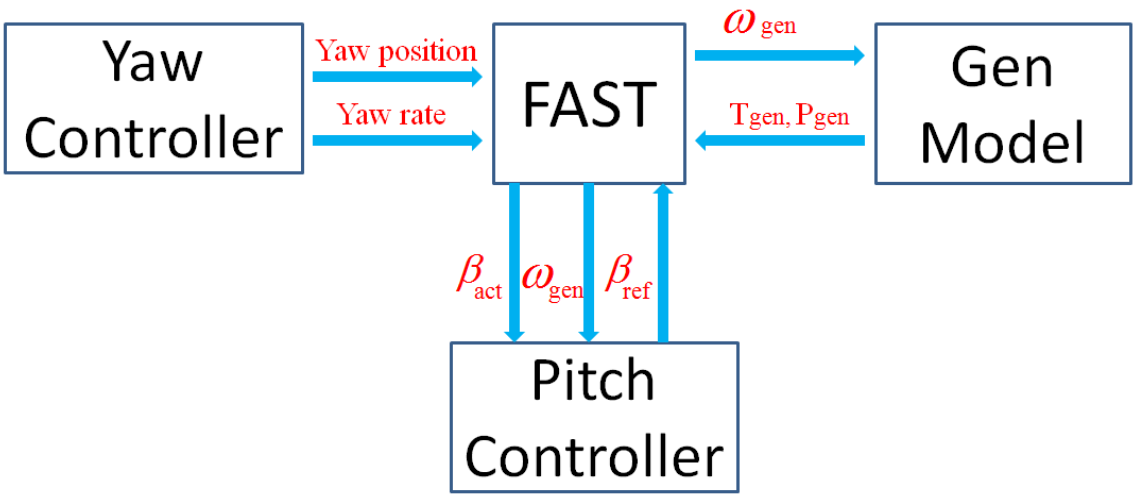

Figure 3.3 Simple flowchart of the CART2 baseline Simulink model

3.3 CART2-PMSG Integrated Model

As discussed before, the CART2 turbine at NREL consists of multi-blade turbine system connected to a variable frequency controlled induction generator via a mechanical gearbox. For the purpose of research objectives intended in this project, the aerodynamic model of CART2 turbine is used, whereas the electrical generator and the power converter used for this simulation is a PMSG with a full power conversion (Type 4). This integrated model is named as "CART2-PMSG".

To be specific, the simplified generator in the CART2 model is fully replaced with a detailed PMSG and average back-to-back power converter to constitute a 600-kW CART2-PMSG integrated model [82]. In addition, the major operating scheme is fulfilled by the generator-side converter control, so that this model resembles the realistic operating characteristics of the CART2 machine in view of different wind speeds. The fundamental control structure of the CART2-PMSG integrated model is shown in Figure 3.4. And Figure 3.5 shows the overall configuration of CART2-PMSG in Matlab/simulink.

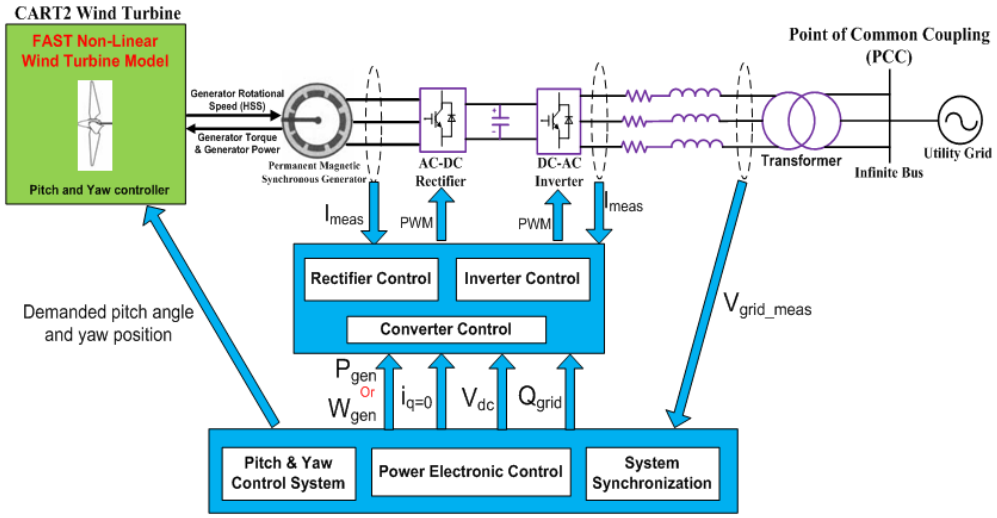

Figure 3.4 Fundamental control structure of the CART2-PMSG integrated model

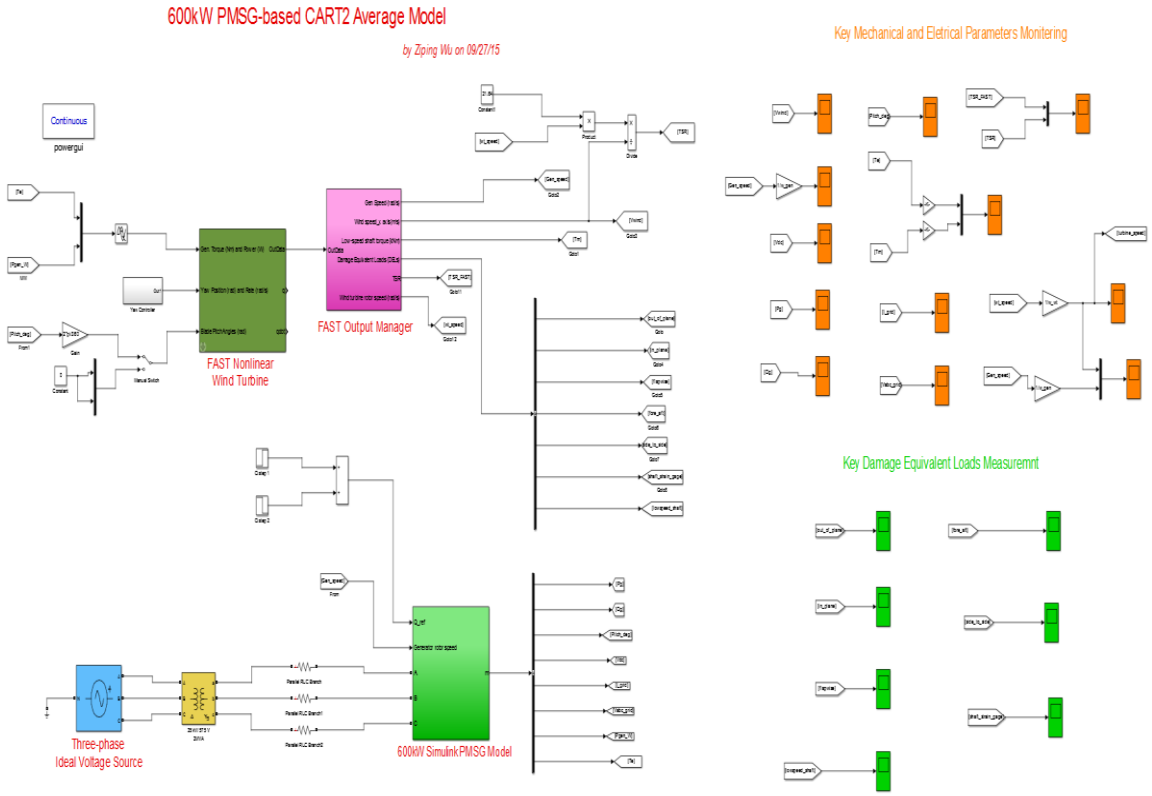

Figure 3.5 CART2-PMSG integrated model in Matlab/Simulink

The values of key parameters for the developed CART2-PMSG integrated model are summarized in Table 3.1.

Table 3.1 List of CART2 modified parameter values

R (rotor radius)	21.336 m
ρ (air density)	1.03kg/m3
C_{p_max} (the maximum power coefficient)	0.396
λ_{opt} (the optimum TSR)	8.49
τ_{rated_gen} (generator rated torque)	3524.4 N-m
ω_{rated_gen} (generator rated speed)	1800rpm (188.5rad/s)
ω_{rated_wt} (wind turbine rated speed)	48.32rpm (5.06rad/s)
N_{gear} (gearbox ratio)	37.25
The pitch angle for C_{pmax}	-1 degree
Rated wind speed (m/s)	12.718
Rated mechanical power	6e5 W
Rated apparent power	664349.4 W
Rated power factor	0.903

3.3.1 Modeling of Pitch control model

One typical model of wind turbine pitch controller is used to carry out the dynamic pitch angle regulation in the operational zone 3 in Figure 3.1. The basic control block diagram of this wind governor is shown in Figure 3.6 [23].

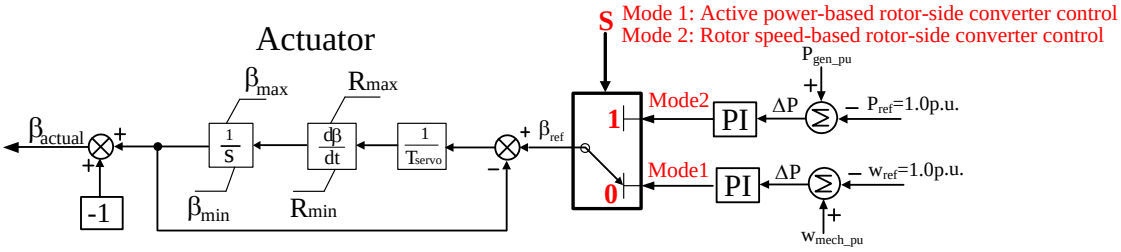

Figure 3.6 Schematic of pitch angle control

In this work, a model of 2 blades pitch mechanism is developed for CART2 model in order to carry out the generator power regulation or rotor speed regulation in coordination with the rotor-side converter control. For the rotor speed-based rotor-side converter control in mode 2, dynamic pitch control strategy is designed to maintain the actual output power of generator within the rated capacity (1.0 p.u.) for the sake of security by increasing the pitch angle when the wind speed exceeds the rated value. But, it is worth noting that modern PMSG-WTG system, including the power converter and generator, is actually capable of carrying out the overloaded operation (1.0p.u.-1.5p.u.) for a specified short period of time (30seconds to several minutes). For the active power-based side converter in mode 1, the pitch angle control is employed to keep the rotor speed of generator below the rated rotor speed (1.0 p.u.) by increasing the pitch angle when the wind speed exceeds the rated value. In this way, the mechanical and electrical components of CART2-PMSG can be protected effectively under the over-wind speed

condition. Note that Figure 3.4 shows a baseline pitch angle control that doesn't consider any other additional control such as frequency regulation control or load mitigation.

3.3.2 Modeling of Permanent Magnet Synchronous Generator

The general dq-axis model of permanent magnet synchronous generator is established in MATLAB/Simulink. The rotor excitation of the PMSG is generated by permanent magnets as constant value, so the model of PMSG in the synchronous reference frame is given as [19],[83]:

$$\begin{cases} V_{ds} = -R_s i_{ds} + \omega_e L_q i_{qs} - L_d p i_{ds} \\ V_{qs} = -R_s i_{qs} - \omega_e L_d i_{ds} + \omega_e \lambda_r - L_q p i_{qs} \end{cases} \quad (3.1)$$

The electromagnetic torque produced by PMSG-WTG is calculated as follows:

$$T_e = 1.5P((L_d - L_q) i_{ds} i_{qs} + i_{qs} \psi_f) \quad (3.2)$$

The PMSG rotor mechanical speed ω_{rm} is given by motion equation

$$\omega_r = \frac{P}{JS}(T_m - T_e) \quad (3.3)$$

where, subscripts ‘d’ and ‘q’ respectively represent the physical quantities transformed into the d-q synchronous rotating reference frame; R_s is the stator resistance; L_d and L_q are the generator inductances on the d- and q-axis, respectively (For the nonsalient PMSG applied, the d- and q- axis magnetizing inductances are equal L_d=L_q); V_{ds} and V_{qs} are the d- and q- axis components of stator voltage, respectively; i_{ds} and i_{qs} are the d- and q-axis components of stator current, respectively; ω_e is the rotor electrical angular speed; ω_r is the rotor mechanical speed; P is number of pole pairs; ψ_f is the permanent magnetic flux; T_e is the electromagnetic torque; T_m is the mechanical torque; J is moment of inertia.

3.3.3 Modeling of Power Converter System

a) Rotor-Side Converter

As shown in Figure 3.7, a coordinated control strategy of back to back double PWM converter is proposed based on the dynamic characteristics of CART2 test bed. There are currently two types of control methods available to achieve the MPPT operation of PMSG-WTG. One method is to have a direct control over the generator electromagnetic power P_{ele}, based on the measured rotor speed to ensure that the rotor speed runs at the optimal power capture mode in Region 2. The other method is to directly adjust the rotor speed based on the measured wind speed so as to maintain the optimal tip speed ratio that enables the PMSG-WTG to extract the maximum wind energy under the different wind speeds. In this work, these two types of control schemes have been considered for the MPPT operation of rotor-side converter, respectively. Moreover, the synchronous generator of CART2-PMSG system is controlled by the rotor-side converter using the rotor magnetic flux oriented control technique, which is implemented at the rectifier for a decoupling control of d-and q-axis stator current components of PMSG. For this purpose, the controller of the rotor-side converter has a cascaded structure: a faster inner current loop for q-axis currents control in conjunction with middle loop for electromagnetic torque control and a slower outer loop for the optimal active power control in mode 1 (optimal rotor speed control in mode 2). By this means, the active power output of PMSG is dynamically modified in accordance with the measured rotor speed in mode 1 (measured wind speed in mode 2) so as to make wind turbine perform at the MPPT mode corresponding to the optimal C_p value [19],[83].

The other control loop is used to regulate the d-axis current component for controlling the excitation flux of the generator. As the i_d is usually set to 0, the stator current can be completely utilized for generating the maximum electromagnetic torque. Furthermore, the d-and q-axis voltage control signals of the machine-side converter are obtained by comparing the d-axis and q-axis currents references with the actual generator stator d-axis and q-axis current values. With this control design, the current-regulated voltage-source PWM converter performs the optimal operation of PMST-WT system.

b) Generator-Side Converter

For the grid-side converter, a control method with a reference frame aligned along the inverter ac voltage (Voltage Oriented Control) is adopted, so that the active power and reactive power delivered from PMSG to the grid can be fully independently controlled. The grid-side converter takes advantage of two outer PI control loops that define reference values i_d^* and i_q^* for two inner current control loops that control the dq-axis decoupling current components. Meanwhile, the inner current control loops define the PWM modulation indices for the inverter control [19],[83].

Using this method, a grid-side converter is able to maintain the dc link voltage constant and control the reactive power at the desired value. In addition, once the reference value of reactive power is set as 0, the inverter is ensured to operate in the unity power factor mode to produce the maximum active power output.

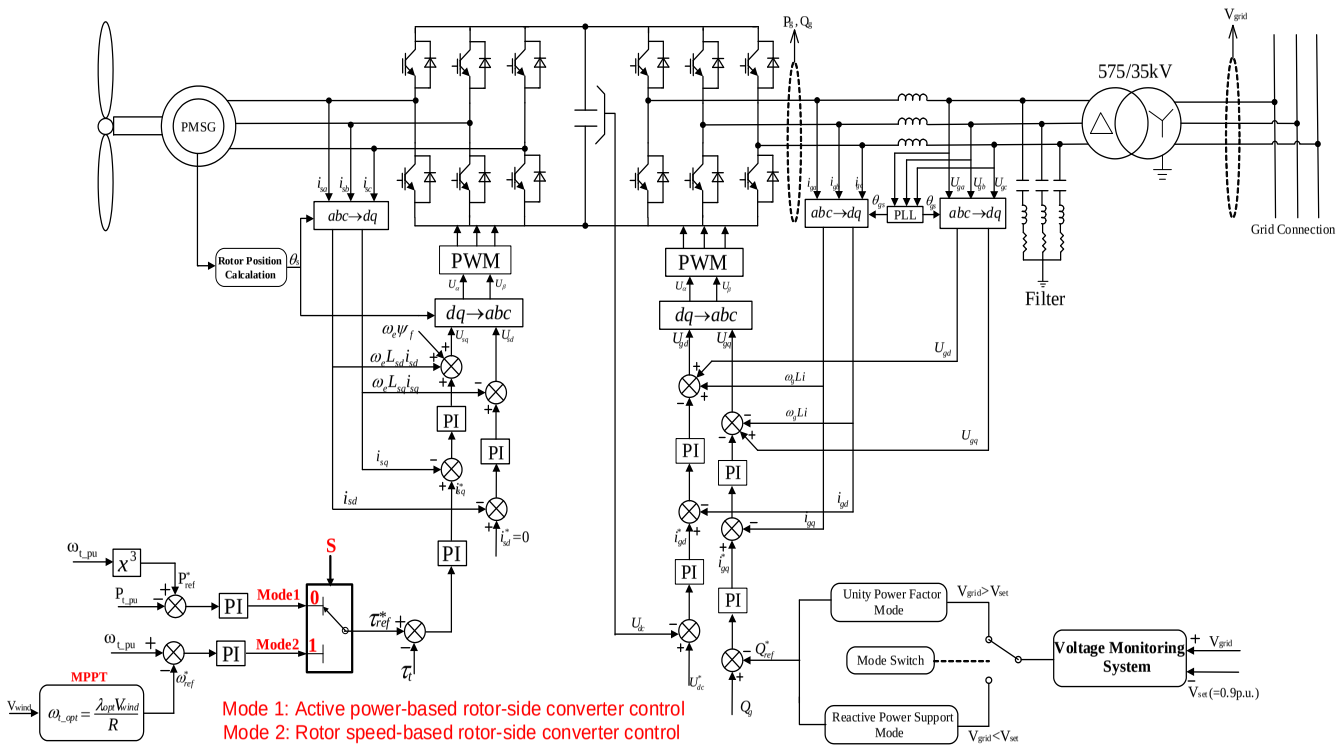

Figure 3.7 The basic control scheme of proposed PMSG-WTG system connected to an infinite bus

3.4 Simulation Results and Discussion

The dynamic response of a single CART2-PMSG based on active power control and rotor speed control are compared through the following three simulation cases: wind speed step change, real wind speed condition as well as transient voltage sag. Simulation results and analysis are presented as follows.

Case 1. Dynamic response of CART2-PMSG model under step-change wind speeds

1) Simulation Results from PMSG Simulink model

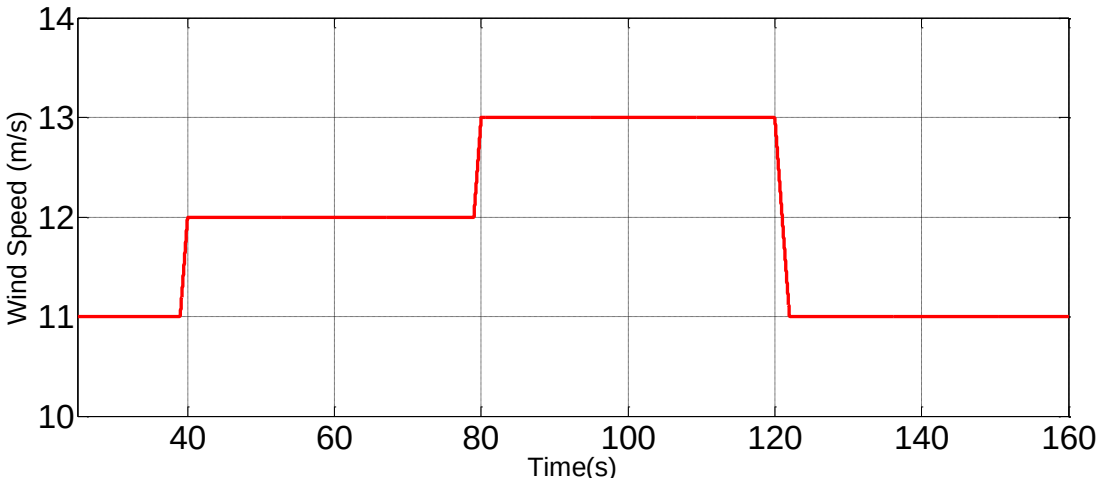

(a) Wind speed

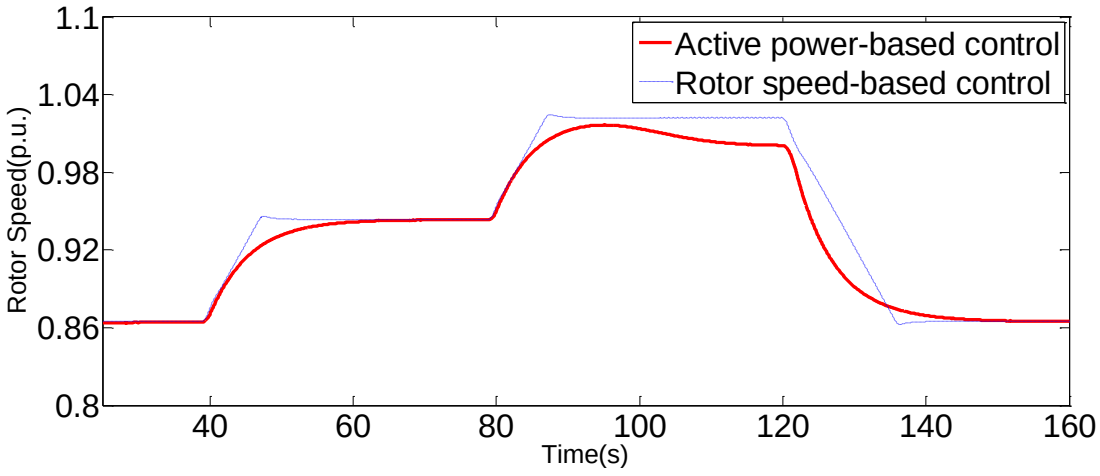

(b) Generator rotor speed

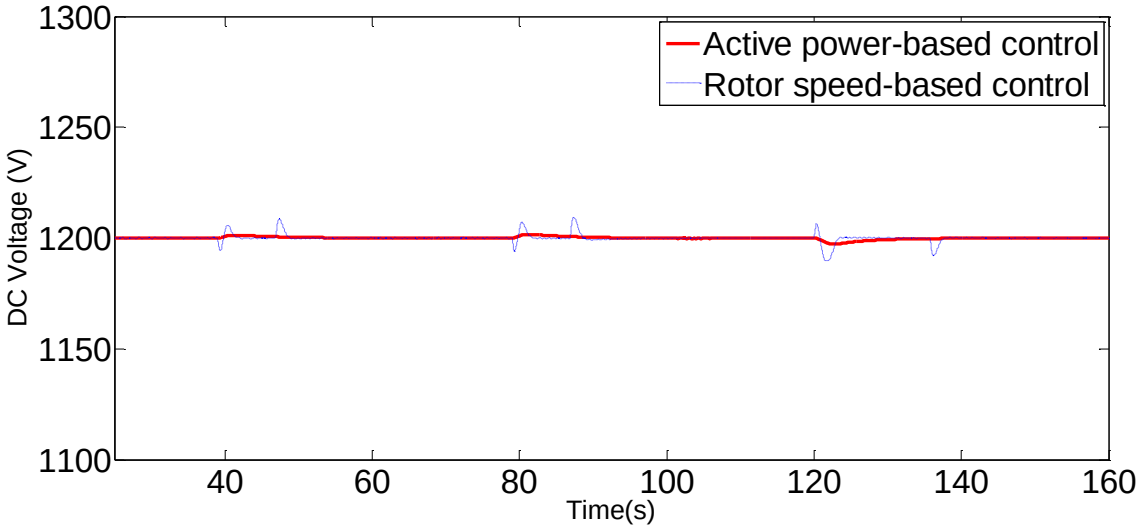

(c) DC-link voltage

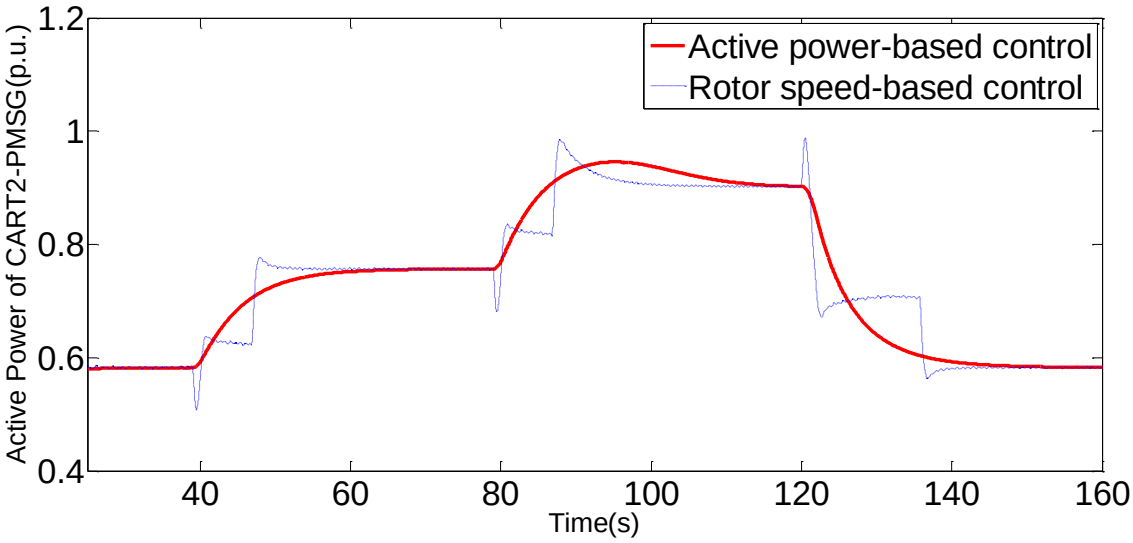

(d) Active power output of CART2-PMSG

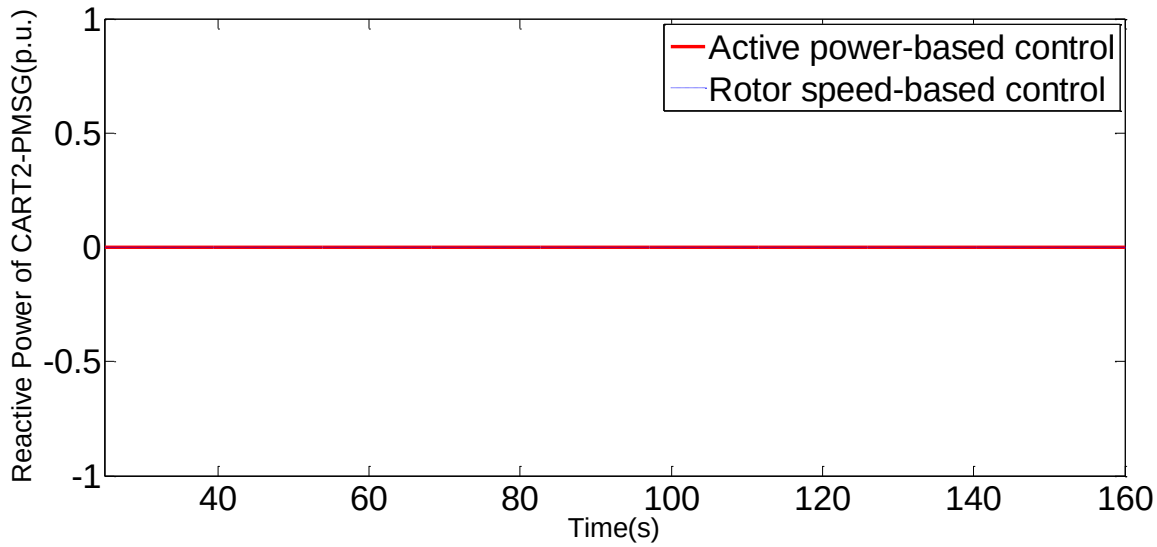

(e) Reactive power output of CART2-PMSG

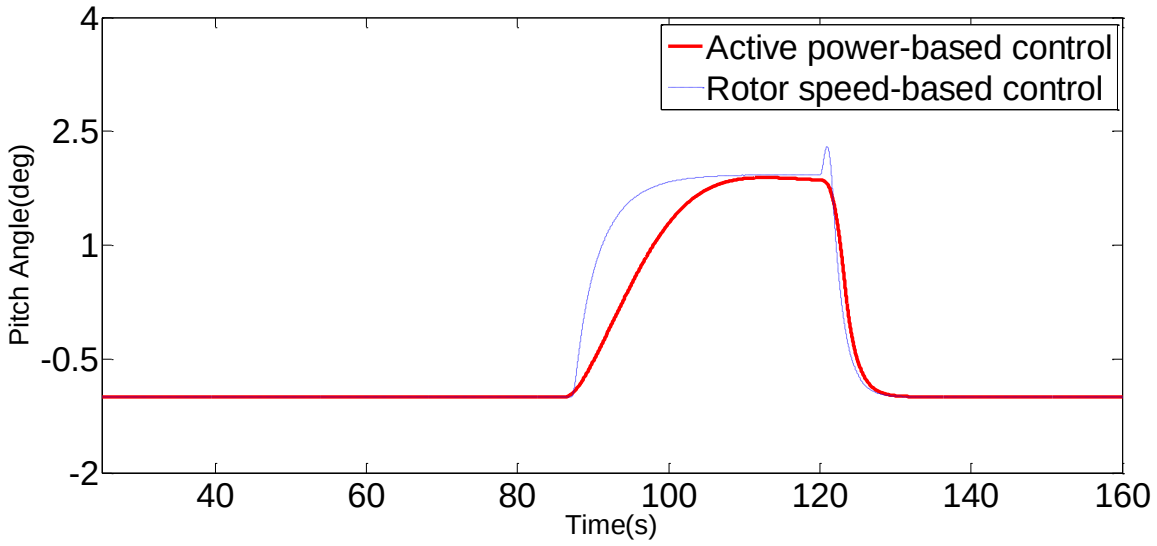

(f) Pitch angle

Figure 3.8 Simulation results for the PMSG model under step-wise wind speed conditions

As shown in Figure 3.8, wind speed changes from 11 m/s to 13m/s and returns to 11m/s with a step change of 1m/s. For the active power-based control, it is observed that the rotor speed have a slight overshoot of 1.5% of the rated value due to the slow response of pitch angle regulation mechanism when wind speed rises from 12 m/s to 13 m/s. For every step change of 1m/s in wind speed below the rated value, rotor speed

regulated by active power-based control takes approximately 22s to reach the steady state because of CART2's large inertia constant. In contrast, it takes about 10s to settle down if the rotor speed-based control is adopted by imposing a direct control over the rotor speed. For the step change in wind speed above the rated value, the rotor speed needs longer duration (35s) to enter another steady status due to the combined large inertia of WT and slow response of pitch control. During the wind speed change, the DC link voltage can be maintained constant around 1200V in the step-change wind speed condition. It is due to the fact that size of DC capacitor is large enough to mitigate the impact resulting from the power imbalance and meanwhile generator-side converter can perform well in maintaining the DC voltage as the targeted value. Although there is a fast step changes in the wind speed, the active power output is well controlled to track the optimal power reference while the reactive power is kept at 0 throughout the entire simulation. By comparison, there is a faster but step-wise change in the active power output when rotor speed-based control is implemented for generator-side converter. That is because the rotor speed variation is subject to the limit of 0.01p.u./s, for the purpose of avoiding the potential risk of power overloading and sudden power drop as a result of excessive inertial power exchange when the rotor speed rapidly varies. The pitch angle motion responding to the step change of wind speed. Note that the variable pitch angle control is hardly activated to regulate and limit the generator rotor speed (active power-based control) or the generator active power output (rotor speed-based control) below 1.0 p.u. until wind speed goes beyond the nominal value.

Thus, the established CART2-PMSG model equipped with the active power-based control and rotor speed-based control are capable of fulfilling the independent real

and reactive power control while the MPPT operation is achieved throughout the stepwise wind speed conditions, respectively.

2) Simulation Results from FAST model

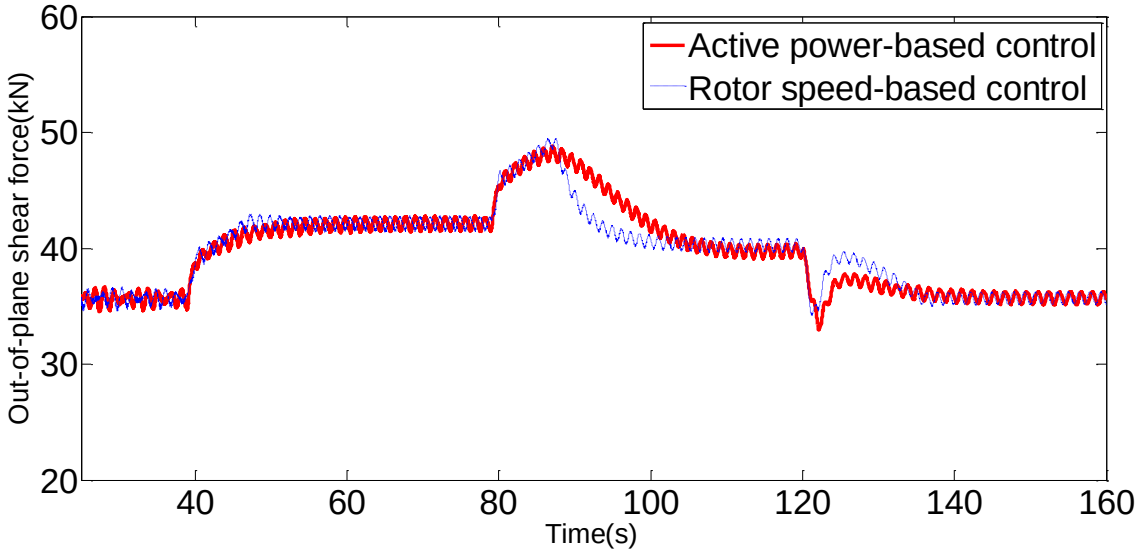

(a) Blade 1 out-of-plane shear force at the blade root

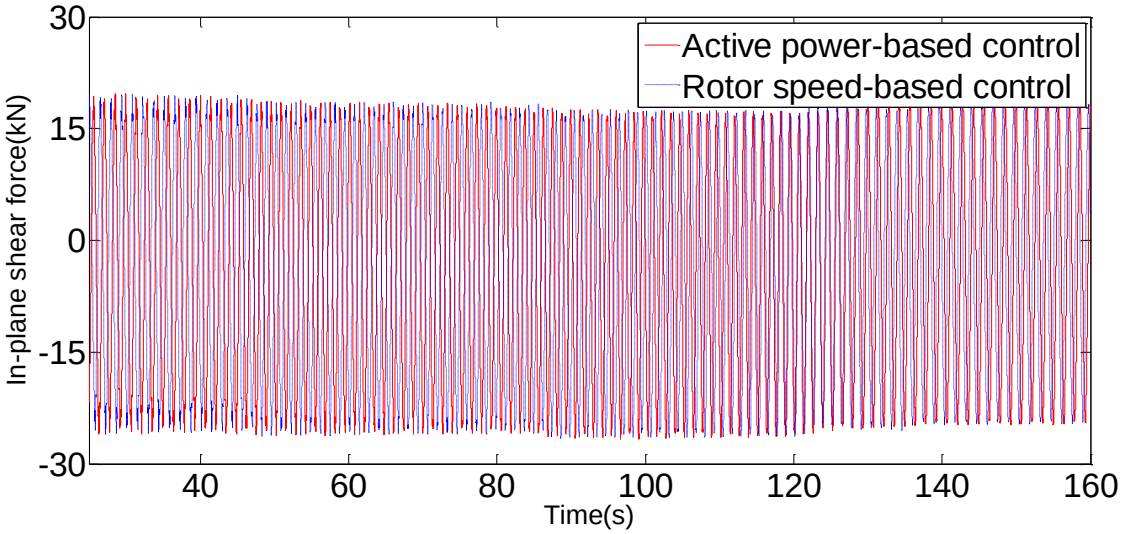

(b) Blade 1 in-plane shear force at the blade root

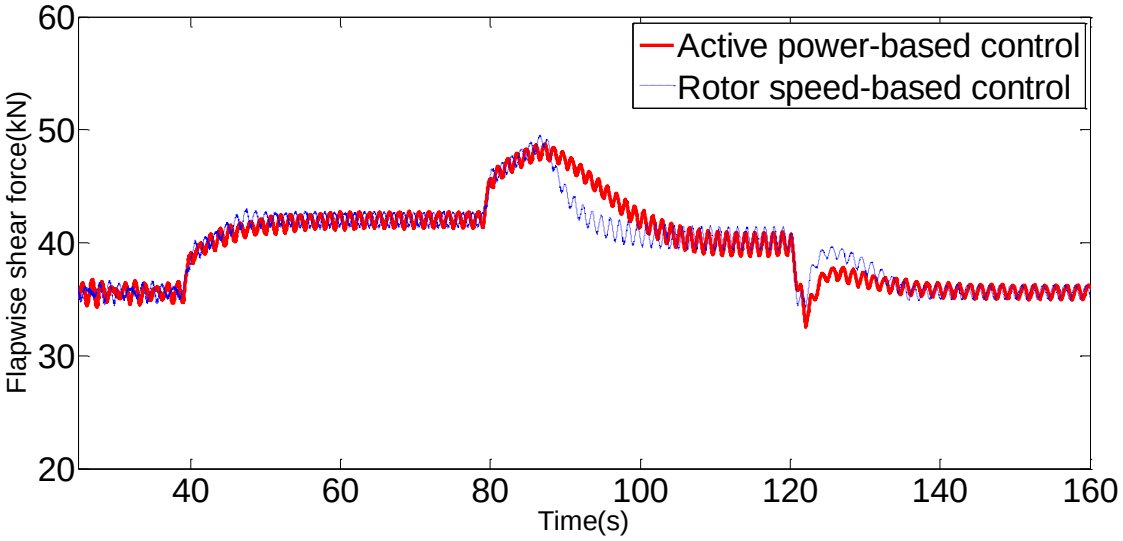

(c) Blade 1 flap-wise shear force at the blade root

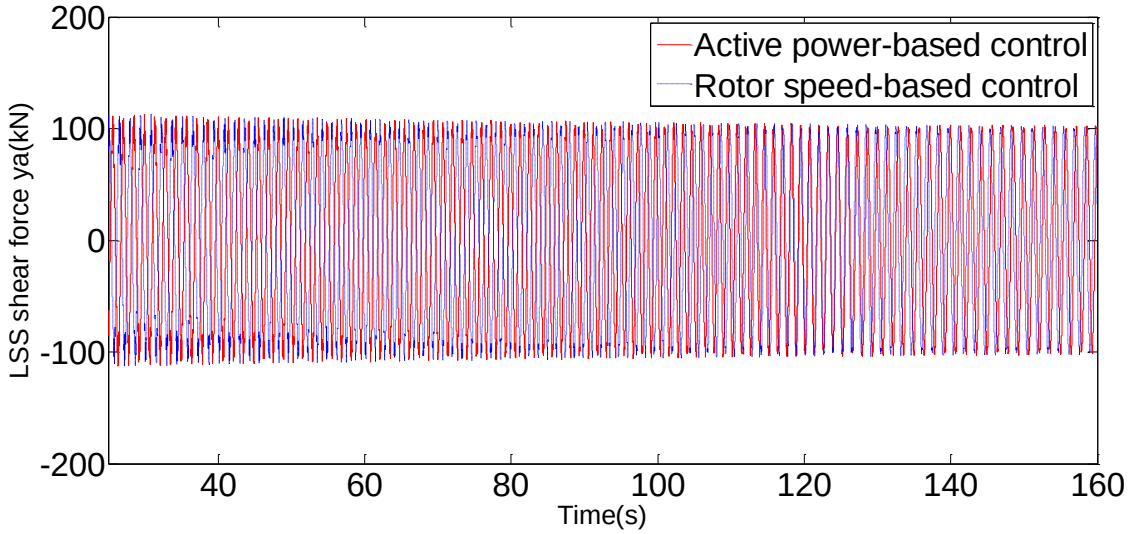

(d) Rotating low-speed shaft shear force (This is constant along the shaft and directed along the ya-axis)

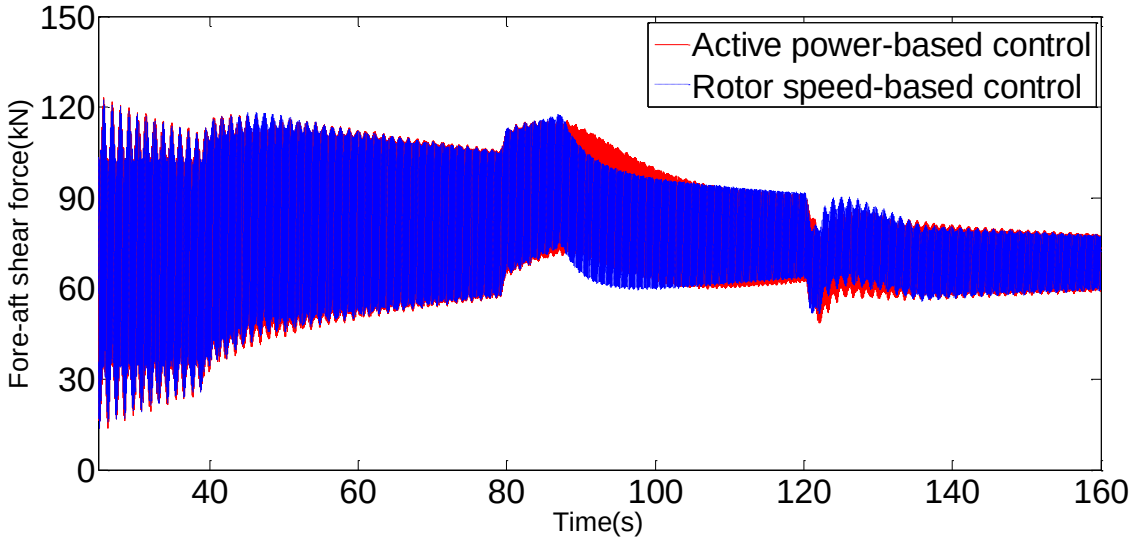

(e) Tower base fore-aft shear force (Directed along the xt-axis)

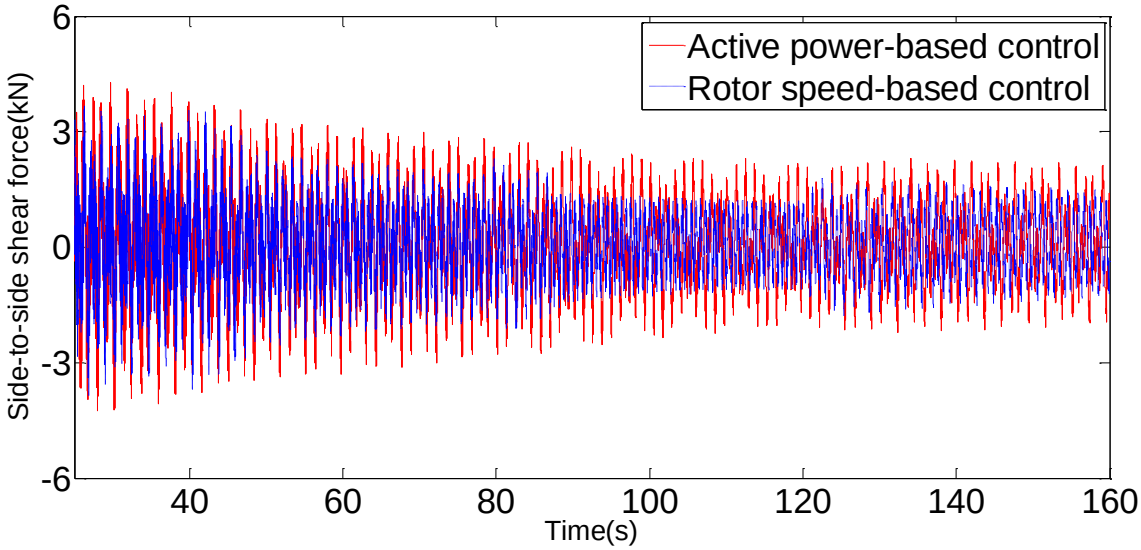

(f) Tower base side-to-side shear force

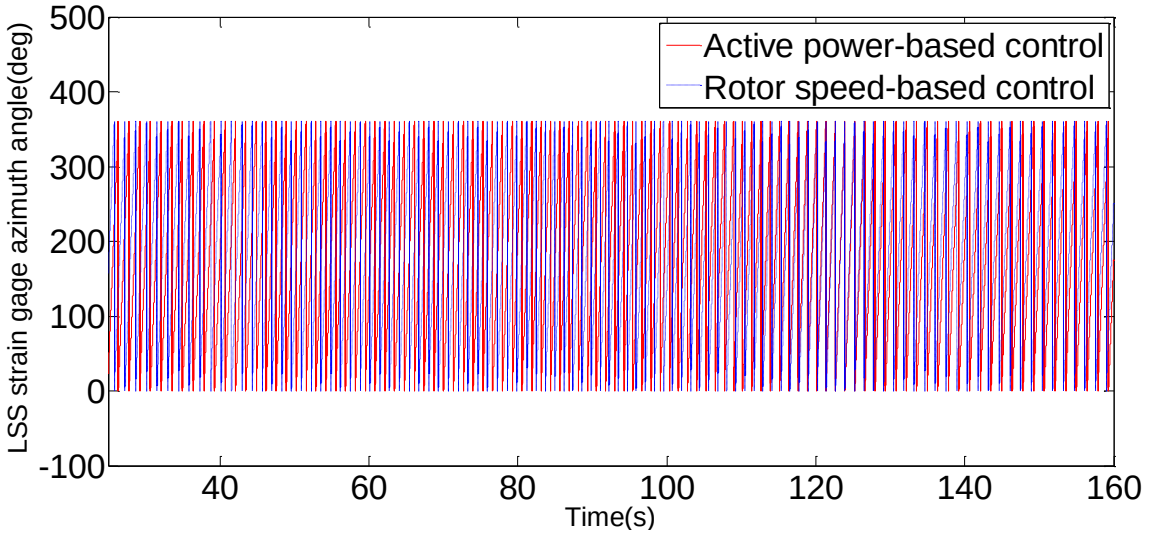

(g) Low-speed shaft strain gage azimuth angle

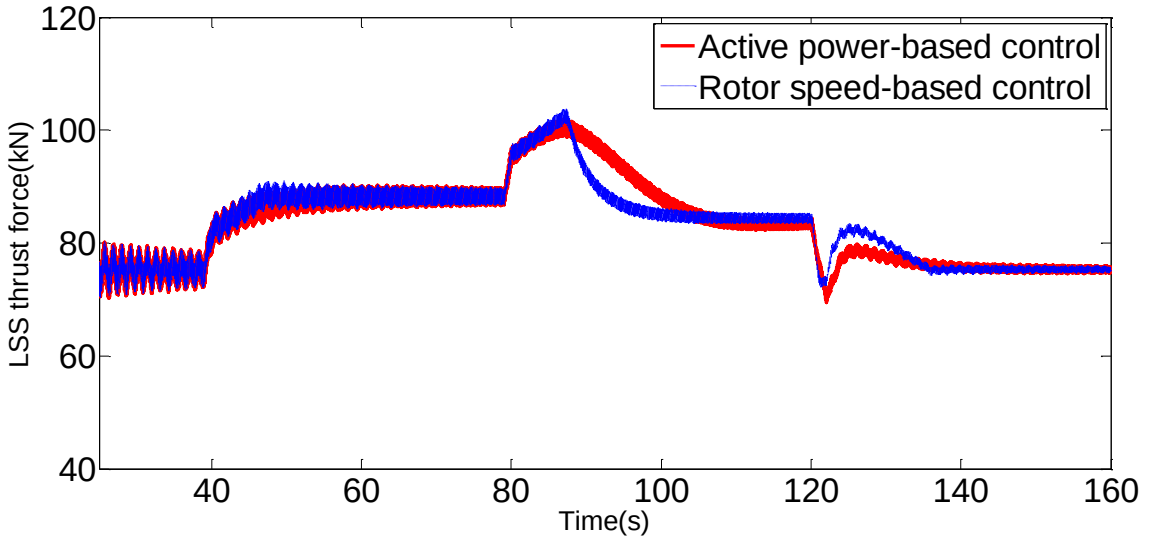

(h) Low speed shaft thrust force/rotor thrust force

Figure 3.9 Simulation results for FAST-based CART2 model under step-wise wind speed conditions

As the wind speed changes, it is noted that significant variations occur in the blade 1 out-of-plane shear force at the blade root, blade 1 flap-wise shear force at the blade root, the tower base fore-aft shear force and low speed shaft thrust force. As wind speed rises at every interval, these shear forces will increase correspondingly due to the increased rotor speed, and vice versa. For other shear forces including rotating low-speed

shaft shear force and Blade 1 in-plane shear force at the blade root, no significant variations can be observed. The low-speed shaft strain gage azimuth angle remains the almost same during the variable wind speeds and shows no difference between two control methods as well. However, there is a smaller oscillation on the tower base side-to-side shear force when rotor speed-based control is used.

Case 2. Dynamic response of CART2-PMSG model under the real wind speeds

1) Simulation Results from PMSG Simulink model

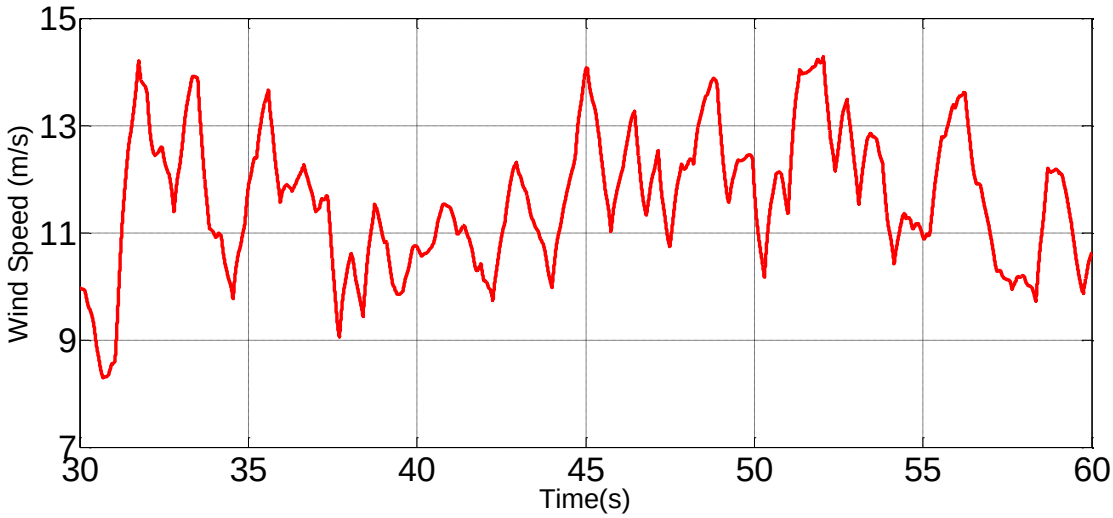

(a) Wind speed

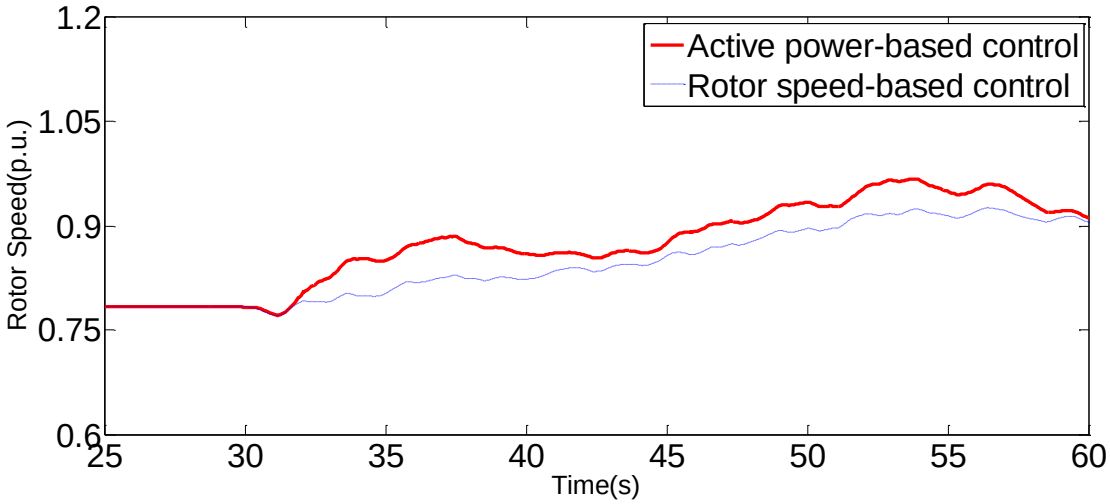

(b) Generator rotor speed

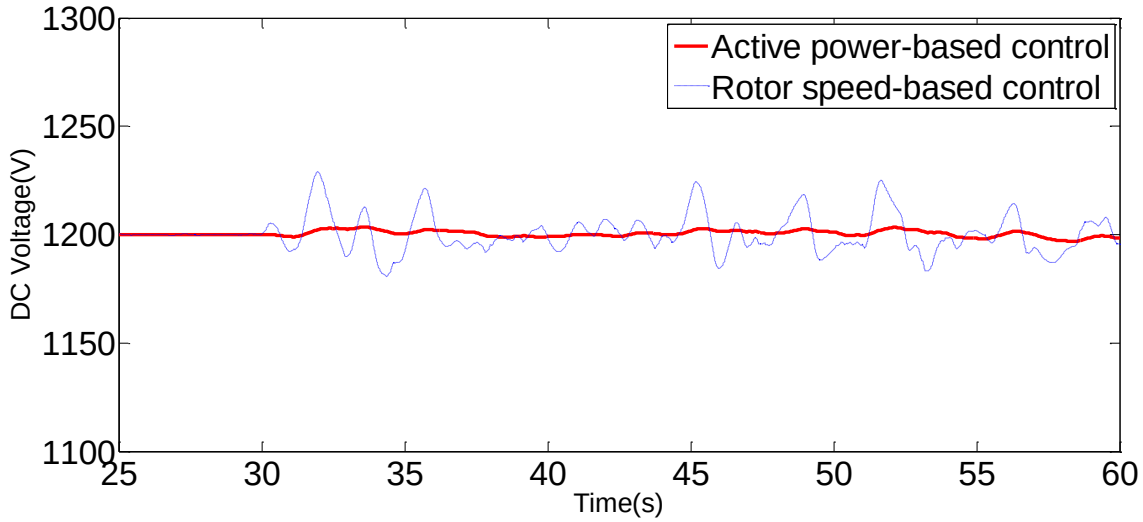

(c) DC-link voltage

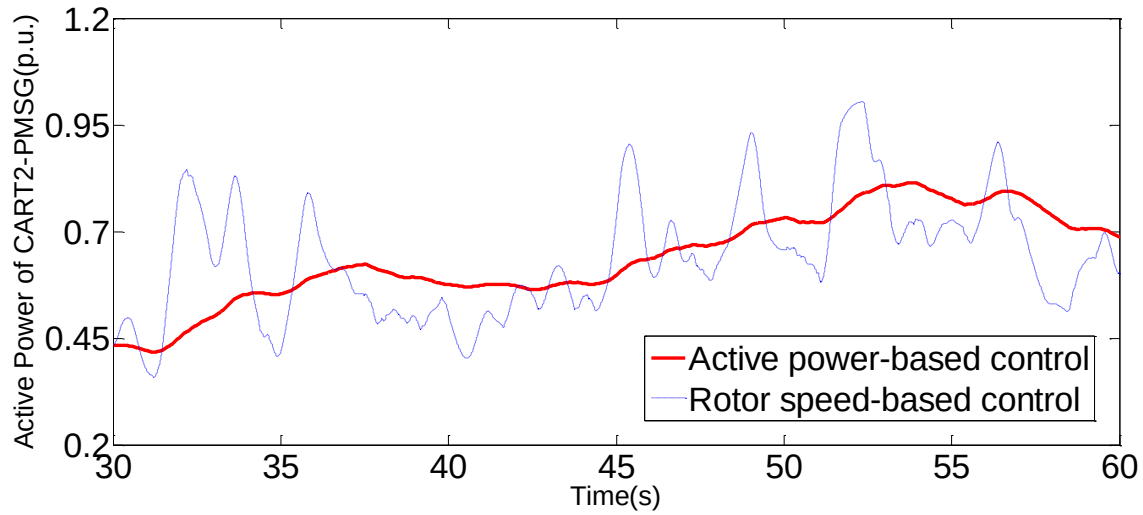

(d) Active power output

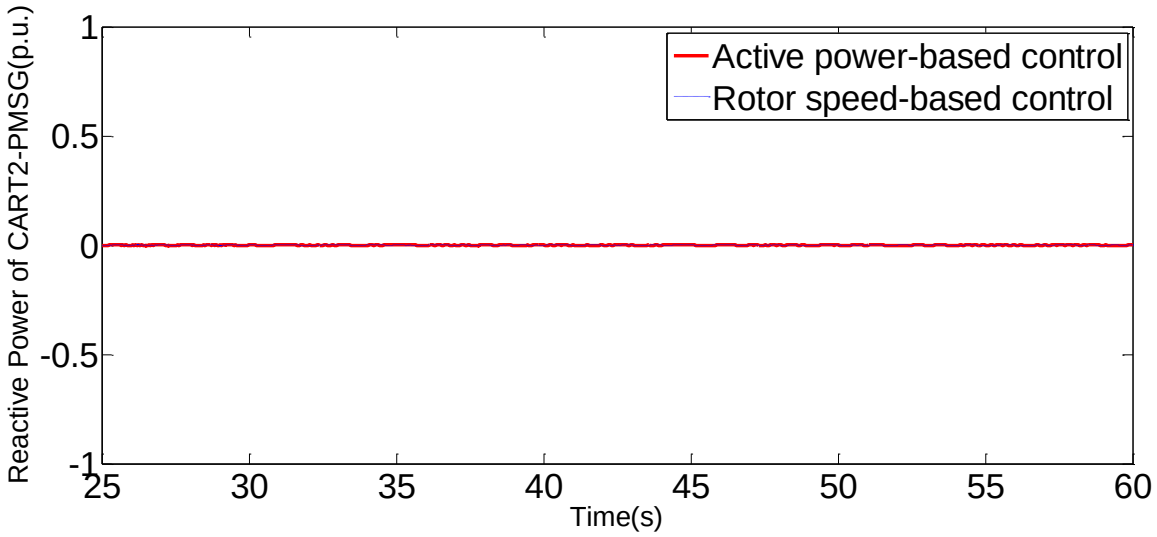

(e) Reactive power output

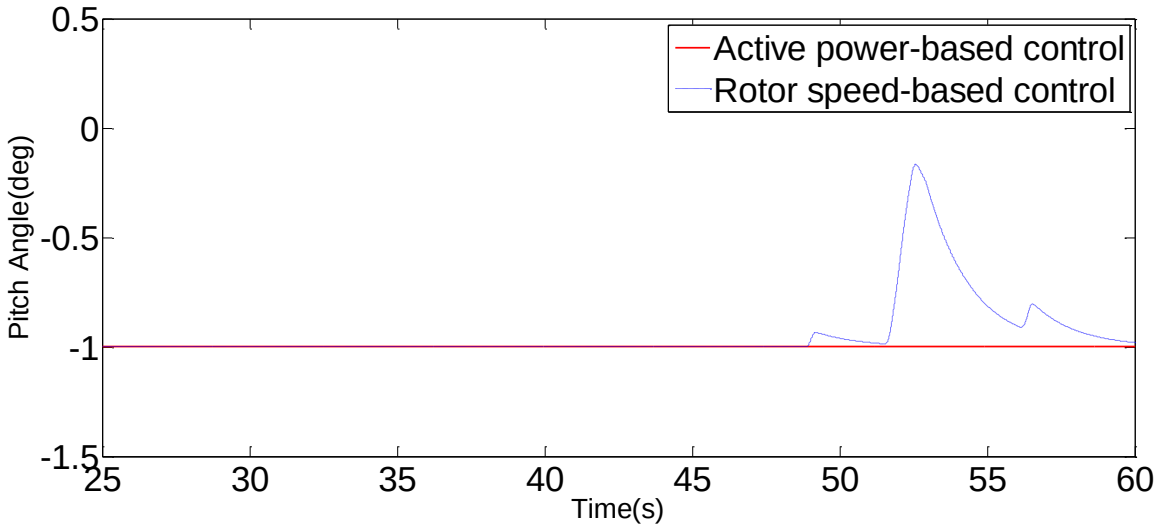

(f) Pitch angle

Figure 3.10 Simulation results for the PMSG model under realistic wind speed conditions

As shown in Figure 3.10, wind speed changes abruptly around the average value of 11 m/s with about 3m/s amplitude of variation (Note: The wind profile is created artificially based on the actual wind speed variations). In this case, rotor speed-based control and active power-based control show different characteristics in terms of rotor speed and active power output, but changing trends seem quite similar for each other. It is shown that the generator rotor speed controlled by active power-based control varies

within the range of 20% of the rated value because of the large inertia of CART2. In contrast, the generator rotor speed adjusted by rotor speed-based control changes within the range of 15% due to the rotor speed upper and lower limit applied.. During the wind speed variation above the 12.718/s (rated value), active power can be well regulated around 0.9 p.u (generator capacity is selected as base value) thanks to the pitch angle control system with which rotor speed-based control is coordinated. However, it cannot be promptly controlled below 0.9 p.u. due to the sluggish mechanical response of pitch angle actuator in the presence of highly rapid wind speeds. For both rotor-side converter control, the DC link voltage is maintained constant at 1200V without obvious oscillation caused by the strong changes in wind speed. With continuous changes in wind speeds, the active power generated through the active power based control has a mean value of 0.537 p.u. over this time period, while the counterpart through rotor speed based control shows a mean value of 0.5353 p.u. during the same period. At the same time, the reactive power generated with both rotor-side converter control remains as zero. The pitch angle of WT is dynamically regulated via pitch mechanism in conjunction with rotor-side converter in limiting the rotor speed or active power output below the rated value. Therefore, the established PMSG-WTG model is demonstrated once again to be effective in realizing the independent real and reactive power decoupling control using a fully decoupled current control strategy in the synchronously rotating d-q frame.

2) Simulation Results from FAST model

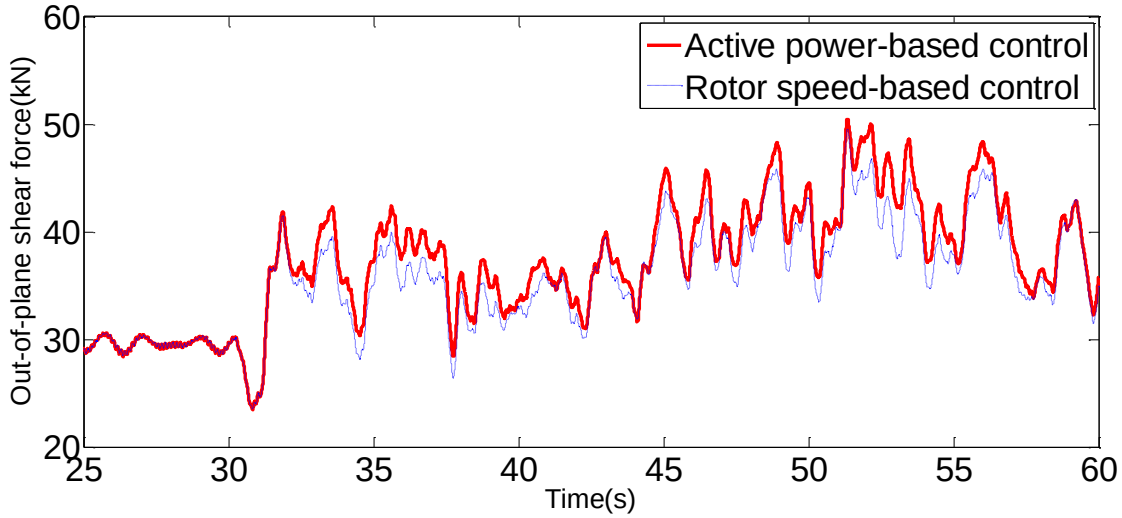

(a) Blade 1 out-of-plane shear force at the blade root

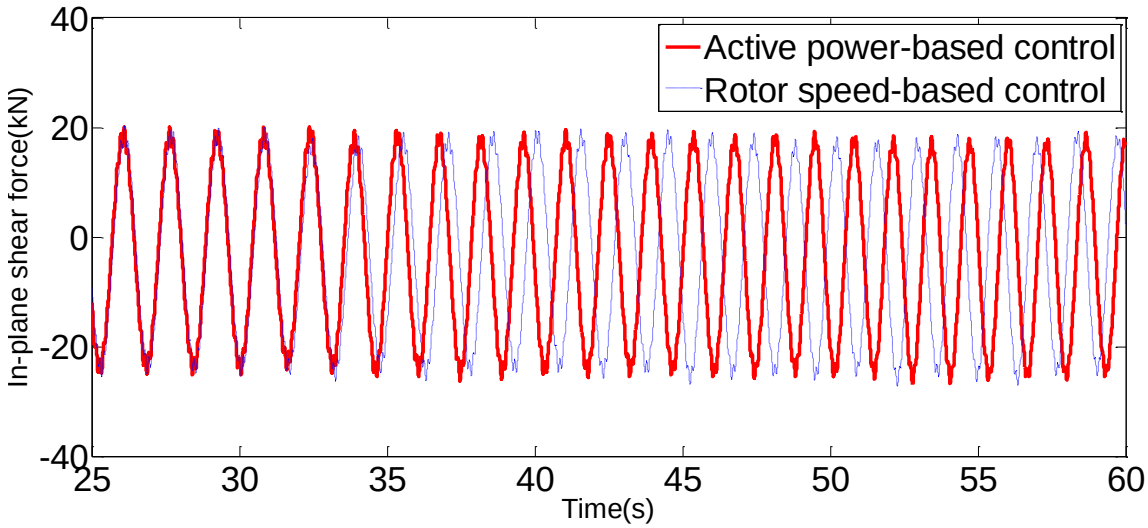

(b) Blade 1 in-plane shear force at the blade root

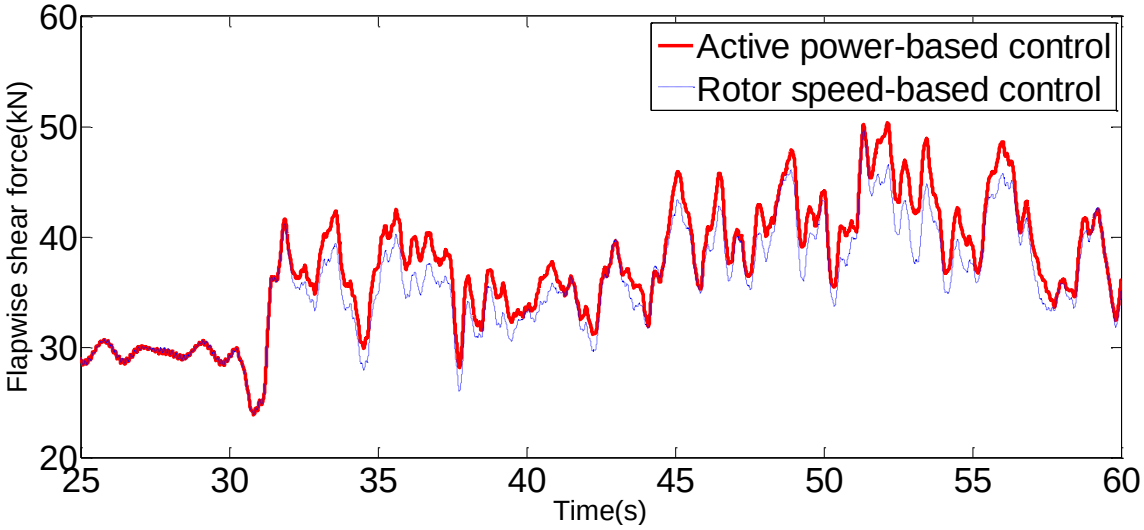

(c) Blade 1 flap-wise shear force at the blade root

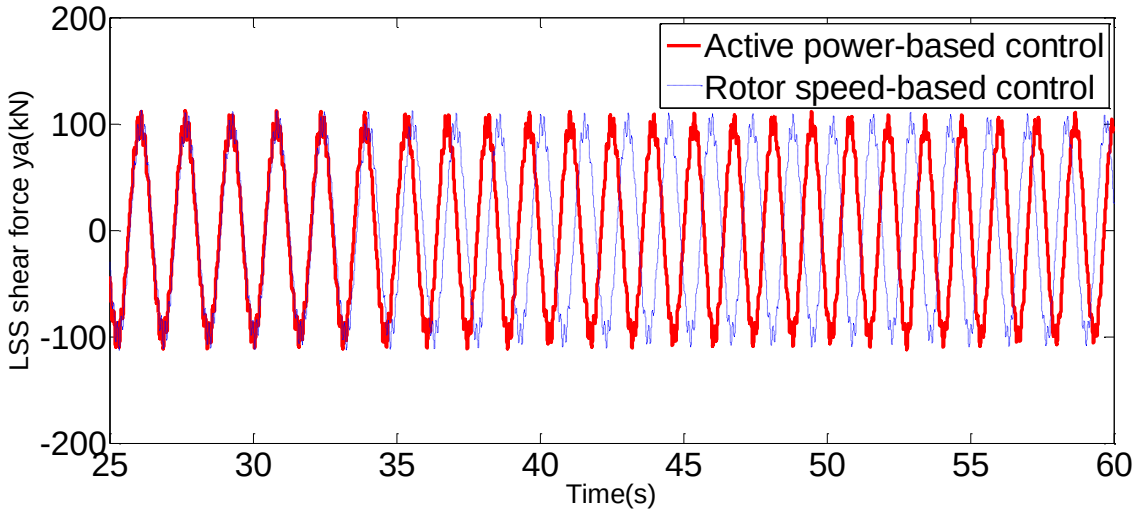

(d) Rotating low-speed shaft shear force (This is constant along the shaft)

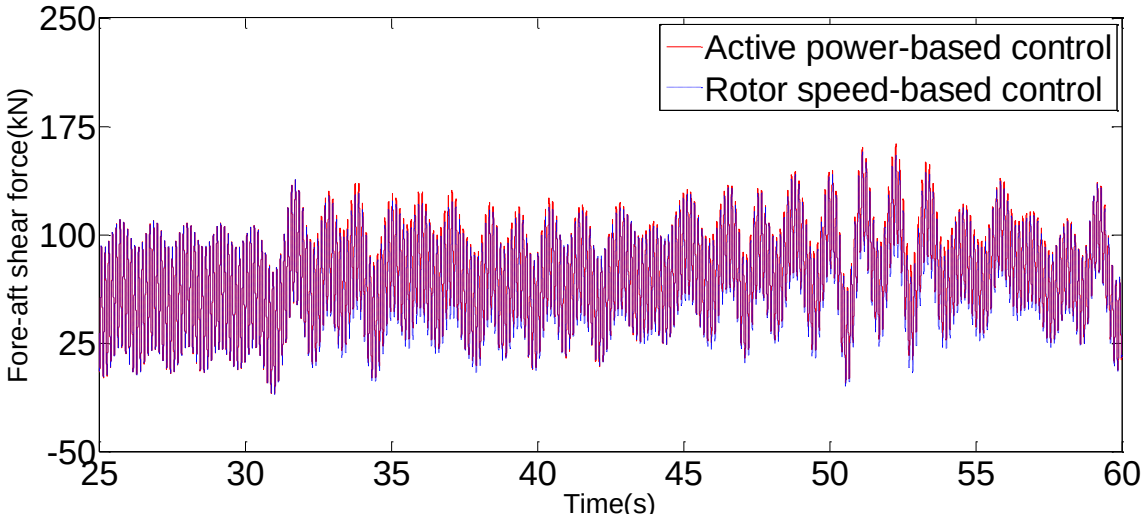

(e) Tower base fore-aft shear force (Directed along the xt-axis)

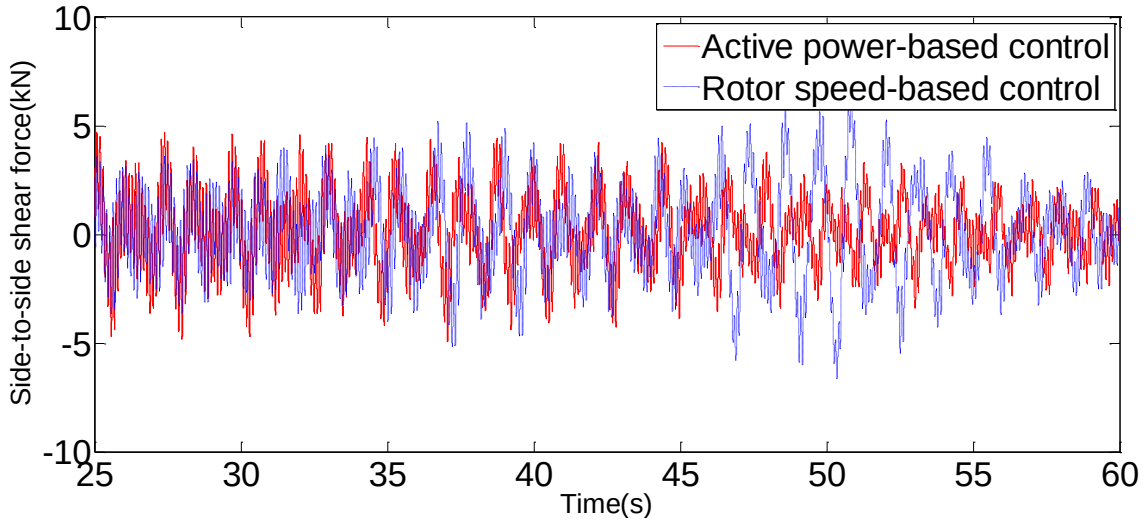

(f) Tower base side-to-side shear force

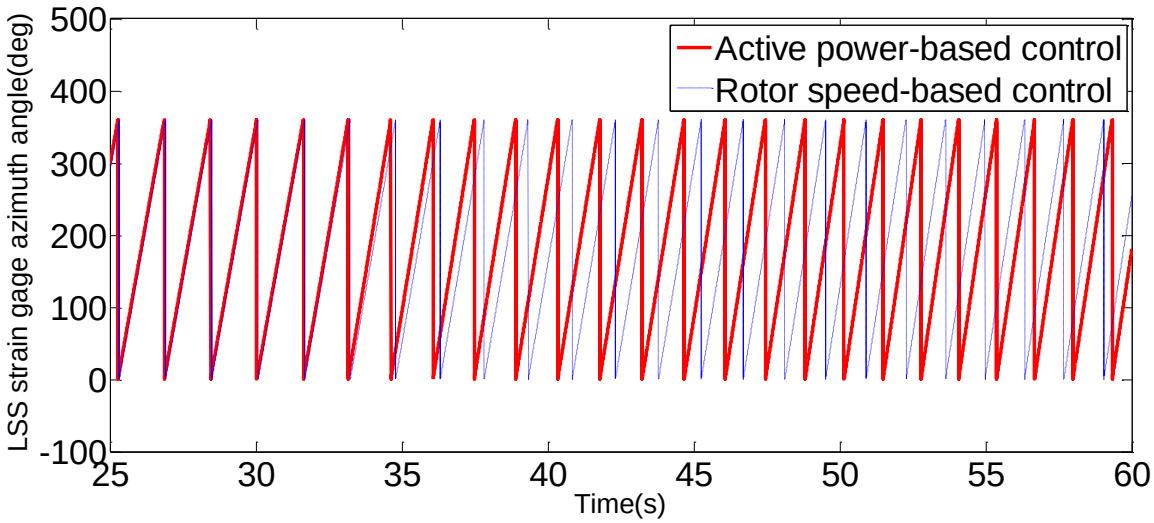

(g) Low-speed shaft strain gage azimuth angle

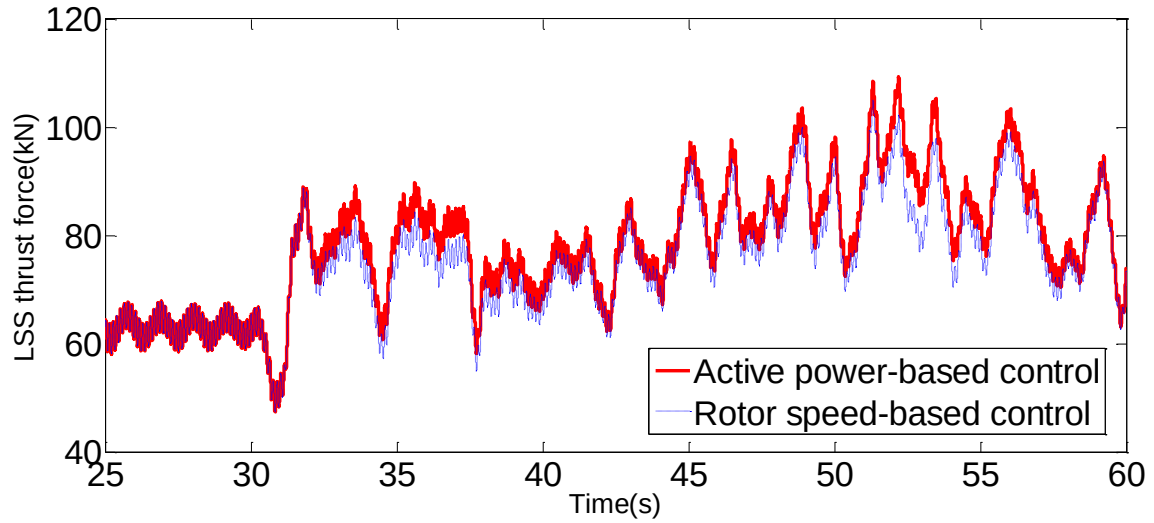

(h) Low speed shaft thrust force/rotor thrust force

Figure 3.11 Simulation results for FAST-based CART2 model under realistic wind speed conditions

As the wind speed changes, significant variations occur in the blade 1 out-of-plane shear force at the blade root, blade 1 flap-wise shear force at the blade root, the tower base fore-aft shear force and low speed shaft thrust force. At the same time, it is worth noting that these shear forces for active power-based control tend to be slightly larger than those for rotor speed-based control. That is due to the fact that its rotor speed

is always smaller than that managed by the active power-based control throughout the variable wind speed conditions. As rotor speed suddenly rises up as a result of increased wind speed, these shear forces will rise correspondingly, and vice versa. Due to the large inertia in wind turbine, the changes in these shear forces tend to become smoother. For other shear forces including rotating low-speed shaft shear force and Blade 1 in-plane shear force at the blade root, no dramatic variations show up in the process of these drastic wind speed variations. Note that the vibrations in those shear forces associated with tower base appear to be much larger once the pitch angle is activated with respect to rotor speed-based control.

3.5 Conclusion

Based on the simulation results of above cases, it can be concluded that the established CART2-PMSG integral model with two different control strategies applied can accurately represent the actual steady-state and dynamic characteristics in terms of both mechanical and electrical aspects. Thus, it can serve as a reliable platform to carry out the design and analysis with respect to the auxiliary frequency regulation control for PMSG-WTG.

Chapter 4 A Comprehensive Frequency Regulation Scheme for PMSG-WTG with pre-deloaded operation

In this work, a novel comprehensive frequency regulation (CFR) scheme is proposed for PMSG-WTGs based on rotor speed control by combining rotor speed control with modified pitch angle control. Constant inertial power control emulates the inertial response using the kinetic energy stored in the rotating mass so as to achieve a short-term frequency support. The rotor speed and pitch angle controls are coordinated to curtail the wind power output for maintaining a certain reserve margin during the de-loaded operation, but also prepared to fulfill the long-term frequency regulation through variable slope droop control during severe frequency event. Furthermore, this CFR control strategy is integrated into the CART2-PMSG model so as to investigate the potential impact on the wind turbine's structural loads when CFR is implemented. From simulation results considering three different types of wind speed scenarios, the proposed CFR can dramatically enhance the frequency regulation capability of PMSG-WTG and well damp the frequency oscillation over a full range of wind speed conditions. Meanwhile, no significant negative impact is imposed on the major mechanical components of wind turbine .

4.1 Coordinated Frequency Controller Design for PMSG-WTG System

In Figure 4.1, the general control structure of a single PMSG-WTG equipped with the proposed CFR control is illustrated. The constant inertial control and droop control are added into the rotor-speed controller to generate the rotor speed reference for the generator-side controller through which the frequency regulation function is enabled. Under the normal grid operation, the rotor-speed controller regulates the rotor speed so that the PMSG-WTG is able to operate in the de-loaded mode regardless of wind speed conditions. At this moment, both Switch 1 and Switch 2 remain in 0 mode.

Based on the measured wind speed and monitored grid frequency at the point of interconnection, the coordinated frequency controller can carry out the specific frequency control strategy where sub-controllers are coordinated to execute the inertial response and frequency regulation when severe frequency disturbance occurs. If a large frequency drop is detected through the coordinated frequency controller, the sub-controller I changes Switch 2 mode from 0 to 1. Once the inertial response is completed, sub-controller I returns Switch 2 mode from 1 to 0 and meanwhile the sub-controller II mode changes the Switch 1 mode from 0 to 1. Since then, the droop controller and de-loaded controller function together to generate a new rotor-speed reference for the primary frequency regulation. In the medium and high wind speed conditions, sub-controller III aims to coordinate the modified pitch angle controller with rotor speed controller for inertial response and frequency regulation. However, in the low wind speed, it serves to maintain the pitch angle fixed at -1 degree. By this means, the frequency

change is linked with the rotational speed variation so as to fulfill the PMSG-WTG's frequency regulation function.

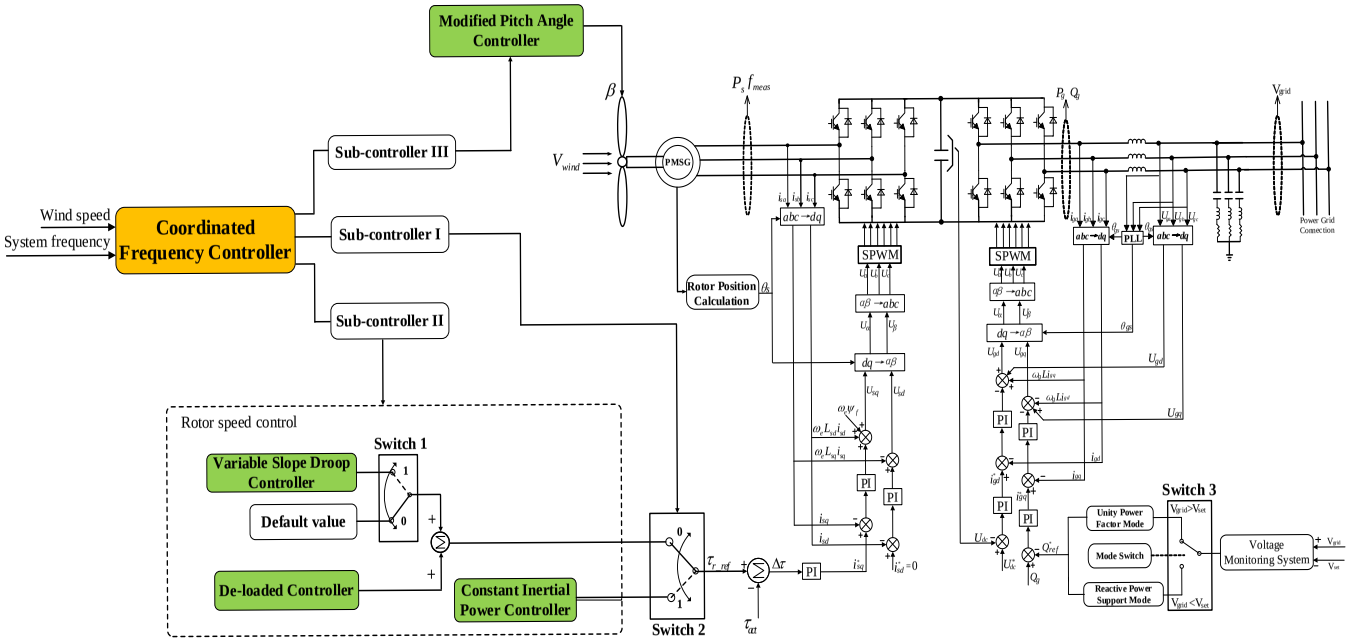

Figure 4.1 Overall control configuration of a typical PMSG-WTG system equipped with the CFR

4.1.1 Rotor Speed Control

a. Constant inertial power control

Using inertial controller, a portion of rotor kinetic energy is quickly delivered to the grid through power converter. The main purpose of this control is to mitigate the rate of change of frequency (ROCOF) and arrest the frequency nadir during the initial few seconds of the frequency event [16]. Until now, there are three main types of inertial control methods including natural inertial, constant inertial and virtual inertial response [4],[42],[79]. In this study, the constant inertial power response is employed since it is more suitable for PMSG-WTG based on the rotor speed control to achieve the controllable and fast inertial response by directly adjusting the rotor speed.

As for constant inertial power control, the inertia refers to a constant amount of active power extracted from WT's kinetic energy in the rotating mass, which is utilized to improve the system frequency performance for a specified duration [4]. The equation for constant inertial power is defined as

$$P_{in}t = \frac{1}{2}J\omega_{r0}^2 - \frac{1}{2}J\omega_{rt}^2 \tag{4.1}$$

where, t is the duration of time for the constant inertial power injection (s), ω_{r0} is the initial rotor rotational speed (rad/s) and ω_{rt} is the rotor rotational speed (rad/s) at the moment t. So, the reference value for rotor rotational speed is given by:

$$\omega_{ref} = \omega_{rt} = \sqrt{\omega_{r0}^2 - 2\frac{P_{in}}{J}t} \tag{4.2}$$

By defining $\omega_{p.u.} = \frac{\omega}{\omega_{base}}$ as per-unit rotor speed and $P_{in\_pu} = \frac{P_{in}}{S_{base}}$ as per-unit inertial power output (S_{base} is the nominal apparent power of PMSG-WTG), the total

moment of inertia of the rotating masses $J = \frac{2HS}{\omega_{base}^2}$ is substituted into (4.2) so that the per-unit rotor speed reference is expressed as

$$\omega_{rt\_pu} = \sqrt{\omega_{ro\_pu}^2 - \frac{P_{in\_pu}}{H} t} \tag{4.3}$$

The constant inertial power response mainly aims to reduce the ROCOF by providing a continuous and steady amount of extra active power P_{in_pu} for a required period of time t. In general, the desired duration t and power magnitude P_{in_pu} are largely dependent on the disturbance magnitude and current grid operation condition [79]. In this paper, the appropriate duration of inertial response alone is determined as 3s through trial and error method. According the equation below, P_{in_pu} is set as 20% of the current deloaded power output and emulated H time constant is set to 7.118s according to Table 3.1.

$$P_{in\_pu} = 0.2 \times P_{de\_pu} \tag{4.4}$$

It is assumed that inertial response is still available in the high wind speed condition due to transient overloading capacity of power converter. The block diagram of constant inertial power control is shown in Figure 4.2. According to Eq.(4.3) and Eq.(4.4), rotor speed reference ω_{ref} is calculated and then error between ω_{ref} and measured $\omega_{r,meas}$ passes through PI controller to generate the direct-axis current reference that controls the active power output.

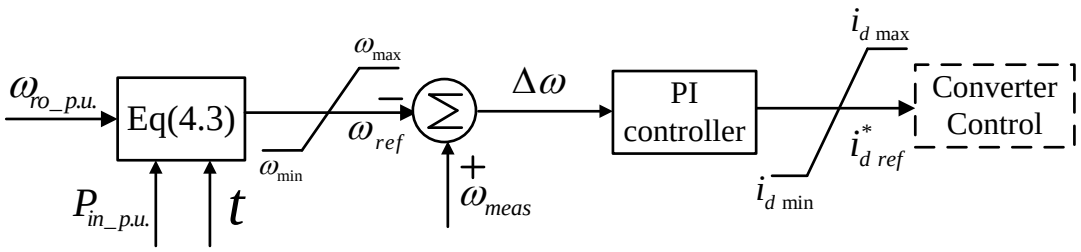

Figure 4.2 Control block diagram of constant inertia response

b. De-loaded operation

In order for PMSG-WTG to participate in the primary frequency regulation, a certain amount of spinning power reserve needs to be made in the acceptable range of wind speed conditions.

According to the power reserve requested from system operator, the primary power reserve is carried out through either “balance” or “delta” control method [40]. In this paper, delta control is adopted based on MPPT strategy so as to allow PMSG-WTG for the de-loaded operation with a fixed percentage of available aerodynamic power. In view of upper rotor speed limit, PMSG-WTG operation is classified into low, medium and high wind speed modes. Regardless of wind speed, the rotor speed reference is obtained from the de-loaded operation curve, which is established through the de-loaded algorithm and implemented by the look-up table in the Simulink simulation.

In Figure 4.3, the left and right de-loaded operation curves are depicted in terms of high, medium and low wind speed regions. Compared with the active-power-oriented control, one of greatest strengths of the rotor-speed-oriented control is to allow PMSG to steadily operate either in the left de-loaded or right de-loaded manner [3]-[4],[14]. With the typical PI controller used, the rotor speed of PMSG can be well controlled to remain stable at the specified rotor speed. In this work, the right de-loaded mode is implemented

since more kinetic energy is available to enhance the constant inertial power response due to its over-rotor-speed condition. Over-rotor-speed condition refers to the scenario that the VSWT remains in the deloaded operation with the rotor speed higher than the corresponding optimal rotor speed under the same wind speed [4], which is represented by dotted line in Figure 4.3.

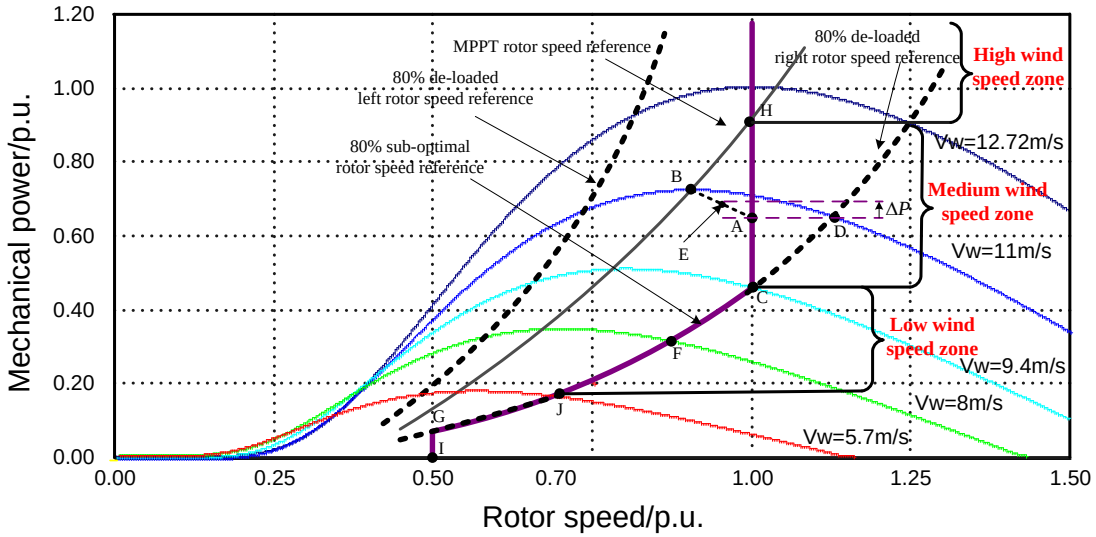

Figure 4.3 80% de-loaded operation curve with the rotor speed limitation (0.5 p.u.-1.0 p.u.) over a full scope of wind speeds

c. Variable slope droop control

Similar to the turbine governor characteristic of traditional synchronous generator, the droop control of PMSG-WTG utilizes the primary reserve power to generate the additional active power as a function of frequency deviation. So, PMSG-WTG is able to coordinate with other synchronous generators to share the load variation. Unlike the inertia control without requiring the deloaded operation, the droop control is dependent on the reserve margin in order to raise up the frequency nadir and minimize the post-disturbance steady-state frequency deviation toward the acceptable range [16]. The extra active power through the droop control is defined as

$$\Delta P_{dr\_pu} = P_{act} - P_0 = -\frac{f_{act} - f_{ref}}{R} \quad (4.5)$$

Where, f_{act} is the actual system frequency [p.u.] and f_{ref} is nominal system frequency [p.u.], R is the rotor speed adjustment rate [%]. P_{act} is the actual active power output [p.u.] corresponding to f_{act} and P_0 is the initial power corresponding to f_{ref}. The value of R usually lies in the range between 3% and 6%, depending on the specified grid codes of different countries [84]. ΔP_{dr_pu} represents the active power change [p.u.] through the droop control. As shown in Figure 4.4, a high pass filter is employed to ensure that small frequency deviation cannot inherently impact the whole control system. Meanwhile, a deadband module is added so that this droop function is activated only through the severe frequency event.

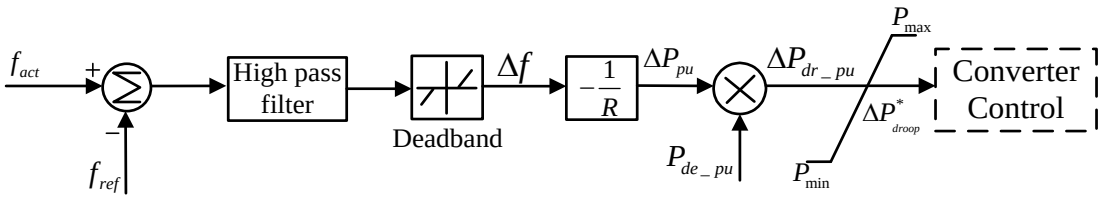

Figure 4.4 Control block diagram of droop response

Considering that reserve power changes throughout the entire frequency regulation, PMSG-WTG operating with higher reserve power is able to deliver more active power that contributes to a stronger droop response than case with lower reserve power. For this reason, the variable droop response is designed to optimize the primary droop response by setting R value inversely proportional to the reserve power margin as shown in Figure 4.5 [66]. Using this method, the hazards leading to WTG's operation instability and excessive mechanical stress on the drive train can be mitigated since

power utilized for the primary frequency support is not allowed to exceed the current reserve margin.

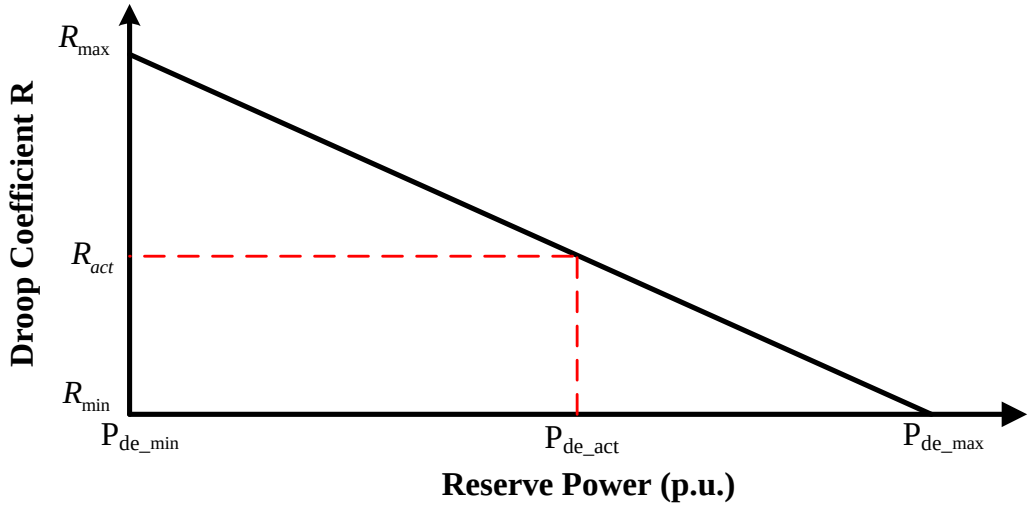

Figure 4.5 The variable slope droop curve versus the reserve power

The value of R_{act} for any specific wind speed is calculated as follows:

$$R_{act} = R_{max} - (R_{max} - R_{min}) \cdot \left[\frac{P_{de\_act} - P_{de\_min}}{P_{de\_max} - P_{de\_min}}\right] \quad (4.6)$$

where, P_{de_act} is the actual power margin [p.u.] corresponding to R_{act} for a specific wind speed. It is obtained from:

$$P_{de\_act} = P_{MPPT} - P_{act} \quad (4.7)$$

where, P_{MPPT} is the maximum wind power output corresponding to the present wind speed [p.u.]. P_{act} is the actual wind power output [p.u.]. In Eq. (4.4-4.6), R_{max} is chosen as 6% and R_{min} is 2% respectively. The maximum margin P_{de_max} is 20 percentage of P_{MPPT} and minimum margin P_{de_min} is 0 percentage of P_{MPPT}, which corresponds to R_{min} and R_{max} respectively.

4.1.2 Modified Pitch Angle Control

A modified pitch angle controller is designed to coordinate pitch angle with rotor speed for the primary frequency regulation in accordance with various wind speed conditions.

As shown in Figure 4.6, variable pitch servo system is represented with a first-order module. S1 is used to pass the pitch angle reference according to different wind speed modes. S2 is applied to maintain the pitch angle control disabled in the low wind speed mode when S2 is set as 0, or conduct the inertial response and droop control in medium or high wind speed mode when S2 is set as 1. Note that the power reference is ΔP_{dr_pu} in the medium wind speed while the power reference is $\Delta P_{dr\_pu} + \Delta P_{inert\_pu}$ in the high wind speed. That is because inertial response in the medium wind speed is a short-term frequency response that can be completely achieved by rotor speed deceleration and acceleration control of the rotor side converter. In contrast, pitch angle is required to perform the inertial response in the high wind speed since the rotor speed remains fixed at around 1.0 p.u. Using this modified control method, the dynamic power balance between the mechanical power input and electrical power output of PMSG is made when performing the proposed comprehensive frequency regulation.

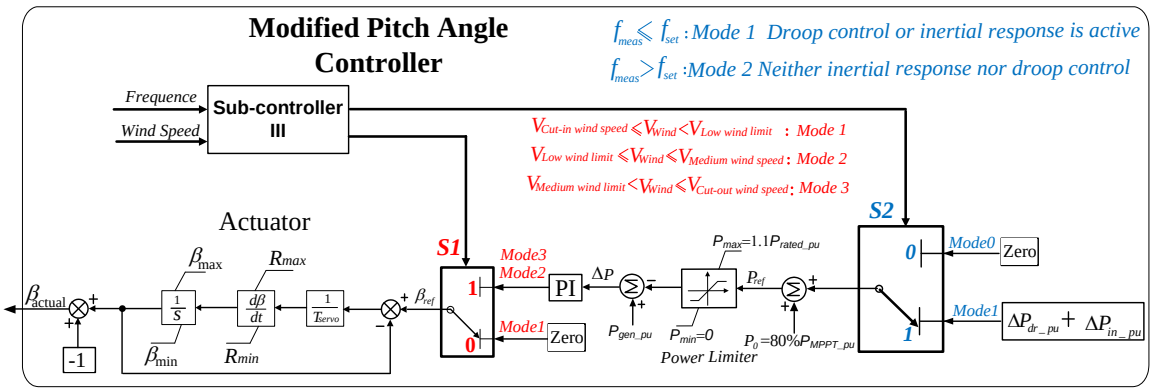

Figure 4.6 Schematic of modified pitch angle controller

4.2 Comprehensive Frequency Control Scheme

From the perspective of operation security, the comprehensive frequency regulation of PMSG-WTG can fit into a wide range of wind speeds. The value of ω resulting from the de-loaded operation in between medium and high wind speeds exceeds the maximum rotor speed limit ω_{max} (1.0 p.u.). Thus, in order to facilitate the proposed scheme with the predefined deloaded margin, three types of wind speed modes are defined: Low wind speed mode where the de-loaded operation and frequency regulation is fulfilled only by rotor speed control; medium wind speed mode where a coordinated frequency regulation is achieved through both modified pitch angle control and rotor speed control; high wind speed mode where modified pitch angle control alone is used for the de-loaded operation and frequency regulation. As shown in Figure 4.3, 80% de-loaded operation is achieved when the generator rotation speed moves along the purple solid line GCH under differing wind speeds.

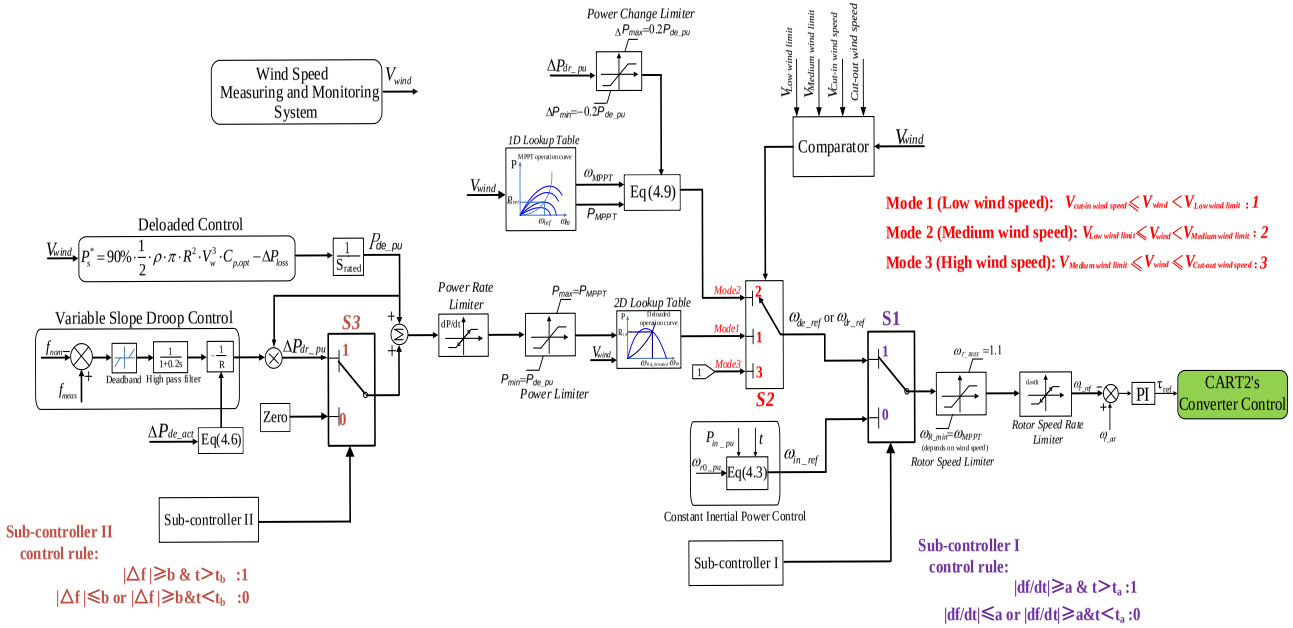

Figure 4.7 Schematic of comprehensive frequency regulation controller at the rotor-side converter

(1) Mode 1: in the low wind speed range from cut-in speed to 9.4 m/s, the rotor over speed control can realize the 80% de-loaded operation without pitch angle control involved. The active power output for inertial response and frequency regulation is regulated only by rotor speed controller as well. The rotor speed reference ω_{ref} is obtained in Figure 4.3 by tracking the line segment G-F-C. Meanwhile, the pitch angle controller is deactivated by setting the pitch angle reference as zero in Figure 4.6. For instance, if frequency abruptly drops, the rotor speed control will inject a constant-wise inertial power into grid through the rotor speed deceleration. Next, the droop control will kick in once frequency deviation goes beyond the safety limit. The operating point moves towards the MPPT curve corresponding to the current wind speed. If rotor speed continues to decline through the inertial response and hit the lower rotor speed limit (0.5 p.u.), it will be locked on to this value with the inertial control suspended. In this case, PMSG-WTG only afford the limited frequency regulation due to its minimum rotor speed constrain.

(2) Mode 2: in the medium wind speed range from 9.4 m/s to rated wind speed (12.718m/s), extra active power for frequency support require a coordinated control between rotor speed and pitch angle controller. That is because that rotor-speed controller alone is unable to maintain 80% de-loaded operation due to the upper rotor speed limit (1.0 p.u.) as indicated in the line C-A-H. The rotor speed control combined with pitch angle control is illustrated in Figure 4.6 and Figure 4.7. Assuming that initial wind speed is 11m/s in Figure 4.3, the rotor speed remains at Point A through the modified pitch angle controller by setting S1 to 1. The final steady-state operating point E is dependent

on the primary droop control in accordance with the dashed straight line A-B. The rotor speed reference value ω_{ref} will change from 1.0 p.u. to ω_E, which is calculated by the linear interpolation method as follows [16].

$$\frac{\omega_E-\omega_A}{\omega_B-\omega_A}=\frac{P_E-P_A}{P_B-P_A} \tag{4.8}$$

Where, ω_B is the optimal rotor speed on the MPPT curve [p.u.]. P_B is the optimal active power [p.u.]. P_A is equal to 80% of optimal active power [pu]. So, if there is an increase $\Delta P = \Delta P_{dr\_pu}$ on top of the active power output P_{de_pu}, the total power output P_E corrresponding to operating point E will be $P_E = P_A + \Delta P = 0.8P_{MPPT} + \Delta P$ with $\omega_A = 1.0\ \text{p. u.}$ The rotor speed reference ω_{ref} for generator-side converter is expressed as

$$\omega_{ref} = \omega_E = 1.0 + \frac{\Delta P}{0.2P_{MPPT}}(\omega_{MPPT} - 1.0) \tag{4.9}$$

All the variables in Eq. (4.4-4.9) are measured in per unit. Using this method, combined rotor speed and pitch angle controller is capable of operating wind turbine at the deloaded operation and meanwhile participate in the constant inertial power response and primary frequency regulation under the medium wind speed.

(3) Mode 3: in the high wind speed range from rated wind speed to cut-out speed, only pitch angle control is responsible for maintaining 80% de-loaded operation as well as implementing the variable droop and inertial response in the frequency event.

From the perspective of response time, the proposed comprehensive frequency control strategy is implemented through the following two stages in case that system frequency abruptly declines due to a heavy load increase or a large-capacity generator trip. At the initial state, once the absolute value of ROCOF is larger than "a" (e.g.0.8Hz/s) in Figure 4.7. for at least delay period time "t_a" (e.g.100ms), inertial control comes into a

play. As shown in Figure 4.7, the sub-controller I will switch the S1 from normal deloaded mode 1 to constant inertial power control mode 0 while S3 remains in the default mode 0. Then the new rotor speed reference is generated for PMSG-WTG generator-side converter to perform the constant inertial power response. This process assists in arresting the initial ROCOF to prevent the triggering of under frequency load shedding (UFLS) relay protection. (2) Primary frequency regulation will be activated to take over the subsequent frequency regulation when the absolute value of frequency deviation exceeds deadband threshold "b" (e.g. 0.3Hz) for at least delay time period "t_b" (e.g. 50ms). In Figure 4.7, sub-controller II will change S2 from default mode 0 to variable droop control mode 1 and meanwhile the sub-controller I switches S1 from 0 back to 1. In the case of medium and high wind speed conditions, rotor speed controller needs to be coordinated with pitch angle controller to achieve a long-term primary frequency regulation using the reserve power [16]. Furthermore, Rate Limiter for rotor speed is used to eliminate the impact of undesirable inertia on the active power output that results from the overly fast rotor deceleration or acceleration. The power rate limiter with 0.45 p.u./s and torque limiter with 1.1 p.u./s are added to reduce mechanical stresses on the drive train. Therefore, inertial response and primary frequency regulation are performed safely within the available reserve margin, namely 0.2 p.u. of maximum power output P_{MPPT}. Accordingly, upper limit and lower limit of Power Limiter are set as $0.2P_{MPPT}$ and $-0.2P_{MPPT}$ respectively. The upper limit of power limiter for modified pitch angle controller is set as 1.1 p.u. of rated power with the assumption that both generator and power converter are able to undertake a certain short-term overload.

4.3 Test System with Integration of CART2-PMSG Model

A small power system model is established in the Matlab/Simulink platform. As depicted in Figure 4.8, a 60Hz simple power system consists of an aggregated CART2-PMSG based wind farm, three synchronous generators and one constant power load. The 3MW wind farm consisting of 5 single CART2 wind turbines is connected to the point of common coupling (PCC) via a 575/35kV step-up transformer. The three synchronous generators are based on the thermal power plant with IEEE standard steam turbine governor and type 1 excitation system [47]. The inertial time constant for the 12-MVA SG1, 5-MVA SG2, and 0.8MVA SG3 are set as 5s, 4.2s and 3.5s respectively while droop coefficient for all generators is uniformly set as 5%. The baseline operating points for SG1 and SG2 are set to 0.8 p.u. of their rated capacities to ensure a certain power headroom for performing the primary frequency regulation. And the initial operating point of SG3 is 1 p.u., namely operating at the rated condition. The wind power penetration level of this small grid system is approximately 19.4% when CART2-PMSG operates at the rated wind speed.

In order to evaluate the effectiveness of the CFR method, the SG3 is tripped off the grid at t=30s, resulting in a severe frequency decline due to the power imbalance and reduced system inertia. Thus, differences in the frequency regulation performance can be noticeably observed through the following four scenarios: no auxiliary frequency control, constant inertial power control, fixed slope droop control as well as the proposed CFR control.

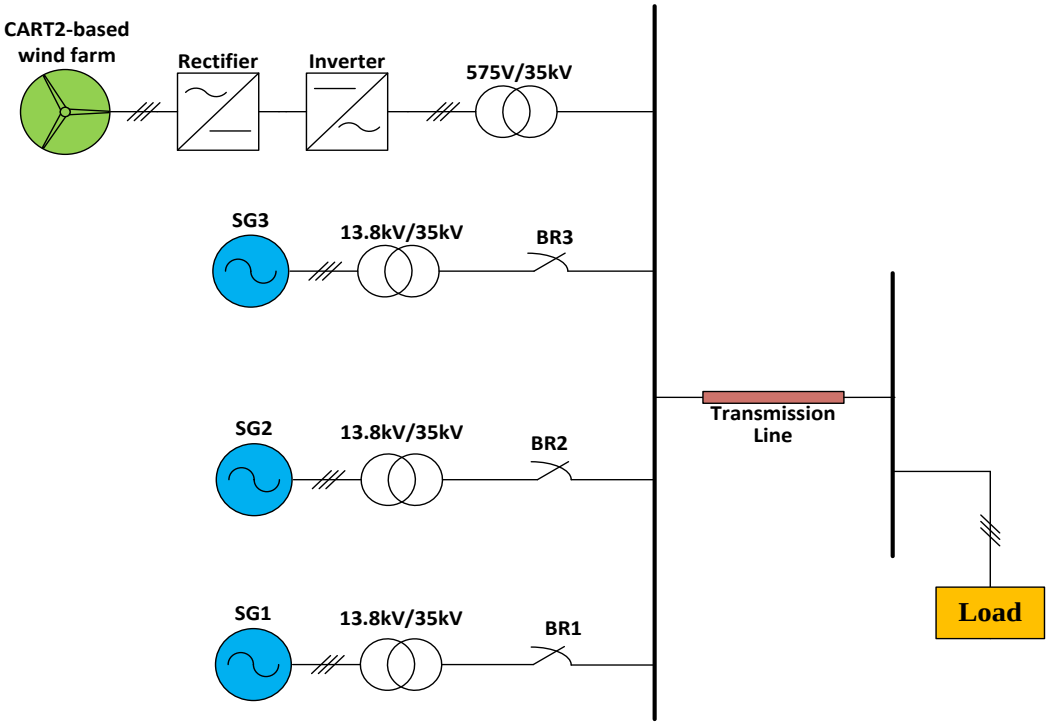

Figure 4.8 Basic configuration of a small test system

4.4 Simulation Results

4.4.1 Simulation Results for Electrical System

Case 1. Low wind speed condition (8/s)

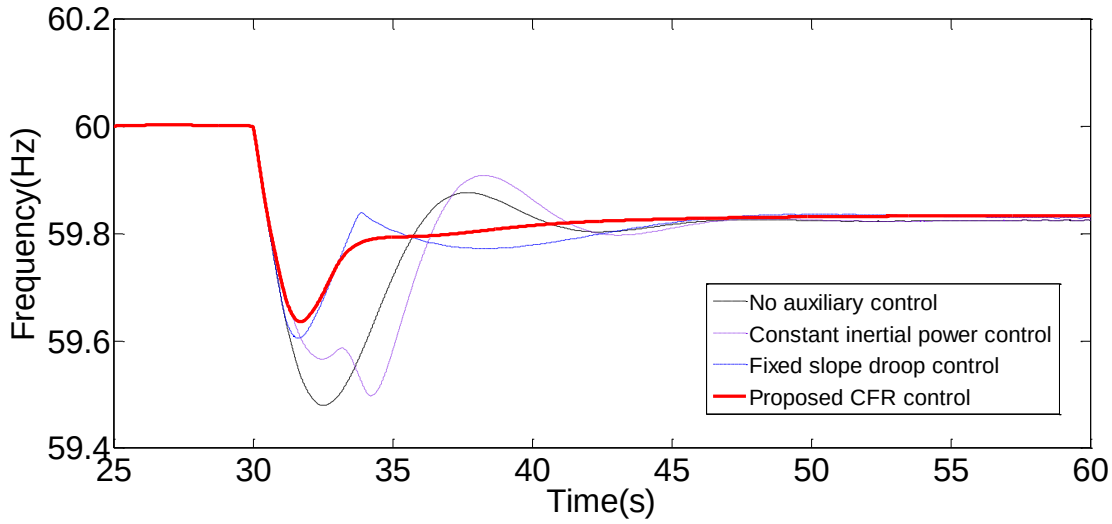

(a) System frequency

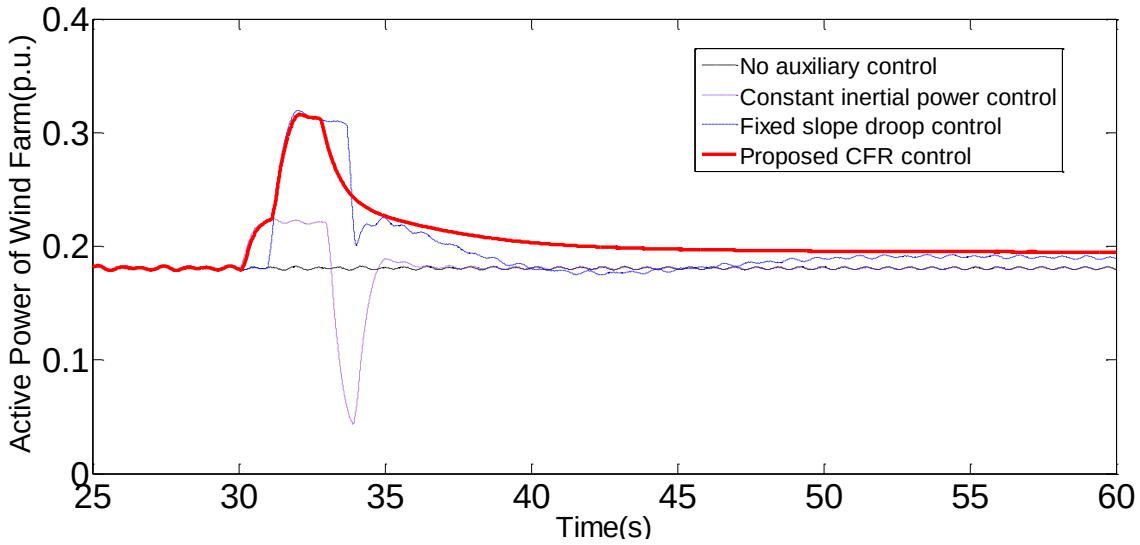

(b) Active power output of CART2-PMSG based wind farm

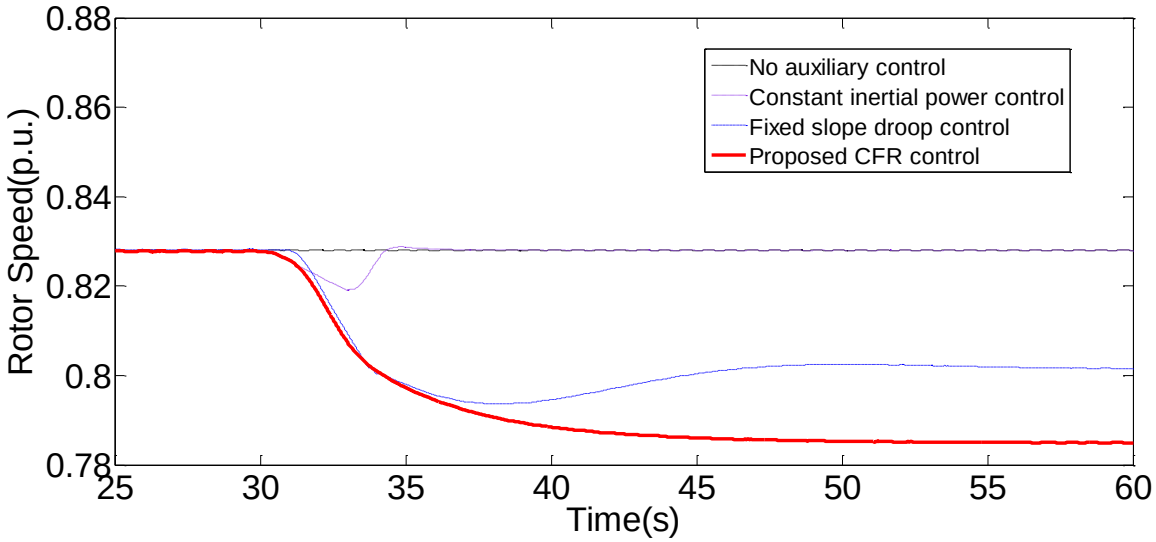

(c) Rotor speed

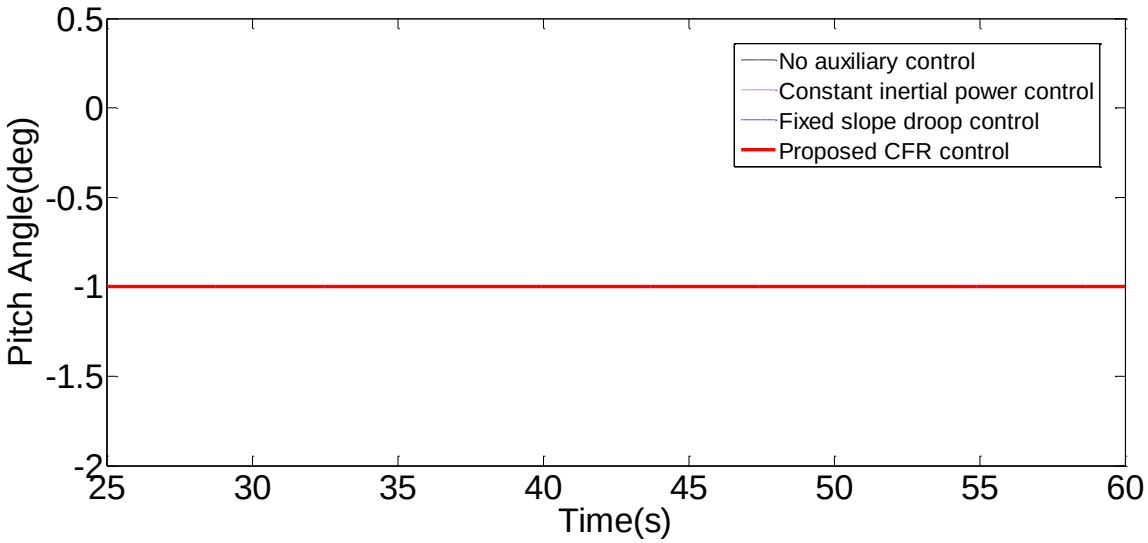

(d) Pitch angle

Figure 4.9 Simulation results of electrical system under the low wind speed.

Case 2. Medium wind speed condition (11/s)

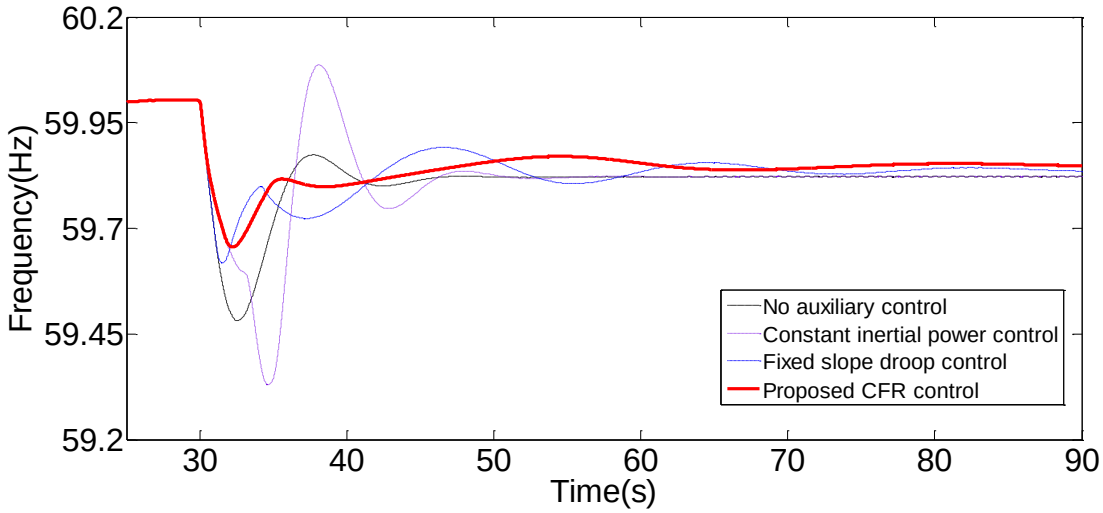

(a) System frequency

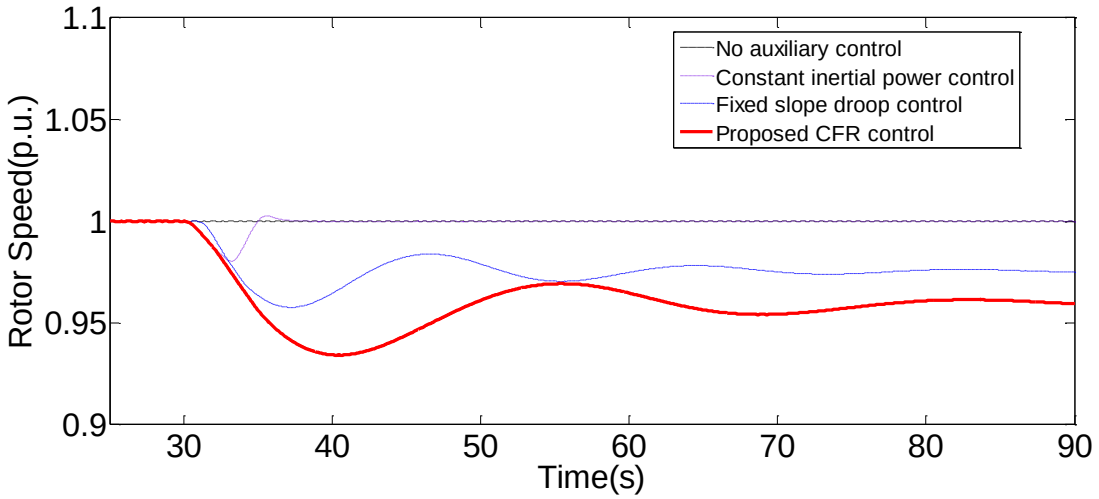

(b) Active power output of CART2-PMSG based wind farm

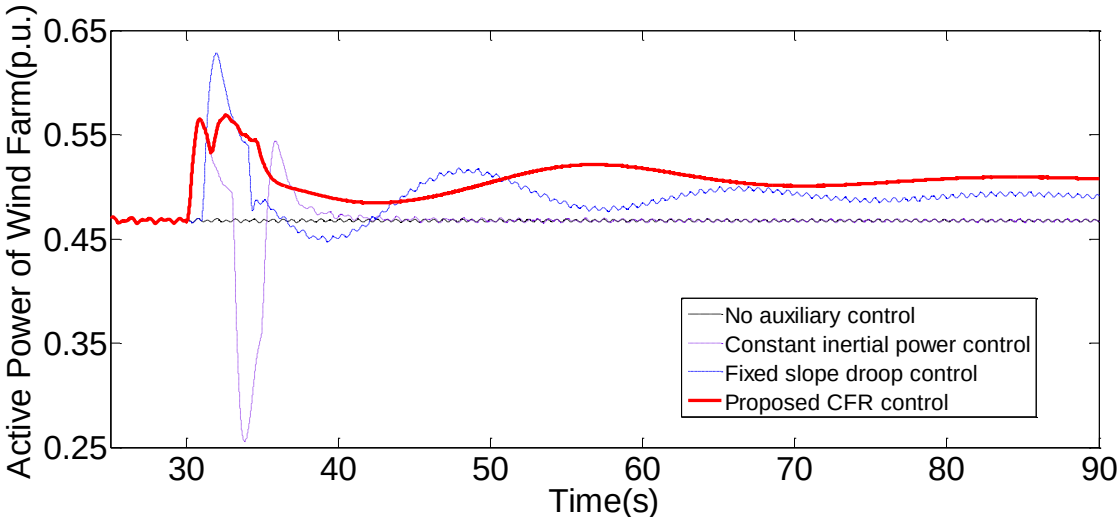

(c) Rotor speed

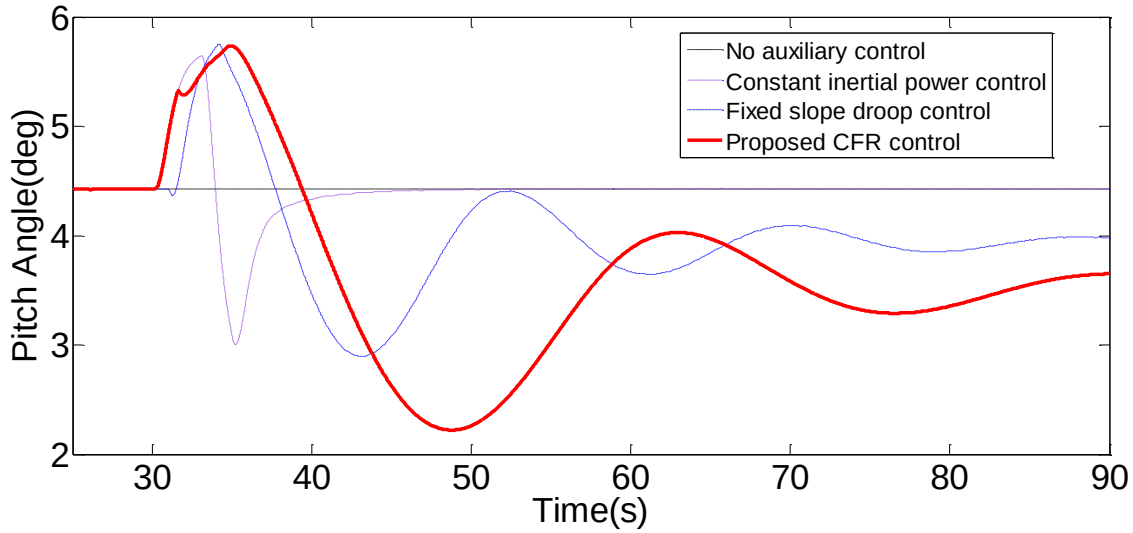

(d) Pitch angle

Figure 4.10 Simulation results of electrical system under the medium wind speed.

Case 3. High wind speed condition (14m/s)

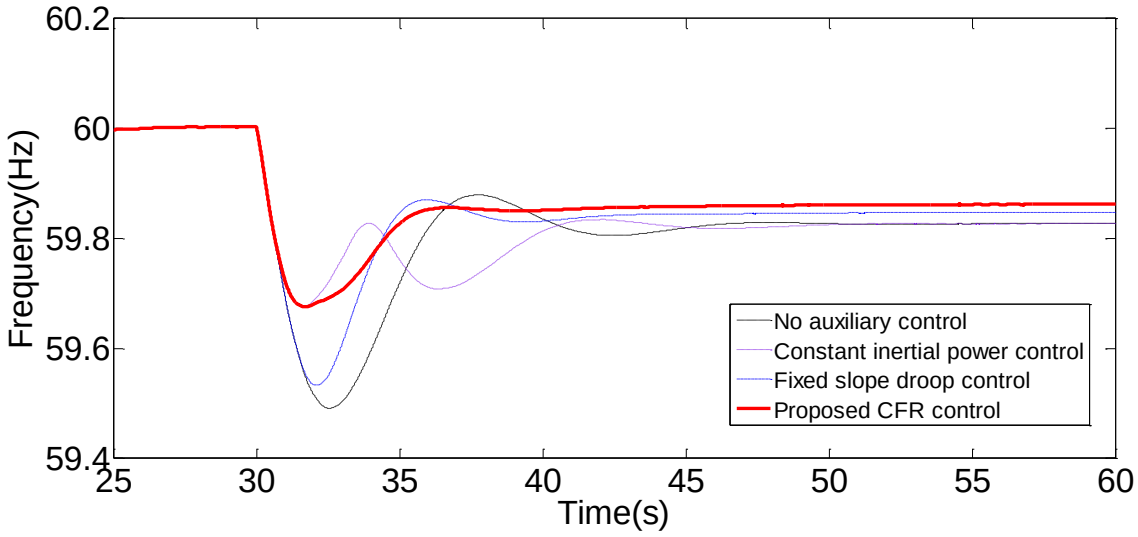

(a) System frequency

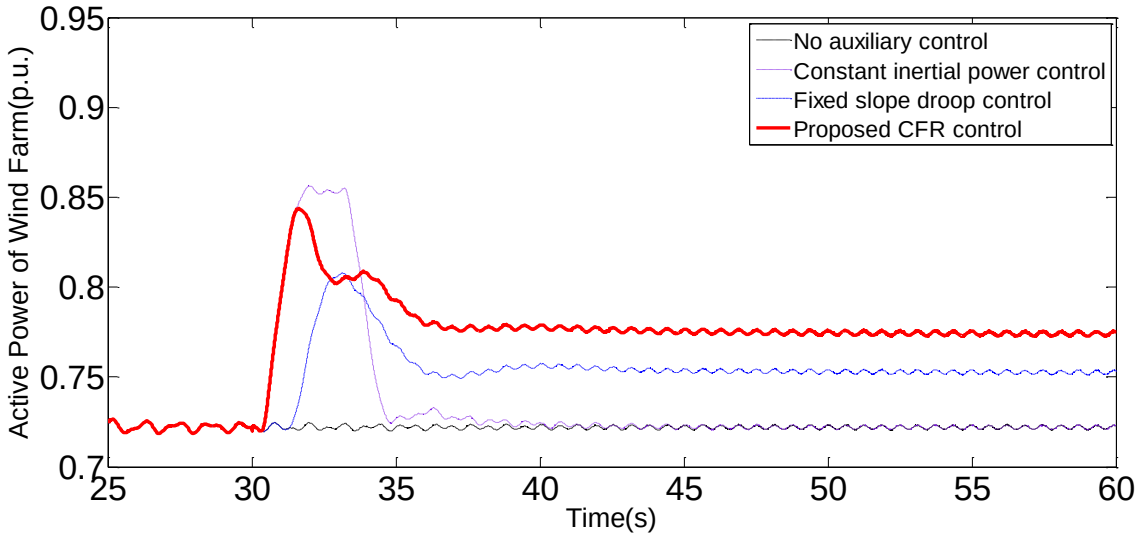

(b) Active power output of CART2-PMSG based wind farm

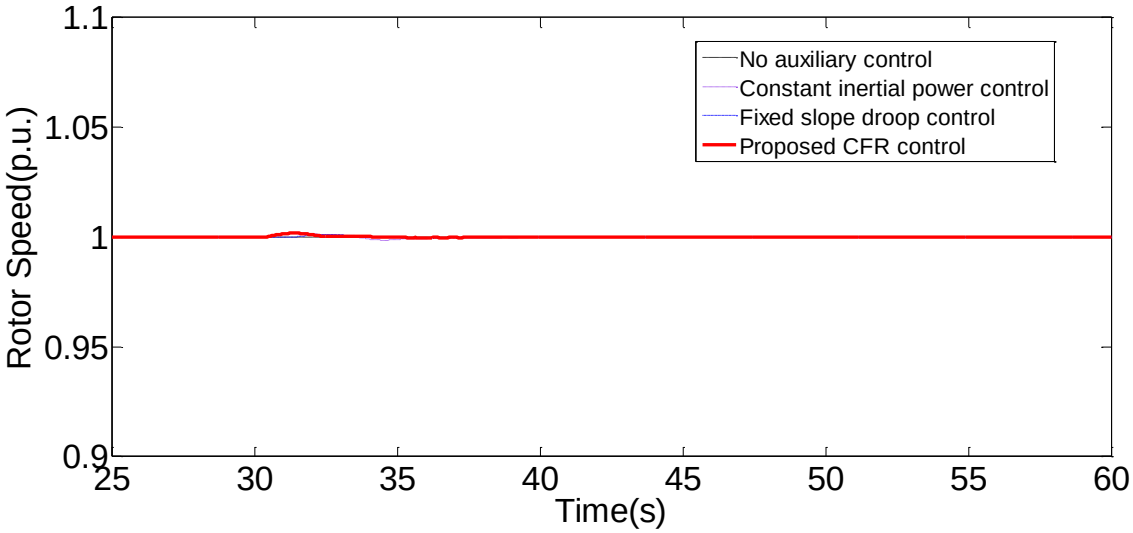

(c) Rotor speed

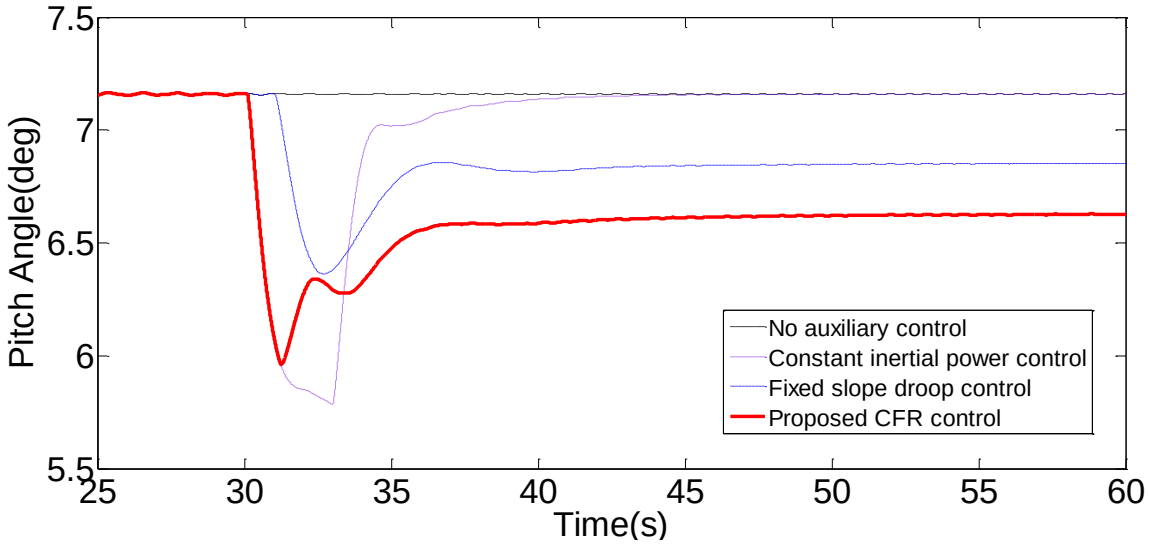

(d) Pitch angle

Figure 4.11 Simulation results of electrical system under the high wind speed.

4.4.2 Simulation Results for FAST Mechanical Stresses

Case 1. Low wind speed

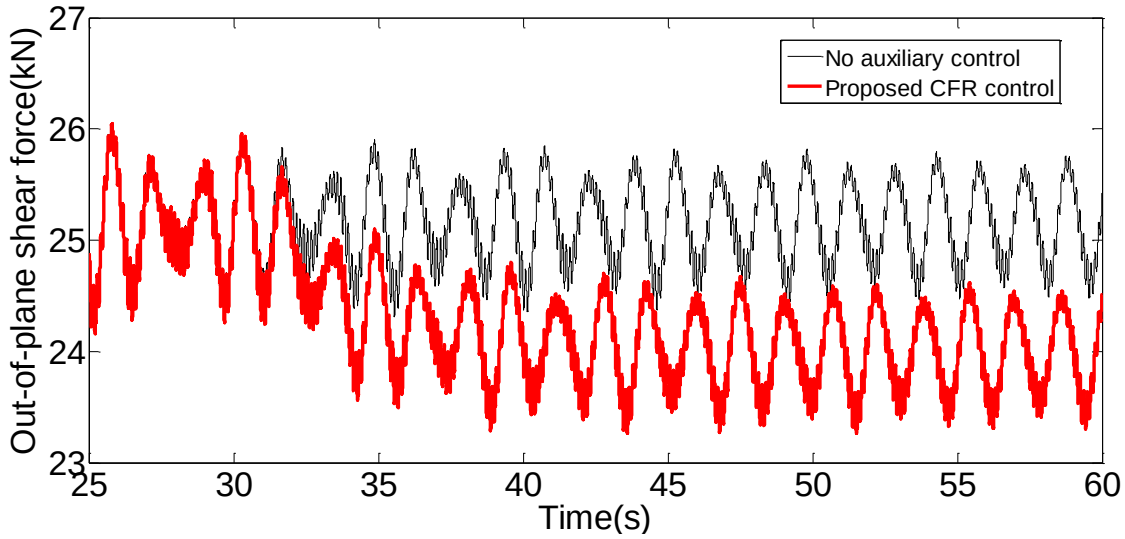

(a) Blade 1 out-of-plane shear force

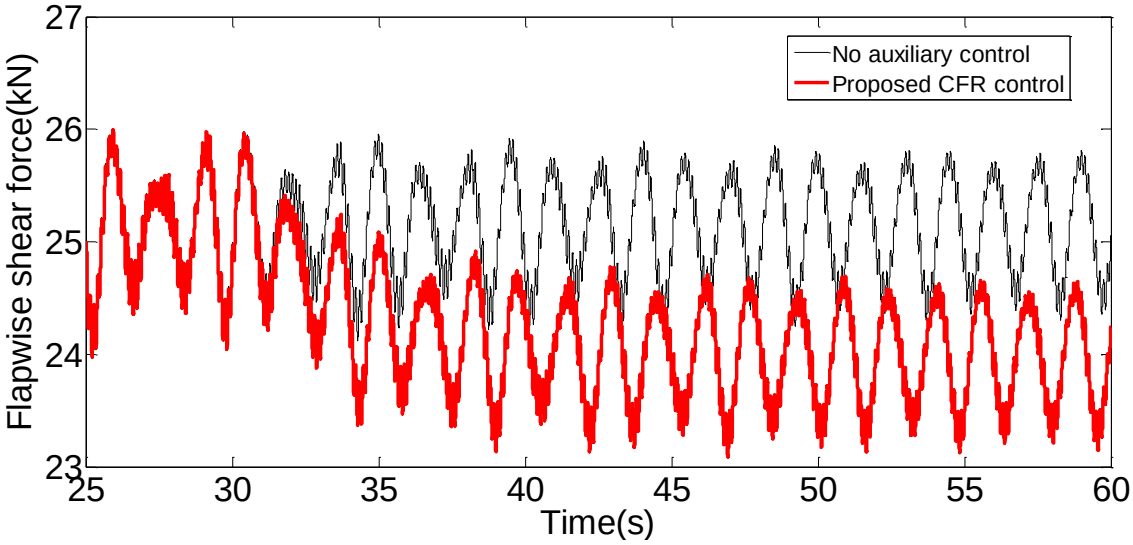

(b) Blade 1 flap-wise shear force

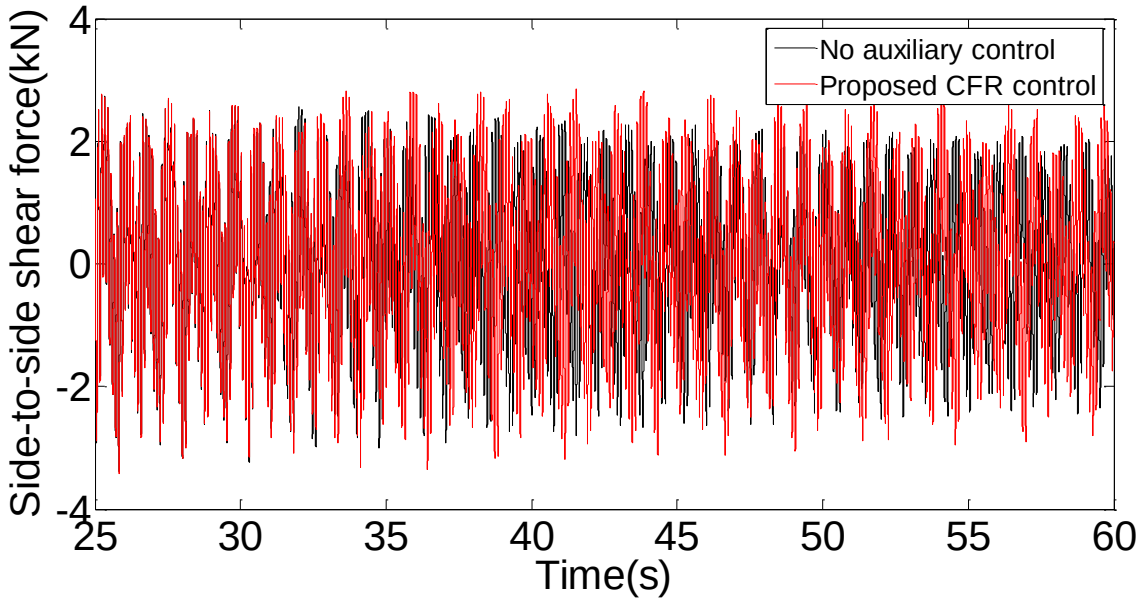

(c) Tower base side-to-side shear force

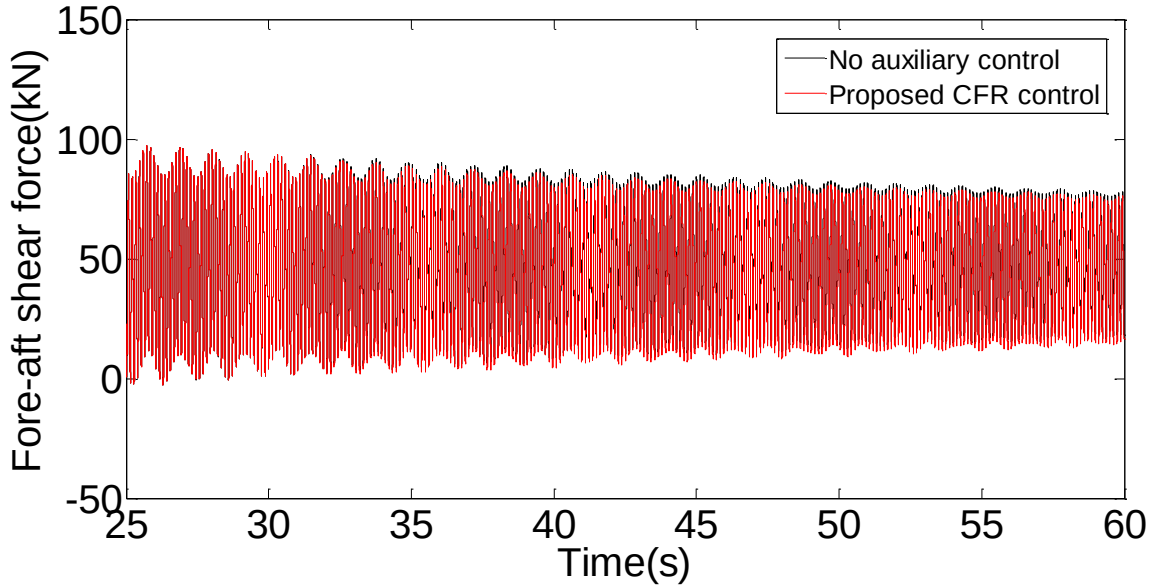

(d) Tower base fore-aft shear force

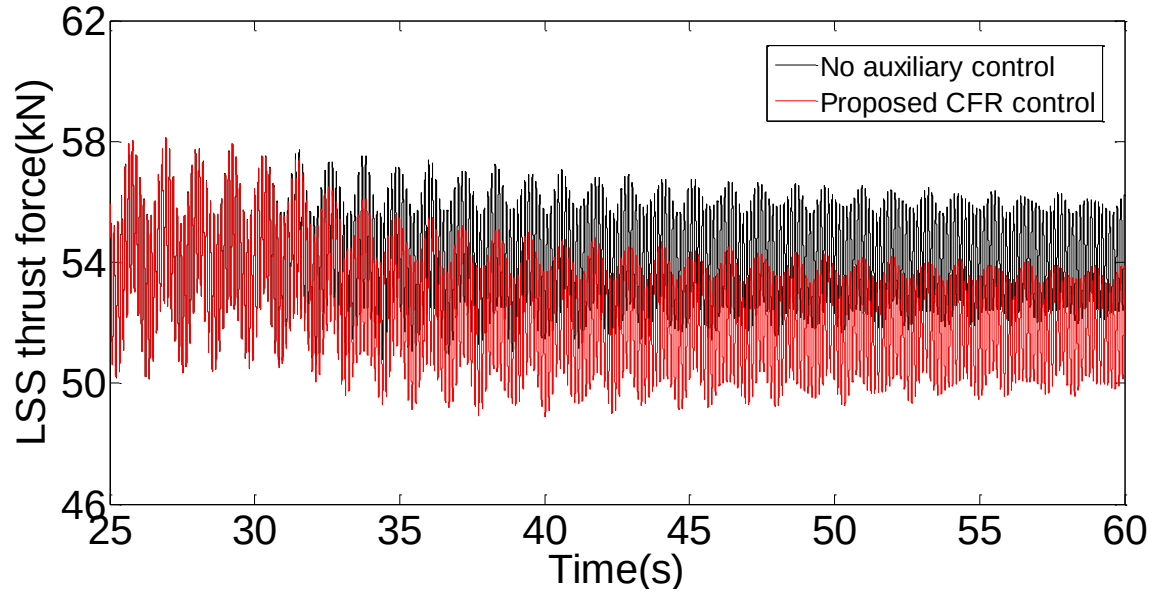

(e) Low speed shaft thrust force/rotor thrust force

Figure 4.12 Simulation results of mechanical stresses under the low wind speed.

Case 2. Medium wind speed

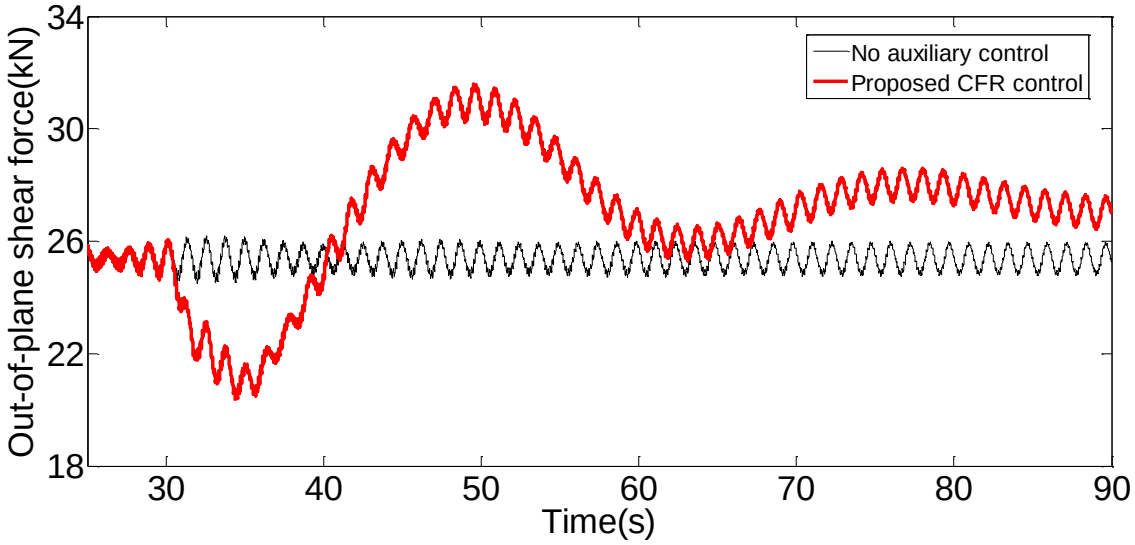

(a) Blade 1 out-of-plane shear force

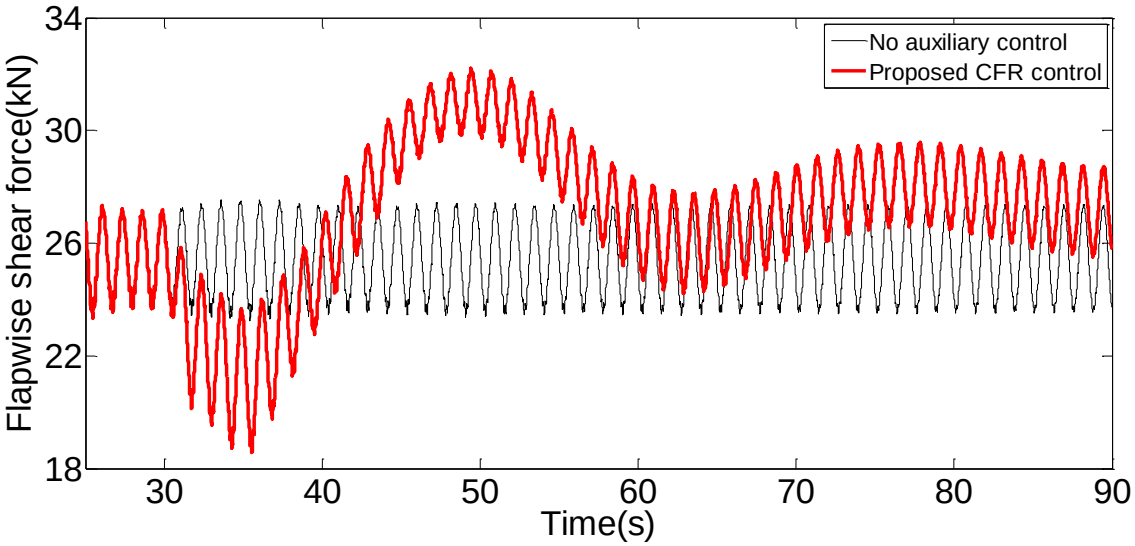

(b) Blade 1 flap-wise shear force

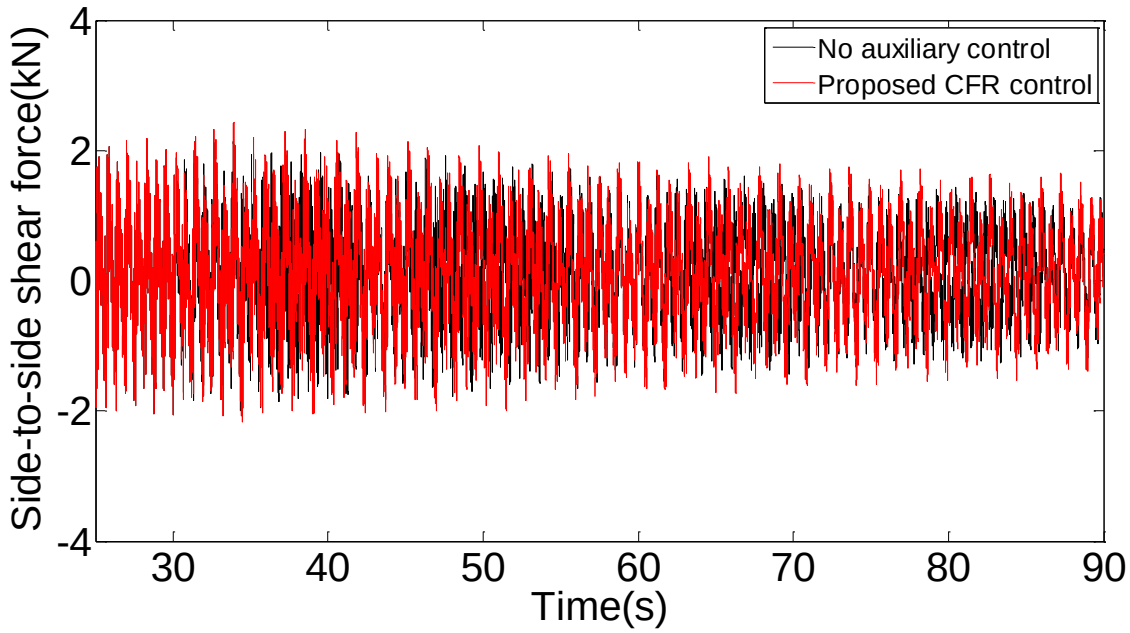

(c) Tower base side-to-side shear force

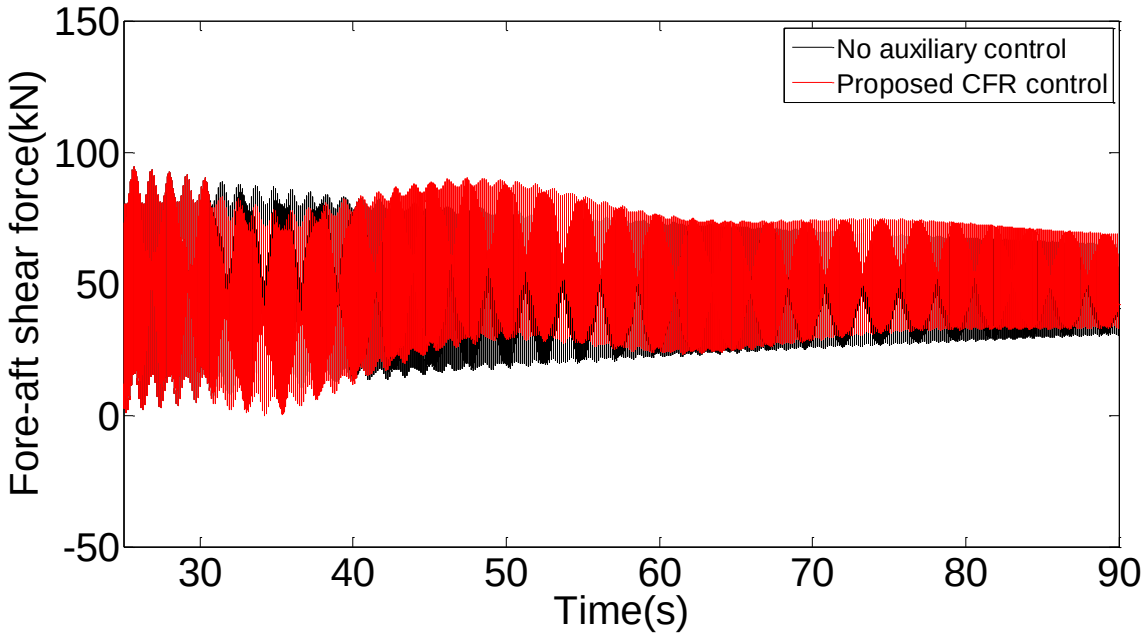

(d) Tower base fore-aft shear force

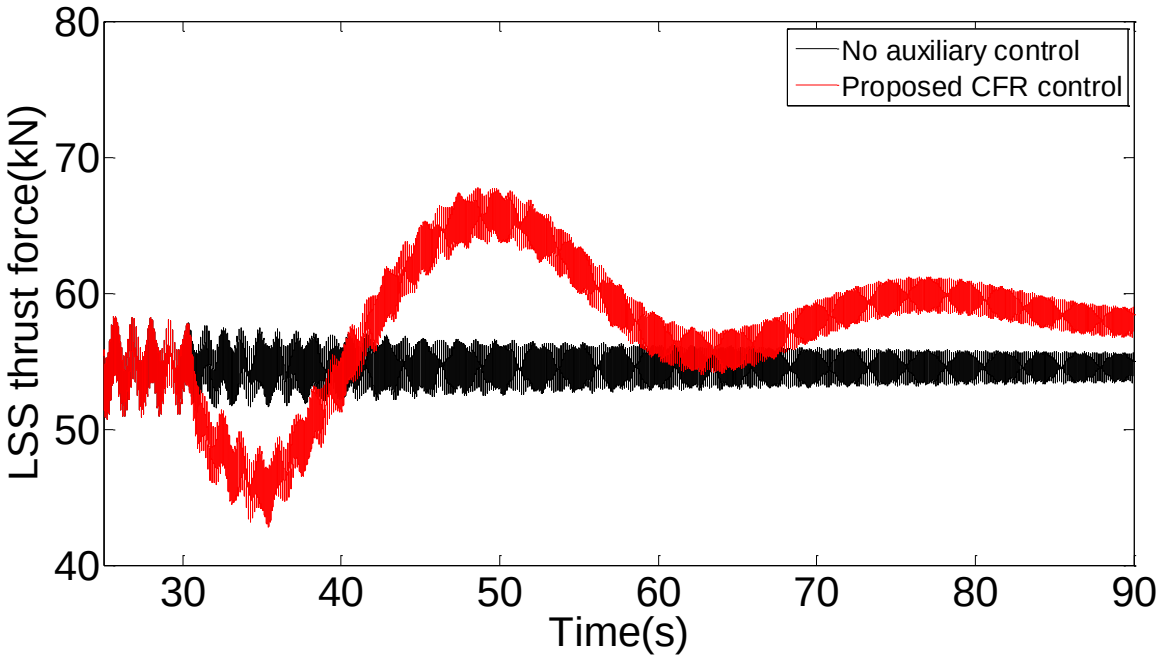

(e) Low speed shaft thrust force/rotor thrust force

Figure 4.13 Simulation results of mechanical stresses under the medium wind speed.

Case 3. High wind speed

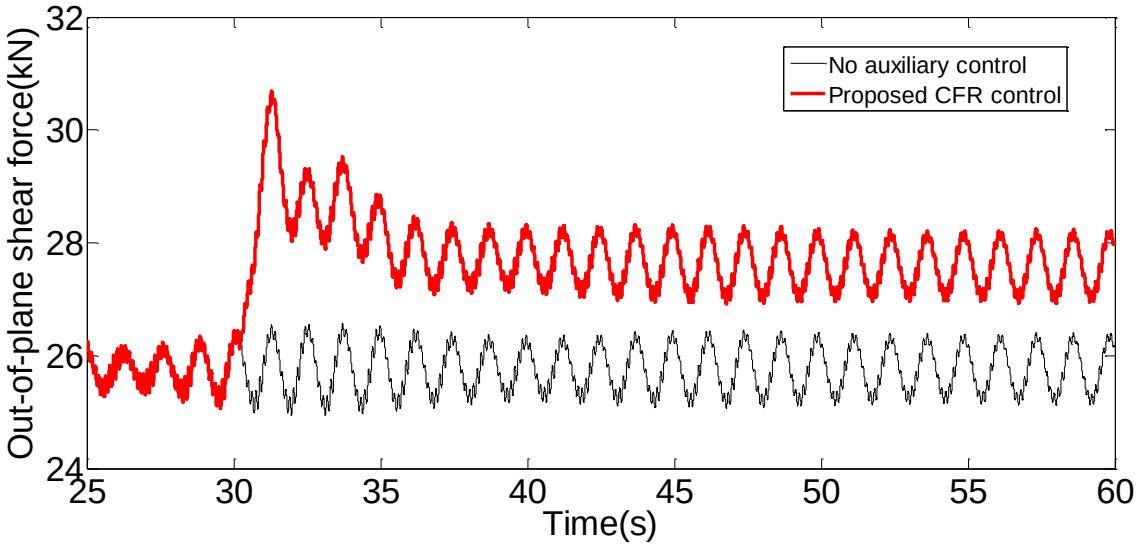

(a) Blade 1 out-of-plane shear force

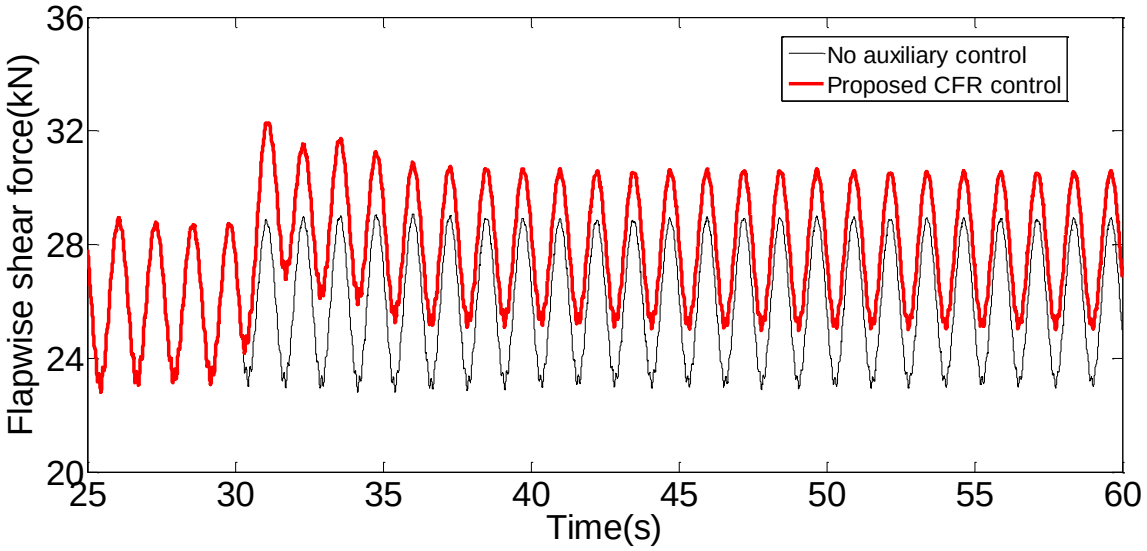

(b) Blade 1 flap-wise shear force

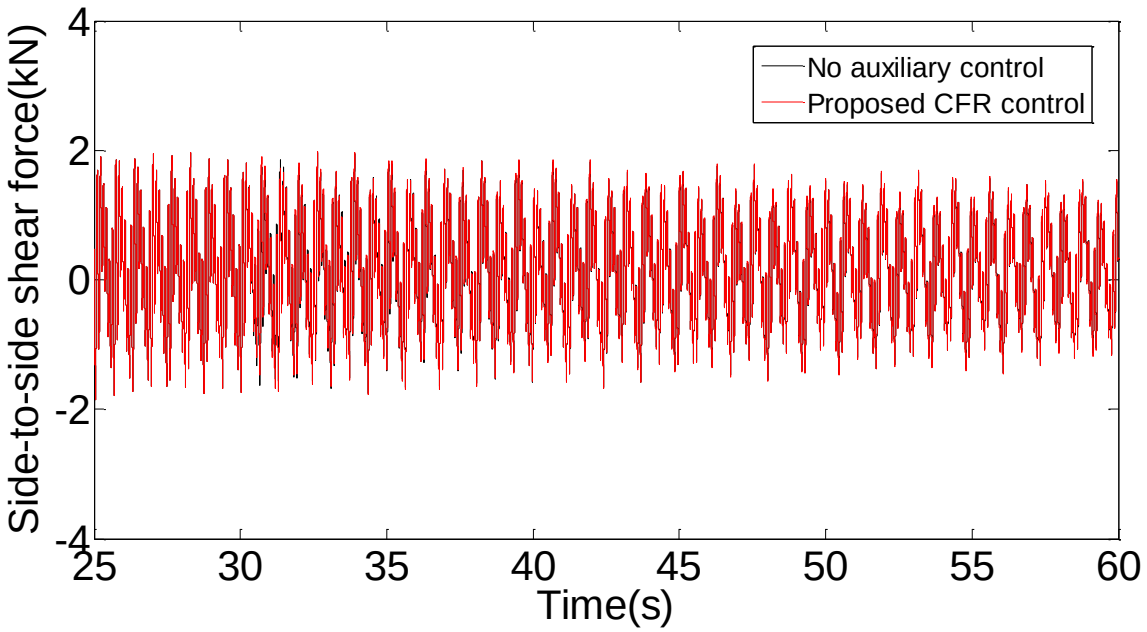

(c) Tower base side-to-side shear force

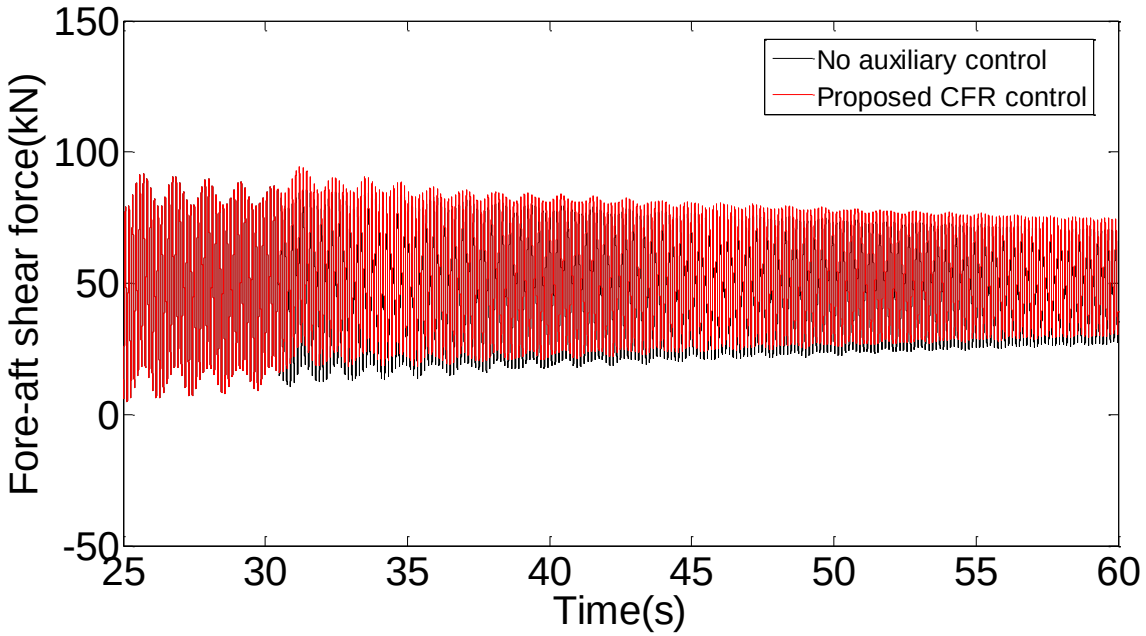

(d) Tower base fore-aft shear force

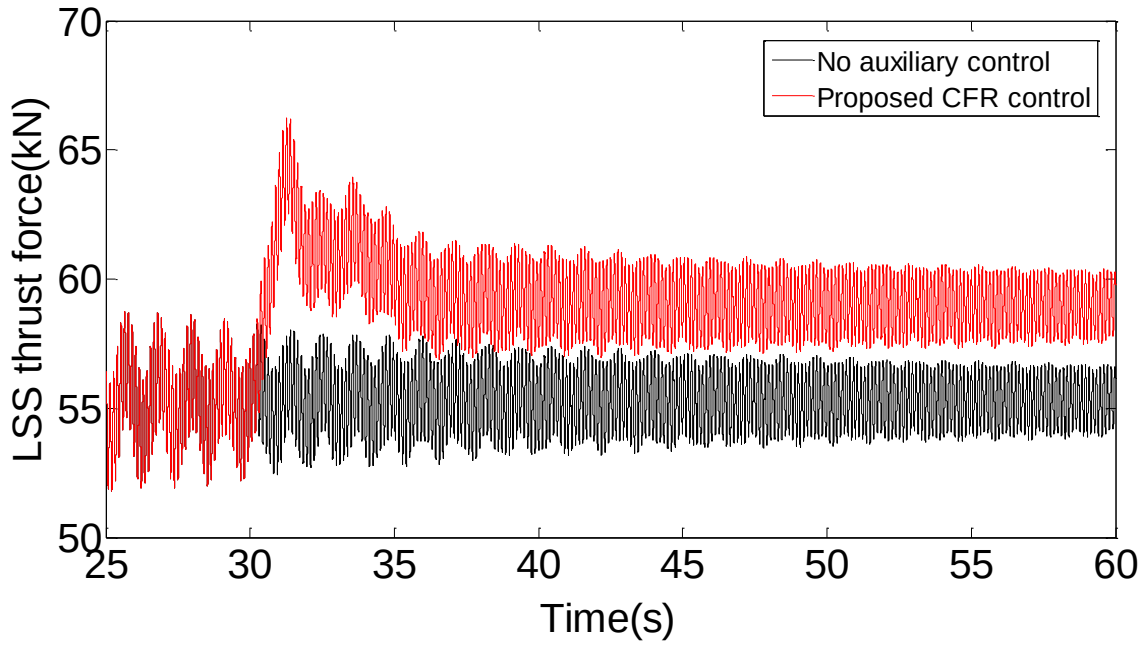

(e) Low speed shaft thrust force/rotor thrust force

Figure 4.14 Simulation results of mechanical stresses under the high wind speed.

4.4 Comparison and Discussion

From Figure 4.9. to Figure 4.11, dynamic characteristic and frequency regulation performance of CART2-PMSG are compared between using proposed CFR and other single traditional controls under various wind speed modes. Meanwhile, the impact of CFR control on the essential mechanical components including blade, shaft and tower is examined by comparing with the baseline case as shown in Figure 4.12-Figure.4.14. In case 1, additional active power is regulated only by using the rotor speed control while the modified pitch angle is maintained as -1 degree. In case 2, pitch angle control and rotor speed control are coordinated as a means of generating the extra active power. In case 3, the extra power is controlled entirely by the modified pitch angle control while the rotor speed remains around 1 p.u..

Without the auxiliary frequency control scheme, the output of CART2-PMSG does not respond to the frequency disturbance. So, from the Figure 4.9(a) to Figure 4.11(a), the overall frequency performance is the least desirable. The frequency nadir dropped below 59.5Hz (assumed as the minimum permissible frequency), so that the Under Frequency Load Shedding (UFLS) relay is triggered by tripping a certain amount of loads. In contrast with the natural inertia response in [26], constant inertial power response is able to deliver the additional active power in a controllable and sustainable manner. During the inertial response in Figure 4.9 (b) to 4.11 (b), the kinetic energy stored in the rotating mass is extracted and injected into the grid in conjunction with the released reserve power when rotor speed decreases. By doing this, this combined active power fed into the grid can significantly enhance the short-term frequency regulation by

mitigating the ROCOF and lifting the frequency nadir. In this case, the UFLS load shedding is avoided under the disturbance conditions. Nevertheless, the steady-state frequency deviation cannot be reduced since the power output of CART2-PMSG finally returns to the pre-disturbance value. Moreover, once the frequency begins to rise following the frequency nadir, a significant portion of aerodynamic wind energy will be utilized to accelerate the rotor speed and restore the kinetic energy rather than being converted to additional real power. As a result, due to this temporary decline in the electrical power output, a secondary frequency drop (SFD) may takes place, even with the subsequent nadir lower than the previous one as shown in Figure 4.10 (b). Therefore, it is necessary to choose the appropriate value of P_{in_pu} in equation (4) and rotor restoration speed to achieve a tradeoff between increasing the frequency nadir and mitigating the SFD issue.

With the fixed slope droop control, CART2-PMSG can share the sudden increase in the power load with other conventional synchronous generators, so that frequency nadir can be raised as shown in Figure 4.9 (a) to 4.11 (a) In this way, the spinning reserve of conventional generators for the primary frequency regulation can be reduced by de-loading the wind power output. Moreover, the steady-state frequency deviation is mitigated to a certain extent since a certain amount of reserve power is put into use for a long-term primary frequency support. However, the droop control itself cannot substantially improve the ROCOF because its control effect mainly depends on the magnitude of frequency deviation. During the initial stage of frequency decline, the frequency deviation gradually increases so that the droop control reaches the optimal performance at the frequency nadir by providing the largest additional power.

Table 4.1 Result comparisons among various frequency regulation methods in case 1

Methods	ROCOF （Hz/s）	frequency nadir （Hz）	Post-disturbance stable frequency (Hz)	Settling time （s）	The overshoot during the frequency recovery (Hz)
No auxiliary frequency control	-0.23	59.48	59.82	49.8	59.88
Constant inertia power response	-0.15	59.5	59.82	49.8	59.91
Fixed slope droop control	-0.23	59.61	59.83	48.7	59.84
Proposed CFR	**-0.15**	**59.64**	**59.83**	**41.6**	**59.79**

Table 4.2 Result comparisons among various frequency regulation methods in case 2

Methods	ROCOF （Hz/s）	frequency nadir （Hz）	Post-disturbance stable frequency (Hz)	Settling time （s）	The overshoot during the frequency recovery (Hz)
No auxiliary frequency control	-0.3	59.48	59.82	55	59.87
Constant inertia	-0.18	59.33	59.82	55	60.09

power response					
Fixed slope droop control	-0.3	59.62	59.84	85	59.89
Proposed CFR	**-0.18**	**59.65**	**59.85**	**74**	**59.82**

Table 4.3 Result comparisons among various frequency regulation methods in case 3

Methods	ROCOF （Hz/s）	frequency nadir （Hz）	Post-disturbance stable frequency (Hz)	Settling time （s）	The overshoot during the frequency recovery (Hz)
No auxiliary frequency control	-0.2	59.49	59.83	50.3	59.88
Constant inertia power response	-0.1	59.68	59.83	50.3	59.83
Fixed slope droop control	-0.18	59.53	59.85	42	59.87
Proposed CFR	**-0.1**	**59.68**	**59.86**	**37.7**	**59.86**

As shown in Table 4.1-4.3, the proposed CFR control shows the best performance in enabling the CART2-PMSG to participate in both short-term and long-term frequency regulation. It not only helps arrest the ROCOF, but also boost the frequency nadir as well as avoids the secondary frequency drop. Moreover, the primary frequency regulation is significantly enhanced through the variable droop control in an effort to further reduce the steady-state frequency deviation and smoothen the frequency recovery. The duration that frequency restores to the post-disturbance stable state is shortened with much smaller overshoot in the recovery process. However, it is noted that the frequency recovery

period for CFR in case 2 is much longer compared with other two cases without droop control applied. That is due to the fact that the variable droop control is carried out based on coordinated control between the rotor speed and pitch angle. Thus, it more likely results in a relatively long adjustment process due to the mutual effect between large inertia of rotating mass and slow mechanical response of pitch mechanism.

In Figure 4.12 to Figure 4.14, there are no significant impacts on the wind turbine's tower, blade and shaft because of the sudden increase in the electrical power when CFR control is carried out at the low wind speed condition. Actually, out-of-plane shear force and flap-wise shear force in blade 1, tower base fore-aft shear force as well as rotor thrust force tend to become slightly smaller during the frequency response phase when CFR is deployed. This is mainly because the decreasing rotor speed leads to reduced tip speed ratio and eventually causes less force [85]. Similarly, all the shear forces on the blade and tower as well as the rotor thrust force seems to have the same trend as the rotor speed variation in Figure 4.10 (c). With active involvement of pitch angle control in the high wind speed case, magnitude of these forces are slightly larger than those in Figure 4.12-4.13. In Figure 4.14 (a)-(e), due to the fact that the rotor speed is restricted as 1.0 p.u., these shear force and rotor thrust force change accordingly when the pitch angle is adjusted to increase the active power through the CFR control. Nevertheless, this increase is still regarded as acceptable from the perspective of secure operation when compared with the structural loads imposed by the gusty and turbulent wind conditions. Therefore, the implementation of the CFR approach in the low wind speed mode does not negatively impact the mechanical components, and potentially

induce more but not severe stresses on those components in the medium and high wind speed modes.

4.5 Conclusion

A novel CFR control scheme is developed and implemented into the CART2-PMSG model based on rotor speed control. It comprises the constant inertia power response and dynamic variable droop control, which are carried out during two sequential stages of frequency event: in the short term, constant inertial power controller emulates the inertial response aiming to improve the transient frequency characteristics; in the long term, based on the available reserve margin, variable droop control allows PMSG-WTG to participate in the enhanced primary frequency regulation along with other synchronous generators. More importantly, this control scheme needs to be achieved through the coordinated control of both rotor speed and pitch angle in accordance with various wind speed modes. To verify the effectiveness of CFR control and its impact on the mechanical loads, a series of simulation cases are carried out in Matlab/Simulink.

It is concluded that the CFR can enable PMSG-WTG to contribute to the active power regulation and promote the overall frequency regulation performance in case of frequency disturbance. The presented CFR control is capable of reducing the initial ROCOF, raising the frequency nadir as well as minimizing the steady-state frequency deviation. Also, this control scheme can retain a constant percentage of delta reserve power ready for the long-term frequency regulation. Moreover, the presented method can be widely applied for the rotor-speed-control-oriented PMSG-WTG or DFIG-WTG over a wide range of wind speeds. What is important, the implementation of CFR does not do

large damage to major mechanical components of wind turbine and affect wind turbine's safe operation. In this sense, the established CART2-PMSG model with CFR function can serve as a theoretical tool to study the secure integration of PMSG-WTG-based wind farm and their potential contribution to the system frequency regulation as well.

Chapter 5 Frequency Support of PMSG-WTG Based on Improved Inertial Control without Pre-deloaded Operation

In this work, an improved inertial control method based on the maximum power point tracking operation curve is introduced to enhance the overall frequency support capability of PMSG-WTGs in the case of large supply-demand imbalances. Moreover, this method is implemented in the CART2-PMSG integrated model in MATLAB/Simulink to investigate its impact on the wind turbine's structural loads during the inertial response process. Simulation results indicate that the proposed method can effectively reduce the frequency nadir, arrest the rate of change of frequency (ROCOF) and mitigate the secondary frequency drop (SFD) while imposing no negative impact on the major mechanical components of the wind turbine.

5.1 Improved Inertial Control Method of PMSG-WTG

Figure 5.1 shows a complete set of improved inertial control strategy, which is composed mainly of three sequential stages as highlighted in the red line: inertial response (Line A-B-C), temporary deloaded operation (Line C-D-E), and rotor speed recovery (Line E-A). The blue line represents the maximum power characteristics under different rotor speeds, and the black line indicates the mechanical power characteristics corresponding to a given wind speed and optimal pitch angle. Besides, the dashed magenta line presents the torque limit that WT's active power output must comply with.

The green line shows the electrical power reference that is in parallel with the maximum mechanical power curve by ΔP. During the inertial response, the kinetic energy stored in the rotating mass can be released by decelerating the rotor speed, ω_{WT}, because the electromagnetic torque is larger than the available mechanical torque. The rotor speed declines along Line B-C and eventually settles down at Point C due to the decreasing power imbalance. To achieve this function, the active power command P_{ref_1} of rotor-side converter comprises a constant ΔP and the regular reference P_{MPPT}. ($P_{MPPT} = K\omega_t^3, k = \frac{1}{2}\rho\pi R^5 \frac{C_{pmax}}{(\lambda_{opt})^3}$).

$$P_{ref\_1} = P_{MPPT} + \Delta P \tag{5.1}$$

where, P_{MPPT} is the maximum active power captured from the wind energy at a certain wind speed, ΔP is a constant value in proportion to the rotor speed; ω_{WT}, which is a certain percentage of the actual output power level instead of the wind turbine's rated power. It is more favorable to provide stronger inertial response in the relatively high rotor speed condition by setting a larger value of ΔP. On the other hand, a lower inertial response is still available for system frequency support in the low wind speed condition without causing the over-deceleration of the rotor speed. It is worth noting that the value of ΔP cannot be set too high because the green line should intersect with or be tangent to the black line to assure the rotor speed stabilizes at the ω_1. Moreover, due to the maximum torque limit and maximum power constrain of the power converter, the value of ΔP cannot be kept setting high but being reduced especially as rotor speed rises toward the rated one. So, the proper adjustment of ΔP in the high rotor speed condition is very necessary in order to optimally perform the SAI function. It will be further studied in the

later work. For the temporary deloaded operation, the active power command P_{ref_2} is described as

$$P_{ref\_2} = P^* - \Delta P_{de} \tag{5.2}$$

where, P^* is the active power value corresponding to the intersection Point C between the mechanical power curve and the electrical power curve, and ΔP_{de} is a constant value for the deloaded margin that drives the rotor speed to be accelerated due to the power imbalance. The larger the ΔP_{de} value is, the faster the rotor speed returns to the optimal Point E, but the more likely a secondary frequency drop (SFD) occurs. So it is necessary to determine the appropriate value for ΔP_{de} to achieve a desirable trade-off between the recovery speed and frequency performance. During the rotor speed recovery, the rotor speed can smoothly move toward the original Point A along Line E-A, and it finally settles down at Point A due to the decreasing power imbalance. At this stage, the active power command P_{ref_3} remains constant as the optimal value:

$$P_{ref\_3} = P_{MPPT} = K(\omega_t)^3 \tag{5.3}$$

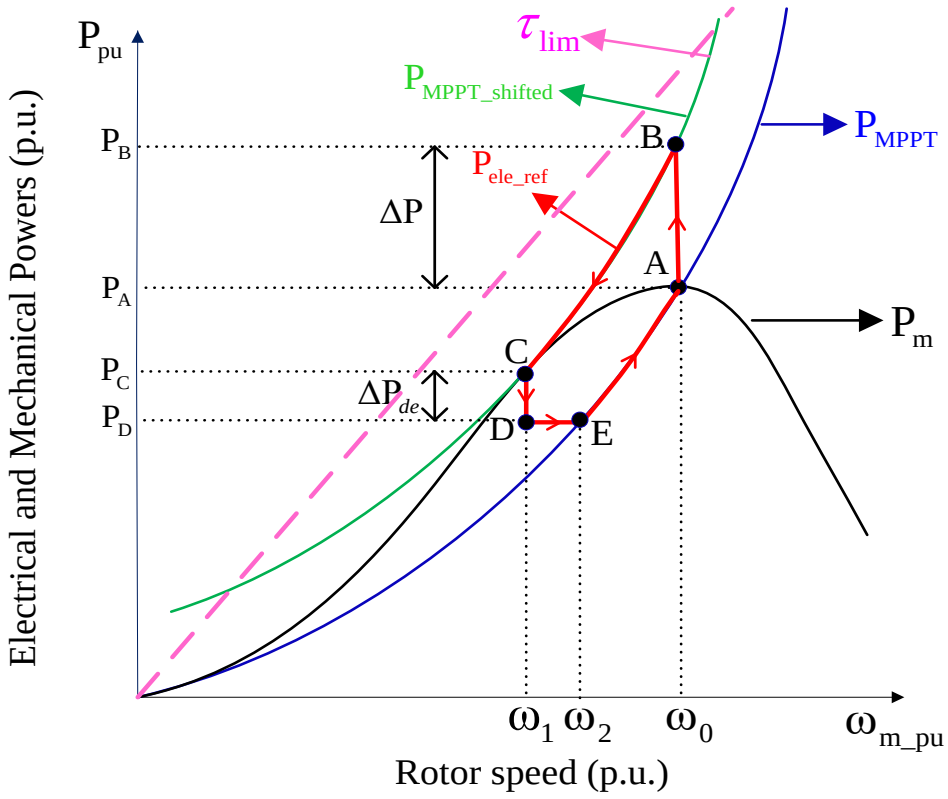

Figure 5.1 Power–rotor speed trajectory

The specific control strategy of improved inertial response implemented in MATLAB/Simulink is illustrated in Figure 5.2 [86]. A disturbance detector is utilized to trigger the inertial response as the frequency deviation exceeds 0.02 Hz and sustains for a period of 100 ms. When the rotor speed decreases to ω_1 and the condition (5.4) is met for a specified period of time (1s), in this case the rotor speed has basically reaches the stable state at the point C and the frequency support is completed. At this moment, the power command is switched from the inertial response to temporary deloaded operation through the deloaded operation detector.

$$|\omega_t - \omega_{t-1}| \leq 0.5 \times 10^{-3} \text{ p.u.} \tag{5.4}$$

where ω_t is the rotor speed at the moment t (s) and ω_{t-1} is the rotor speed at the moment t-1 (s). During the deloaded operation, the power command is changed to MPPT mode using the inertial recovery detector if the condition (5.5) is satisfied for a specified period of time (50 ms). This criterion can make sure that the active power output is able to increase from Point E moving along Line E-A without undergoing any possible decline.

$$\omega_t \geq \omega_{MPPT} \tag{5.5}$$

where ω_{MPPT} is the optimal rotor speed when WT operates at the deloaded power level, $P_{ref\_2} = P_D$. In other words, ω_{MPPT} corresponds to the rotor speed ω_2 at the point E.

Note that the power magnitude limiter, torque magnitude limiter, and their rate limiters are added to this integrated model to avoid the excessive stress and overload imposed on the wind turbine's mechanical components (blade, drive train, and tower) when performing the inertial response.

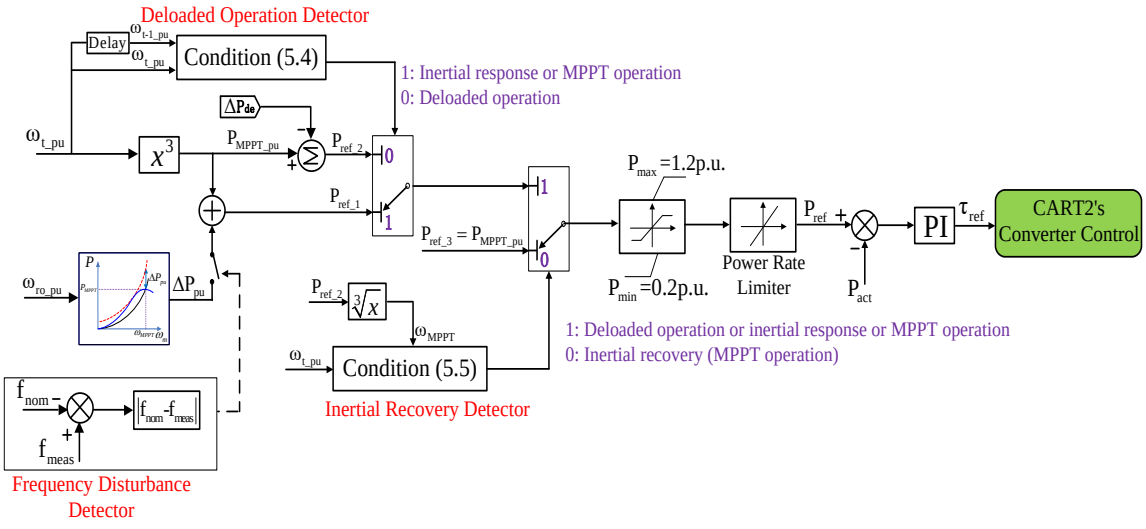

Figure 5.2 Complete set of the improved inertial control scheme

5.2 Model System and Case Study

Figure 5.3 shows a small power grid system consisting of three steam turbine generators and one aggregated CART2-PMSG-based wind farm as established in MATLAB/Simulink. The inertial time constant for the 10-MVA SG1, 5.2-MVA SG2, and 0.9MVA SG3 are set as 5s, 4.2s and 3.5s, respectively while droop coefficient for all generators is set as 5%. The initial operating points for SG1 and SG2 are set to 0.76 p.u. of their rated capacities to secure a certain power headroom to participate in the primary frequency regulation. The initial operating point of SG3 is 1 p.u., namely operating at the rated condition. The 3MW wind farm incorporating 5 single CART2 wind turbines is connected to the point of common coupling (PCC) via a 575/35kV step-up transformer. The pre-disturbance power output of WTG is 0.44 p.u., so the wind power penetration is approximately 10.4% in this scenario. In this work, the penetration level is defined as the percentage of total demand served by the actual wind power output. Automatic generation control is disabled in this work, thus the steady-state error following the frequency disturbance remains.

At the moment of 30 s, the SG3 rated at 900 kW is tripped out of the grid and a rapid frequency decline immediately follows. To eliminate the influence of wind variation on the structural loads, CART2-PMSG operates at the constant wind speed of 10 m/s wherein it is capable of providing 0.3 percentage of the available optimal power output for the inertial response. In this case, the performance of the proposed inertial scheme and its effect on the grid frequency is fully evaluated by comparing it to the case that uses no inertial control. Meanwhile, two different values of the deloaded margin,

ΔP_{de}, are chosen to explore its impact on the system frequency recovery process and structural loads of the wind turbine. Therefore, a series of results regarding the grid side, electrical and mechanical features as well as the selected loading variables are made available in three scenarios. The black line is the basic case without the wind turbine's inertial response. The blue line represents the proposed inertial response with ΔP_{de} = 0.03 percentage of the current wind power output, and the red line shows the proposed inertial response with ΔP_{de} = 0.0044 percentage of the current wind power output.

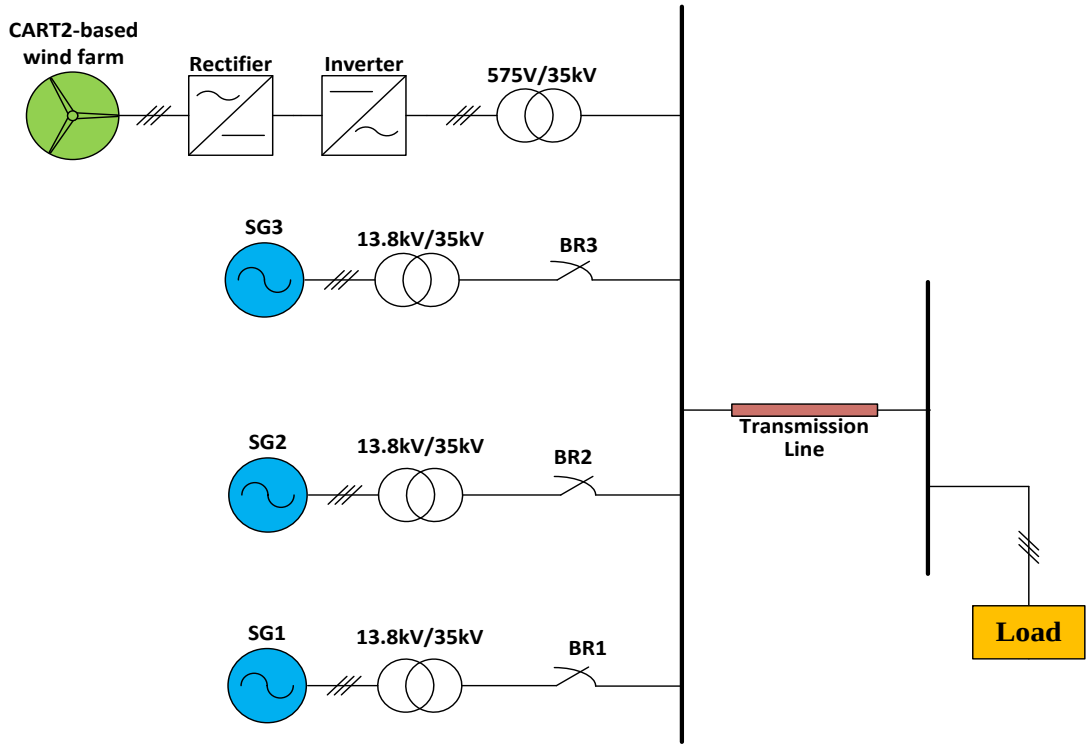

Figure 5.3 Basic configuration of a small-scale power grid system

5.3 Simulation Results

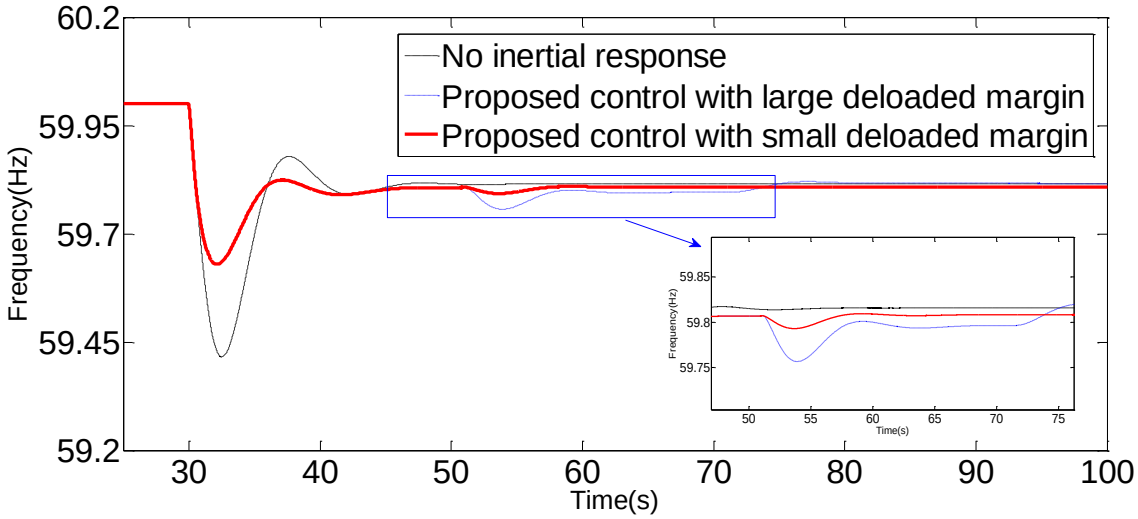

(a) System frequency

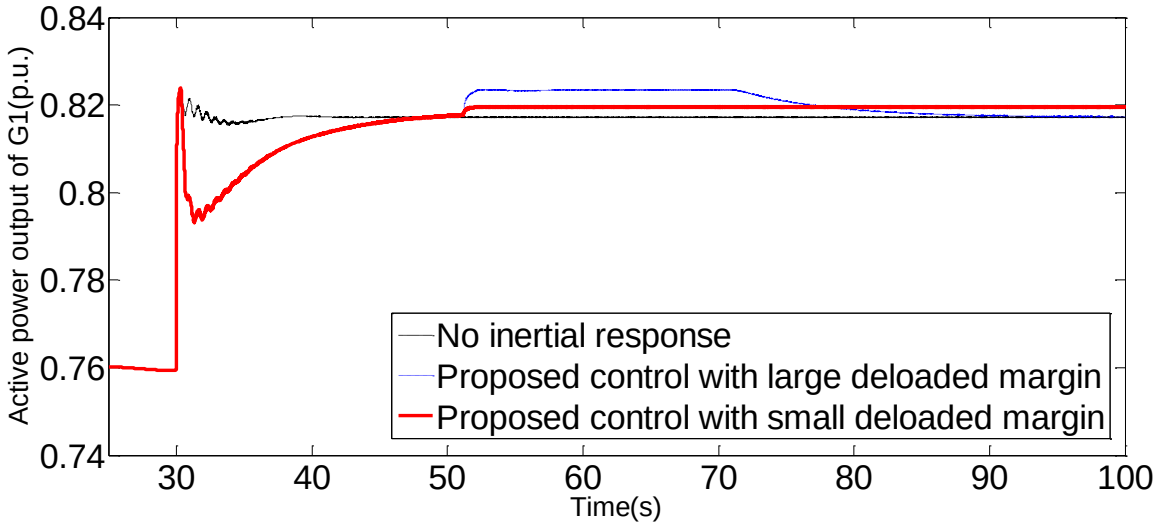

(b) Active power output of SG1

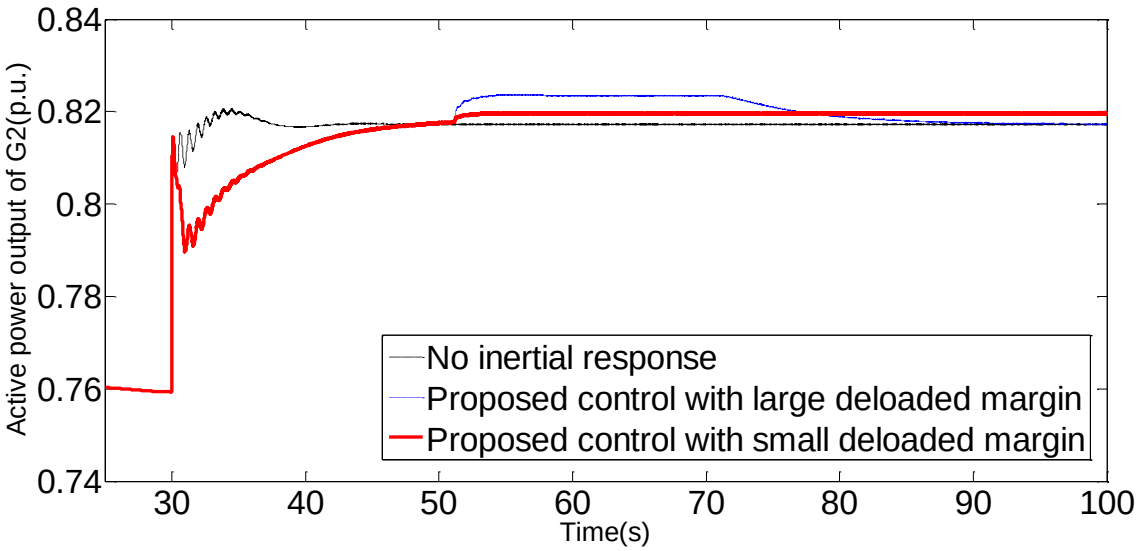

(c) Active power output of SG2

Figure 5.4 Simulation results for the grid side

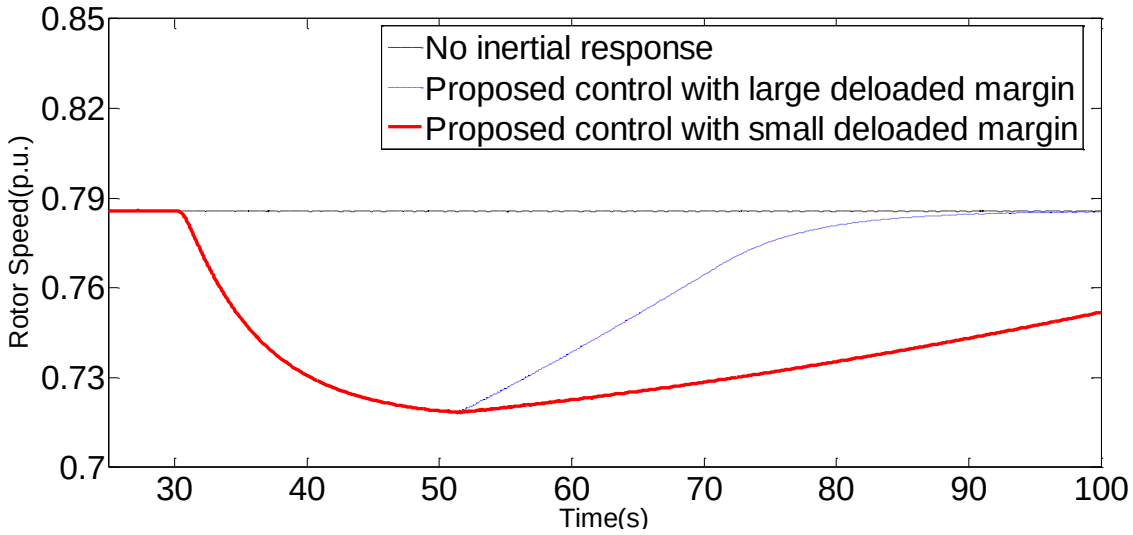

(a) Generator rotor speed

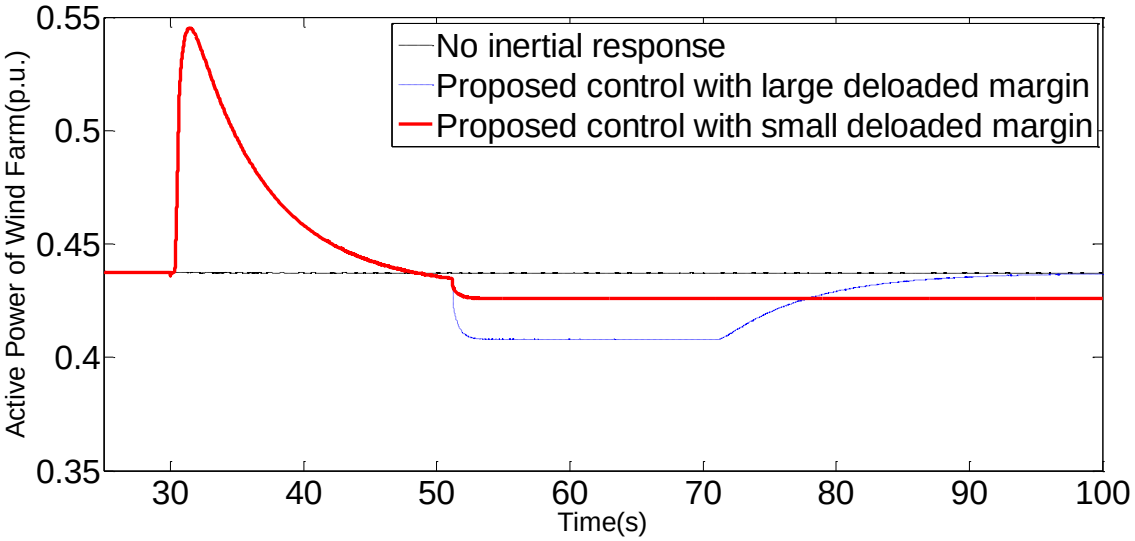

(b) Active power output of wind farm

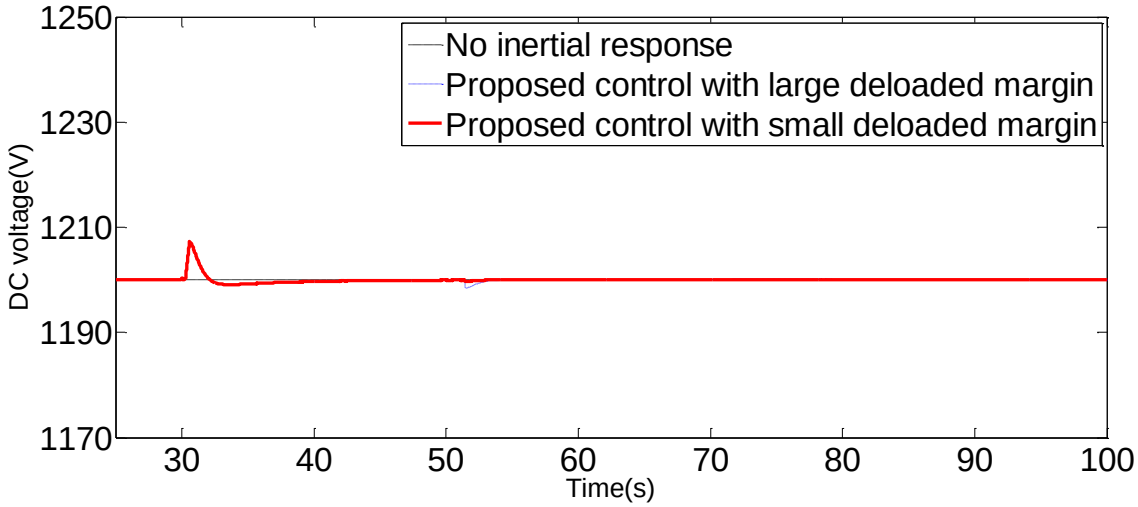

(c) DC-link voltage

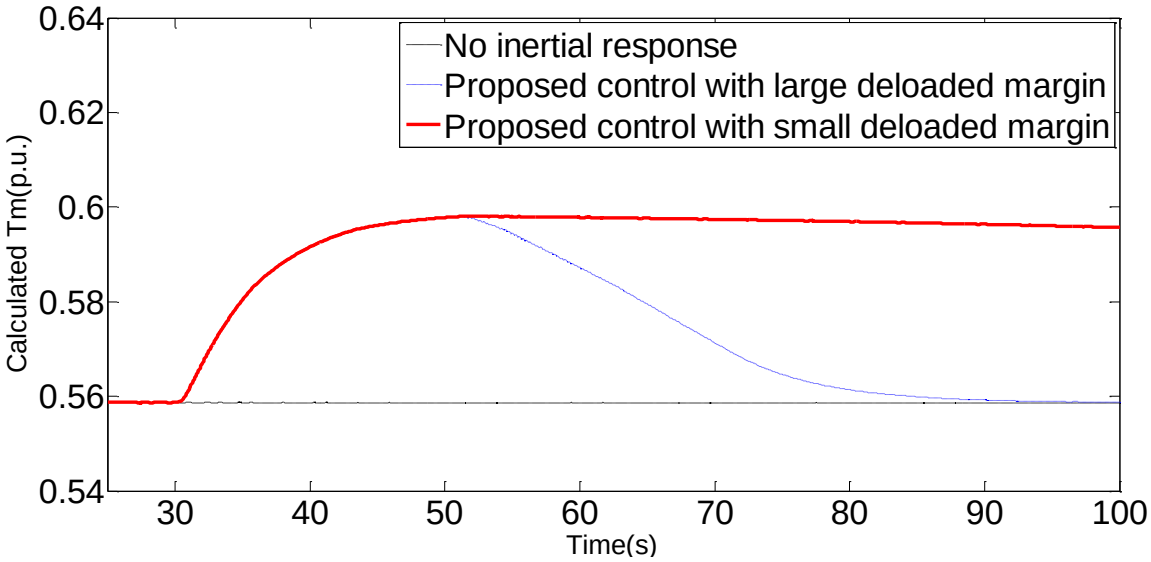

(d) Calculated mechanical torques

Figure 5.5 Simulation results for the electrical system of CART2-PMSG

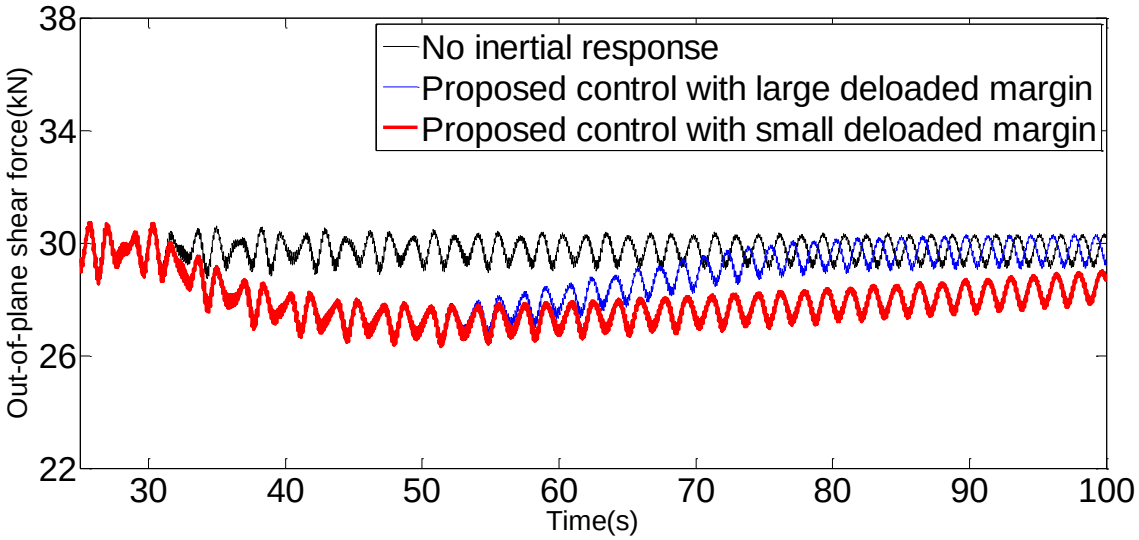

(a) Blade 1 out-of-plane shear force

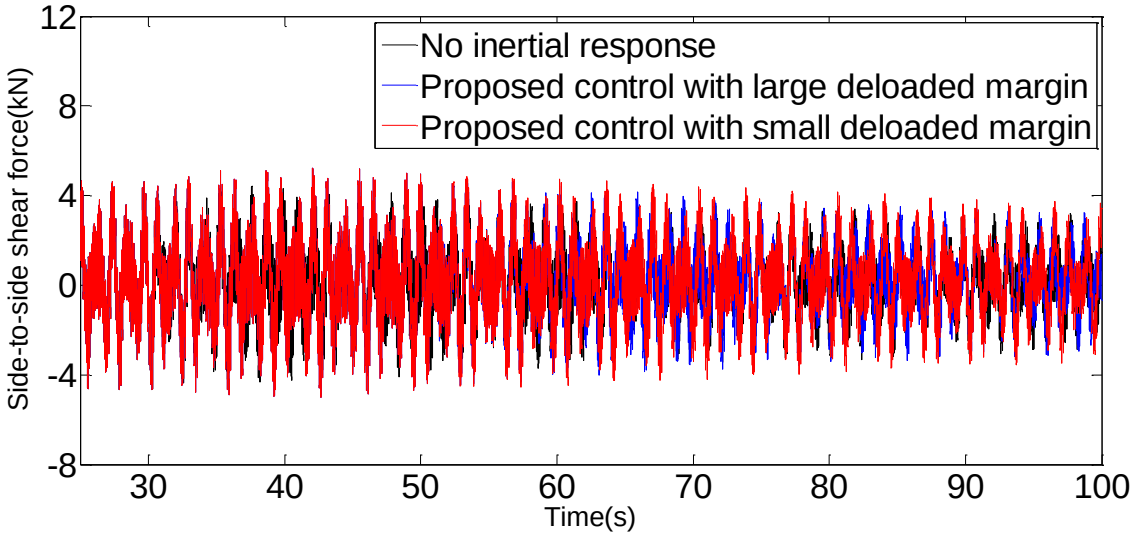

(b) Tower base side-to-side shear force

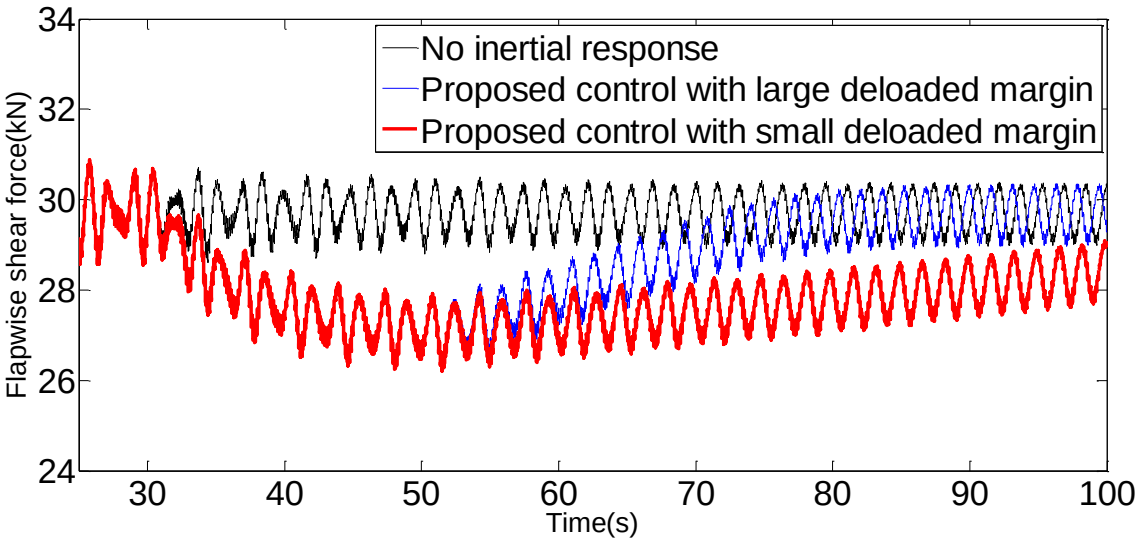

(c) Blade 1 flap-wise shear force

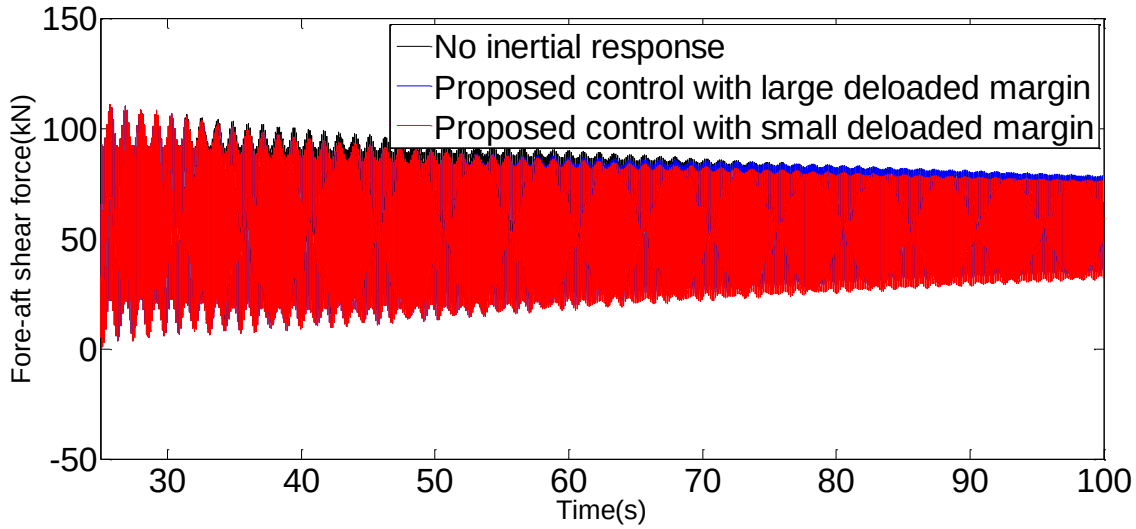

(d) Tower base fore-aft shear force

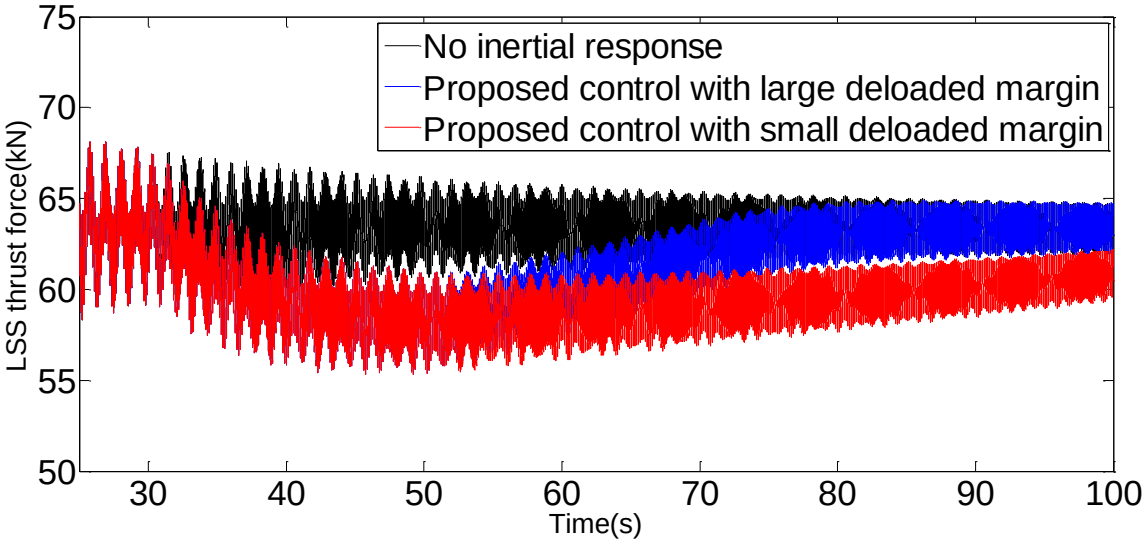

(e) Low-speed shaft thrust force/rotor thrust force

Figure 5.6 Simulation results for the mechanical stresses of CART2-PMSG

5.4 Comparison and Discussion

During the 1st stage of inertial response from 30s to 50s, Figure 5.4 shows the inertial response is activated to increase the electrical power to compensate for the power deficit caused by the SG3 trip. With the proposed inertial response, the kinetic energy stored in the rotating mass of the wind turbine is rapidly released and injected into the

grid through the power converter control. As a result, the overall frequency performance is substantially improved in terms of ROCOF, frequency nadir, and percentage overshoot, as shown in Table 5.1. Meanwhile, the risk of load disconnection triggered by the under-frequency load-shedding protection (UFLS) scheme is reduced throughout the initial inertial response. During this process, more response time is allowed for the online SG1 and SG2 with slow ramp rates to respond and fulfill the subsequent primary frequency regulation after WTG's inertial response. For this reason, the duration of the overloading operation for these two synchronous generators is shortened accordingly.

Table 5.1 Comparison of system frequency characteristics

Methods	ROCOF （Hz/s）	Frequency nadir （Hz）	Post-disturbance stable frequency (Hz)	Settling time （s）	The overshoot during the frequency recovery (Hz)
No auxiliary control	-0.269	59.42	59.81	48.37	59.86
The proposed inertial response with small deloaded margin	**-0.178**	**59.63**	**59.81**	**59.81**	**59.82**

In Figure 5.5, the rotor speed begins to decline as a result of the mechanical and electrical torque imbalance, and eventually it arrives at the secondary steady state, where the torque balance is reestablished. According to the lookup table about the power coefficient C_p versus TSR under a certain pitch angle, it is observed that the calculated

mechanical torque gradually rises until it reaches toward the steady value equal to the electrical torque. That is because the rotor speed, ω_0, corresponding to the MPPT power at Point A is higher than the counterpart corresponding to the maximum torque under a constant wind speed condition. As a result, the new steady-state torque is larger than the previous steady torque since the rotor speed gradually decreases. The DC link voltage is well maintained constant at a rated value of 1,200 V during the entire inertial response.

In Figure 5.6, there are no noticeable impacts on the tower and blade stress because of this sudden increase in electrical power. when the improved inertial response is performed. Actually, Blade 1's shear force, tower base flap-wise shear force as well as shaft thrust force tend to become slightly smaller through this inertial response stage. This is mainly because the decreasing rotor speed leads to decreasing TSR and likely decreasing thrust [85]. Therefore, the implementation of the proposed inertial control scheme in Region 2 does not adversely impact the mechanical components between the blades and the generator and thus is unlikely to jeopardize the wind turbine's lifetime.

During the 2nd stage of deloaded operation from 50s to 72s, the wind turbine with the ΔP_{de} of 0.03 p.u. can accelerate toward ω_2 and enter MPPT mode much faster than the case with the ΔP_{de} of 0.004, as shown in Figure. 5.4. During this course, SG1 and SG2 will increase the active power output by using droop control respectively to offset the reduced power output in the WTG and the frequency declines slightly as a result. Thus, the larger ΔP_{de} can make a quicker recovery of the rotor speed, whereas the more severe SFD occurs as shown in the enlarged image of Figure 5.4 (a). Thus, a small ΔP_{de} is preferred from the perspective of improving the frequency stability. In Figure 5.6, it is

noted that the blade 1 out-of-plane shear force and blade 1 flap-wise shear force gradually increases up toward the pre-disturbance value when rotor speed decelerates back to the previous optimal point. In meanwhile, the tower base fore-aft shear force continue to decline.

During the 3rd stage of the rotor speed recovery from 72s to 90s, Figure 5.5 (b) shows that the active power output of PMSG-WTG finally restores to the initial optimal state when rotor speed arrives at the pre-disturbance value. Due to the increase in the power output of PMSG-WTG, SG1 and SG2 smoothly decrease until getting stabilized at another steady state. For the case with the smaller de-loaded magnitude ΔP_{de}, WTG requires much longer time length to settle down at the MPPT point. However, Figure 5.4 shows there is no obvious impact on the grid frequency stability in contrast with the case with bigger ΔP_{de}. Similarly, all the shear forces tend to increase back to their original values, respectively except the tower base fore-aft one displayed in Figure 5.6.

5.3 Conclusion

In this work, an improved inertial control method based on the MPPT characteristic is presented for the purpose of enhancing the frequency regulation capability of PMSG-WTGs without additional power reserve. To illustrate its effectiveness, an integrated CART2-PMSG model equipped with the proposed inertial control is established in MATLAB/Simulink, and its frequency regulation performance is evaluated in the event of a single generator loss. Simulation results demonstrate that the improved inertial control enables the PMSG-WTG to arrest the ROCOF and improve the frequency nadir even in the low wind power penetration condition, whereas the proper

deloaded value can avoid an SFD throughout the rotor speed recovery process. Moreover, the application of the improved inertial control into the PMSG-WTG cannot cause any potential damage to the wind turbine's mechanical components when it is operating at a certain wind speed.

Chapter 6 Coordinated Control Strategy of BESS and PMSG-WTG to Enhance the Frequency Regulation Capability

A novel control method based on the torque limit (TLC) is proposed in this work for the purpose of maximizing the wind turbine (WT)'s inertial response and thus enhancing the temporary frequency support. To avoid the secondary frequency drop (SFD) caused by the WT's rotor speed recovery and deloaded operation, a small-scale battery energy storage system (BESS) is established and implemented to eliminate this impact and meanwhile assists the wind turbine in restoring to the MPPT mode by using the coordinated control strategy between BESS and PMSG-WTG. For the sake of reducing the costly use of BESS, this control strategy also enables BESS to withdraw smoothly while maintaining the system frequency within the scheduled range through coordination with other conventional generators using automatic generation control (AGC) system. Based on the simulation results, it is concluded the overall system frequency regulation performance can be significantly improved by coordinating BESS with PMSG-WTG for the inertial response. Furthermore, the potential impact of TLC on the WT's mechanical components during the inertial response is investigated by using the CART2-PMSG integrated model.

6.1 Torque Limit Control for Enhanced Inertial Response

Figure 6.1 illustrates the TLC-based inertial control strategy, which consists of three sequential stages as highlighted in the red line: inertial response (Line A-B-C), temporary deloaded operation (Line C-D-E), and rotor speed recovery (Line E-A). The dotted purple line represents the maximum power characteristics versus different rotor speeds along with the torque limit trajectory, and the black line indicates the mechanical power characteristics corresponding to a given wind speed and optimal pitch angle (-1 degree). The black dashed line shows the maximum mechanical power curve. Prior to a severe frequency event, a PMSG-WTG remains stable in MPPT mode, corresponding to ω_{MPPT} and P_{MPPT} at Point A. At the moment when an unacceptable frequency decline occurs, the PMSG-WTG instantly increases its active power output stepwise to Point B corresponding to the torque limit at the current rotor speed:

$$P_{ref\_1} = 1.2\omega_{MPPT} \tag{6.1}$$

Equation (6.1) is presented in per-unit and the torque limit is set to 1.2 p.u. to prevent the permanent damage due to an aggressive incremental torque. During the TLC-based inertial response, a certain amount of kinetic energy stored in the rotating mass is released when the rotor speed ω_{WT} is decelerated, since the electromagnetic torque is larger than the available mechanical torque. The active power output declines along Line B-C as rotor speed slows down.

Next, deloaded operation is triggered as long as rotor speed reaches the lower speed limit (e.g. 0.5p.u.) or frequency hits the nadir at the point C during the inertial

response. For the temporary deloaded operation, the active power command P_{ref_2} is described as

$$P_{ref\_2} = P_{de} = P_{ref\_1} - \Delta P_{de} \tag{6.2}$$

where, ΔP_{de} is the deloaded margin with 0.5p.u. set in this work. Note that the value of ΔP_{de} should be at least larger than the difference between $P_{ref\_1\_t}$ and P_{mec_t} at the moment t when PMSG-WTG switches to temporary deloaded mode from inertial response mode. During the rotor speed recovery, the rotor speed can smoothly move toward the original Point A along Line E-A, and it finally settles down at Point A as a result of the decreasing power imbalance. At this stage, the active power command P_{ref_3} remains constant as the optimal value:

$$P_{ref\_3} = P_{MPPT} = K(\omega_t)^3 \tag{6.3}$$

Note that the duration t for the inertial response and the deloaded value ΔP_{de} for the deloaded operation significantly impact the subsequent rotor speed recovery stage. That is because a relatively long-time inertial response tends to result in a much lower rotor speed and then a larger deloaded power is required to make the mechanical torque larger than the electrical torque so that the rotor speed is able to return to the point D. In this case, the duration for rotor speed from D to E will take much longer accordingly. In addition, a larger ΔP_{de}will more likely contribute to a more severe secondary frequency drop (SFD) due to the resulting temporary power shortage between P_C and P_D. Therefore, the application of BESS is introduced in the following section so as to prevent the SFD issue and assist the fast rotor speed recovery of wind turbine.

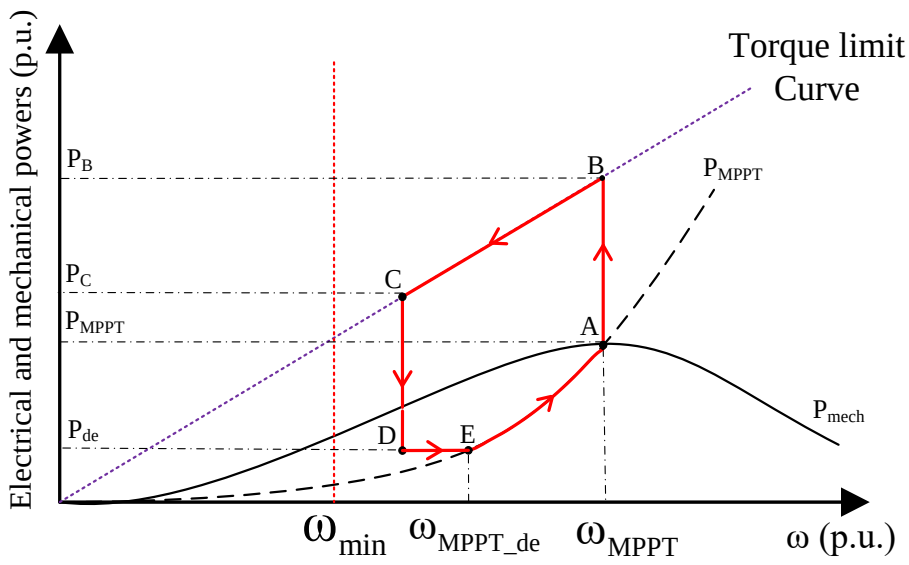

Figure 6.1 Power–rotor speed trajectory for TLC

The detailed control strategy of TLC implemented in MATLAB/Simulink is described in Figure 6.2. A disturbance detector is utilized to trigger the inertial response if the frequency deviation exceeds 0.1 Hz and meanwhile sustains for a period of 50 ms. Provided either condition in (4) is met for a specified period of time (50ms), the deceleration of rotor speed will suspend and then the frequency support is accomplished. At this moment, the power command is switched from the inertial response to temporary deloaded operation via the deloaded operation detector.

$$f_t - f_{t-1} > 0 \;\&\; \omega_t > \omega_{min}\ (0.5\ \text{p.u.})$$
$$\text{or}\ \ f_t - f_{t-1} < 0 \;\&\; \omega_t = \omega_{min}\ (0.5\ \text{p.u.}) \qquad (6.4)$$

where f_t is the frequency at the moment t (s) and f_{t-1} is the frequency at the moment t-1 (s). ω_t is the rotor speed at the moment t (s). During the deloaded operation, the power command is changed to MPPT value through the inertial recovery detector if the condition (5) is met for a specified period of time (50 ms). This criterion ensures that

the active power output can rise from Point E moving along Line E-A without causing any possible decline.

$$\omega_t \geq \omega_{MPPT} \tag{6.5}$$

where ω_{MPPT_de} is the optimal rotor speed when WT operates at the deloaded power level, $P_{ref\_2} = P_{de}$. In other words, ω_{MPPT_de} corresponds to the rotor speed at the point E. Note that the power magnitude limiter and its rate limiters are also added to this integrated model to avoid the excessive stress and over load imposed on the wind turbine's mechanical components when performing the proposed inertial response.

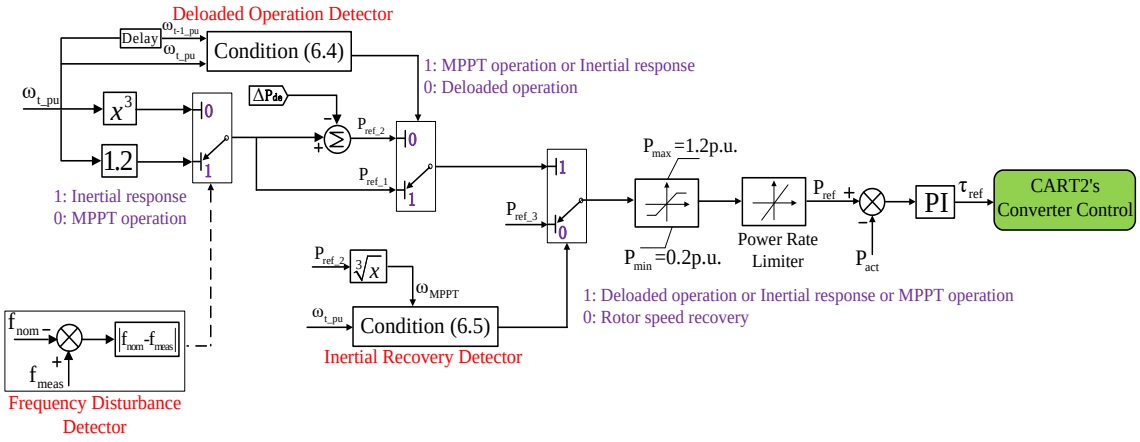

Figure 6.2 Control block of the complete TLC inertial response scheme

6.2 Dynamic Modeling of BESS

6.2.1 Modelling of Battery Module

The dynamic model of 1MWh battery energy storage system (BESS) is designed based on the built-in battery module in MATLAB/Simulink. The basic parameters of BESS are listed in the Table 6.1. An aggregated model is used to represent the general characteristics of energy storage station that comprises a multiple of single cells connected in parallel and series combination. It serves the purpose of improving the

simulation efficiency and accurately representing the dynamic characteristics of BESS that participates in the coordinated system frequency control [87].

Table 6.1 The parameters of lead-acid battery

Battery Type	Lead-acid
Rated power output (MW)	2
Rated energy capacity (MWh)	1
Nominal voltage (V)	769
Rated capacity (Ah)	1302.1
Initial state of charge (%)	50
Fully charged voltage (V)	895.11
Nominal discharge current (A)	2600.8
Internal resistance (ohms)	0.00295
Capacity (Ah) @ nominal voltage	1177.55

The Simulink module of battery implements a generic dynamic model to carry out the corresponding simulations in accordance with various type of rechargeable batteries. Compared with the real physical model, this module shows a maximum error of 5% when SOC is between 10% and 100% for charge current between 0 and 2C as well as discharge current between 0 and 5C. So, it completely satisfied the demand on simulation accuracy. The equivalent circuit of battery model is depicted in Figure 6.3.

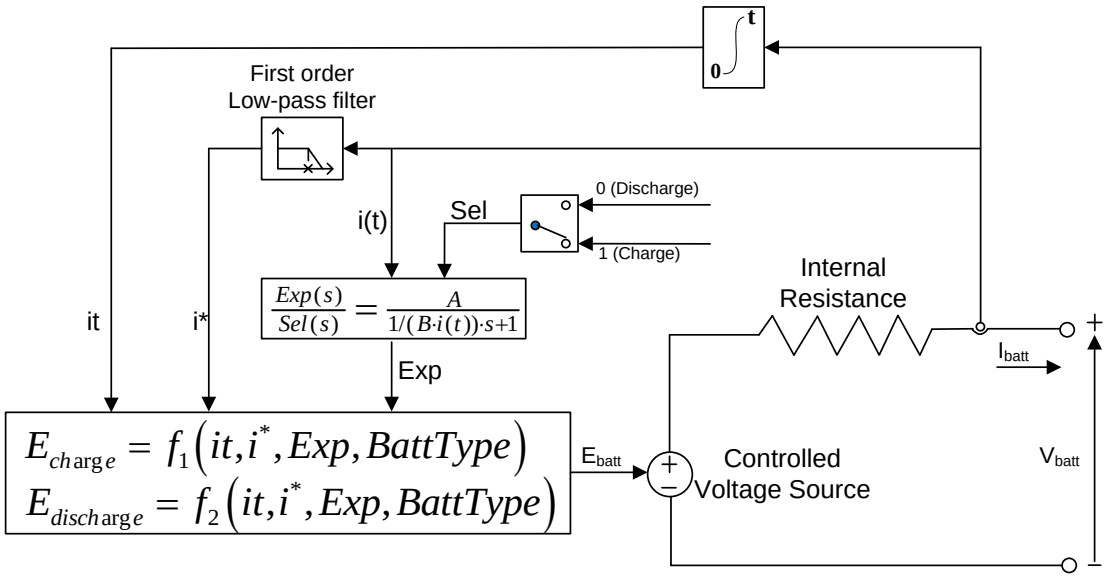

Figure 6.3 Equivalent circuit of the generic battery [87]

The mathematical equations of charge and discharge modes for Lead-Acid model are expressed:

Discharge mode (i*>0)

$$f_1(it,i^*,i,Exp)=E_0-K\times\frac{Q}{Q-it}\times i^*-K\times\frac{Q}{Q-it}\times it+Laplace^{-1}\left(\frac{Exp(s)}{Sel(s)}\times 0\right) \quad (6.6)$$

Charge mode (i*<0)

$$f_1(it,i^*,i,Exp)=E_0-K\times\frac{Q}{it+0.1\times Q}\times i^*-K\times\frac{Q}{Q-it}\times it+Laplace^{-1}\left(\frac{Exp(s)}{Sel(s)}\times\frac{1}{s}\right) \quad (6.7)$$

where,

E_{batt} = Nonlinear voltage (V)

E_0 = Constant voltage (V)

Exp(s) = Exponential zone dynamics (V)

Sel(s) = Represents the battery mode:

Sel(s) = 0 during battery discharge, Sel(s) = 1 during battery charging

K = Polarization constant (Ah^{-1}) or Polarization resistance (Ohms)

i* = Low frequency current dynamics (A)

i = Battery current (A)

it = Extracted capacity (Ah)

Q = Maximum battery capacity (Ah)

Depending on the specific battery type, the typical discharge-characteristic curve can be shown in the Figure 6.4.

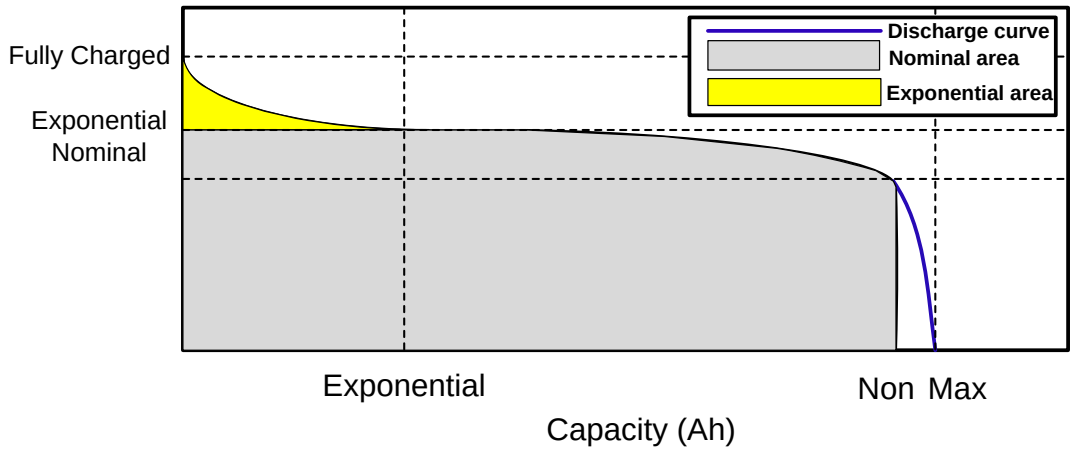

Figure 6.4 Typical discharge characteristics of generic battery [87]

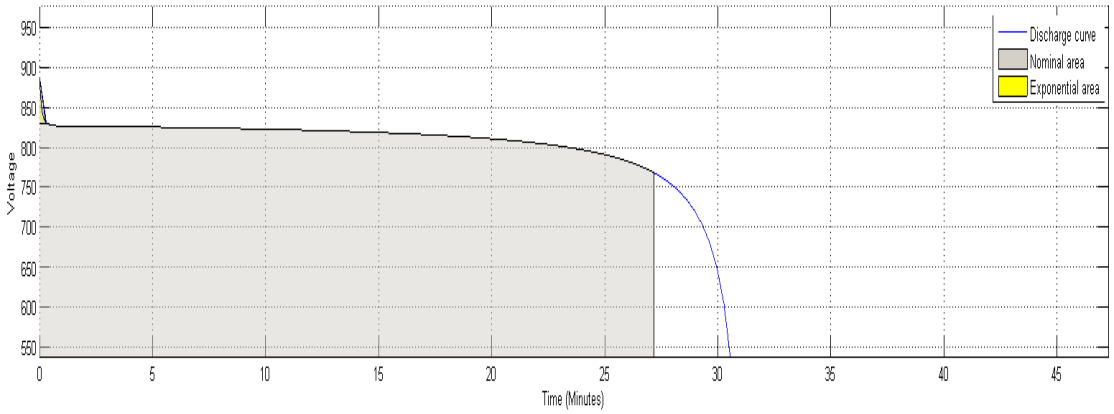

Figure 6.5 Nominal current discharge characteristic for specified lead-acid battery [87]

In Figure 6.5, the curve includes three different sections during the battery discharge process. The yellow exponential area represents the exponential change in the voltage when the battery is in full charge mode. According to various battery types, the size and shape of area vary slightly. The grey nominal area indicates the total energy discharged from the battery until the voltage drops below the nominal value. Lastly, the blank section shows the voltage tends to decline rapidly when the battery totally discharges.

6.2.2 Modeling and Control of BESS Inverter

As shown in Figure 6.6, the DC power output of battery energy storage system can be converted into the three-phase 60Hz AC power through the power inverter[78]-[79].

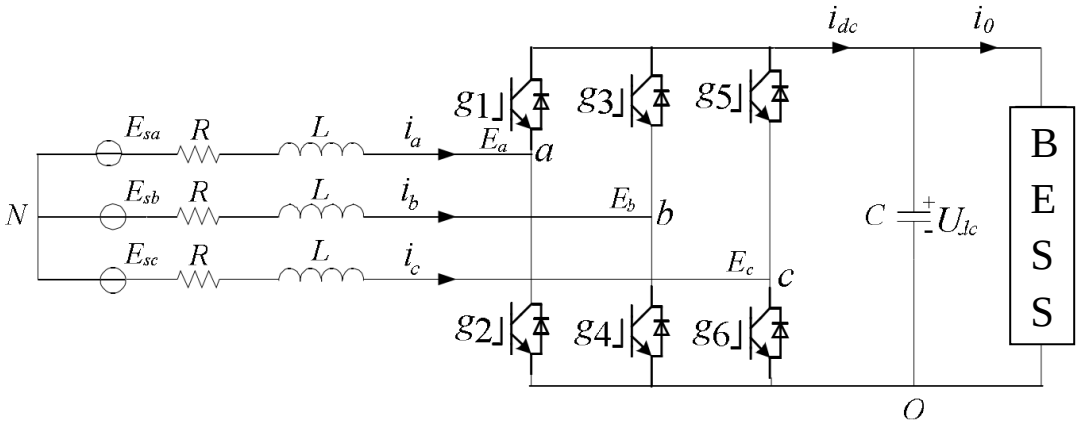

Figure 6.6 Inverter structure of BESS in the charging mode

According to the Kirchhoff's Law, assuming the impact of zero-sequence and modulation frequency is neglected, differential equations of current and voltage in 3-phase coordinate system can be expressed as follows:

$$\begin{cases} L\frac{di_a}{dt} + Ri_a = E_{sa} - E_a \\ L\frac{di_b}{dt} + Ri_b = E_{sb} - E_b \\ L\frac{di_c}{dt} + Ri_c = E_{sc} - E_c \end{cases} \tag{6.8}$$

During the inverter operation, switching signals of upper and lower bridge arms work as complementary PWM signals. At one moment, only one bridge is on while the other is off. The correlation is described as

$$S_k = \begin{cases} 1 & \text{k phase upper bridge arm is on and lower one is off} \\ 0 & \text{k phase lower bridge arm is on and upper one is off} \end{cases} \quad (k=a,b,c) \tag{6.9}$$

Take phase A as an example, when the upper bridge arm is on ($g_1 = 1$), the lower bridge arm is off ($g_2 = 0$). The voltage E_{ao} between point "a" and point "o" should be equal to U_{dc}. In contrast, when the upper bridge arm is off ($g_1 = 1$), the lower bridge arm is on ($g_2 = 1$). The voltage E_{ao} between point "a" and point "o" should be 0. The other two phases can apply in the same way. The correlation equation can be expressed:

$$E_{kO} = s_k \cdot U_{dc} \ (k = a, b, c) \tag{6.10}$$

Assume E_{NO} is voltage between AC-side neural point and DC-side "O" point, the three-phase voltages are obtained:

$$\begin{aligned} E_{aN} &= E_{aO} - E_{NO} \\ E_{bN} &= E_{bO} - E_{NO} \\ E_{cN} &= E_{cO} - E_{NO} \end{aligned} \tag{6.11}$$

From the above equations, we can derive the following ones:

$$E_{NO} = \frac{1}{3}(E_{aO} + E_{bO} + E_{cO}) - \frac{1}{3}(E_{aN} + E_{bN} + E_{cN}) \tag{6.12}$$

Since three phases variables are balanced at AC side, we can have the equation as $E_{aN} + E_{bN} + E_{cN} = 0$. Thus, e.q. (6.12) can be rewritten as

$$E_{NO} = \frac{1}{3}(E_{aO} + E_{bO} + E_{cO}) \tag{6.13}$$

Accordingly , three phase voltages are represented as

$$\begin{cases} E_{aN} = \left(s_a - \frac{1}{3}\sum_{k=a,b,c} s_k\right) \cdot U_{dc} \\ E_{bN} = \left(s_b - \frac{1}{3}\sum_{k=a,b,c} s_k\right) \cdot U_{dc} \\ E_{cN} = \left(s_c - \frac{1}{3}\sum_{k=a,b,c} s_k\right) \cdot U_{dc} \end{cases} \tag{6.14}$$

Based on e.q. (6.14), AC voltages of inverter are determined by the switching signal S_k. And the switching functions are defined as

$$\begin{cases} m_a = s_a - \frac{1}{3}\sum_{k=a,b,c} s_k \\ m_b = s_b - \frac{1}{3}\sum_{k=a,b,c} s_k \\ m_c = s_c - \frac{1}{3}\sum_{k=a,b,c} s_k \end{cases} \tag{6.15}$$

According to three-phase current and voltage equations of inverter, the following equations can be obtained:

$$\begin{cases} L\frac{di_a}{dt} + Ri_a = E_{sa} - m_a U_{dc} \\ L\frac{di_b}{dt} + Ri_b = E_{sb} - m_b U_{dc} \\ L\frac{di_c}{dt} + Ri_c = E_{sc} - m_c U_{dc} \end{cases} \tag{6.16}$$

where, the relation between DC-side voltage U_{dc} and DC-side current i_{dc} is given by

$$C\frac{dU_{dc}}{dt} = i_{dc} - i_0 = m_a i_a + m_b i_b + m_c i_c \tag{6.17}$$

Since the above model is established in the 3 phase stationary reference frame, the voltages and currents at the AC side are time-varying variables. To facilitate the design and application of controllers, the mathematical model represented in three-phase (abc)

stationary reference frame can be transformed into two-phase model in a rotational reference frame defined by the d (direct)-q (quadrature) axes that are perpendicular to each other, so that the DC variables can be acquired. So, equations of inverter at the DC and AC sides are converted as：

$$\frac{d}{dt}\begin{bmatrix} i_d \\ i_q \end{bmatrix} = \begin{bmatrix} -\frac{R}{L} & \omega \\ -\omega_1 & -\frac{R}{L} \end{bmatrix}\begin{bmatrix} i_d \\ i_q \end{bmatrix} - \begin{bmatrix} \frac{U_{dc}m_d - E_{sd}}{L} \\ \frac{U_{dc}m_q}{L} \end{bmatrix} \tag{6.18}$$

$$\frac{dU_{dc}}{dt} = \frac{m_d i_d + m_q i_q - i_0}{C} \tag{6.19}$$

where, ω is angular frequency of phase voltage at the AC side, E_{sd} is direct-axis component of AC voltage, i_d and i_q are direct-axis and quadrant-axis components of AC current, respectively. Similarly, m_d and m_q are the d and q-axis components of switching function respectively.

The real and reactive power output can be given by

$$\begin{cases} P = E_{sd} i_d \\ Q = -E_{sd} i_q \end{cases} \tag{6.20}$$

If the AC side three-phase parameters are exactly same, E_{sd} remains constant value。So, real and reactive power outputs are related with i_d and i_q, respectively. In other words, i_d and i_q can be independently controlled by adjusting P and Q separately. To achieve this objective, the converter model in d-q reference frame is transformed in the following way:

$$\begin{cases} L\frac{di_d}{dt} = -Ri_d + \omega L i_q + E_{sd} - V_d \\ L\frac{di_q}{dt} = -Ri_q - \omega L i_d + E_{sq} - V_q \end{cases} \tag{6.21}$$

where, V_d and V_q are the d-axis and q-axis components of AC-side voltage output of inverter. According to e.q. (6.21), it indicates id and i_q will be affected by the controls of V_d and V_q respectively, but also influenced by current coupling items of ωLi_d and ωLi_q as well as AC voltage E_{sd} and E_{sq}. In order to eliminate their impacts, one feed-forward compensation method is adopted to realize the decoupling control.

v'_d, v'_q and Δu_d, Δu_q can be defined as：

$$\begin{cases} v'_d = L\frac{di_d}{dt} + Ri_d \\ v'_q = L\frac{di_q}{dt} + Ri_q \end{cases}, \quad \begin{cases} \Delta u_q = \omega Li_q \\ \Delta u_d = \omega Li_d \end{cases} \tag{6.22}$$

The inverter model in the d-q reference frame can be transformed as follows：

$$\begin{cases} V_d = E_{sd} - v'_d + \Delta u_q \\ V_q = E_{sq} - v'_q + \Delta u_d \end{cases} \tag{6.23}$$

Due to the first order differential relation between v'_d and i_d as well as v'_q and i_q, decoupling item v'_d and v'_q can be obtained using Proportional-Integral loop:

$$\begin{cases} v'_{d1} = k_{p1}(i_{dref} - i_d) + k_{i1}\int (i_{dref} - i_d)dt \\ v'_{q1} = k_{p2}(i_{qref} - i_q) + k_{i2}\int (i_{qref} - i_q)dt \end{cases} \tag{6.24}$$

where, i_{dref} and i_{qref} are reference values for active power current i_d reactive power current i_q, respectively.

Based on the above analysis, the state equations can be fully decoupled by adding the voltage decoupling compensation items Δu_d and Δu_q. As shown in Figure 6.7, a phase locked loop (PLL) is utilized for the detection of the grid voltage angle that synchronizes the BESS with power grid during the dq/abc or abc/dq transformation. The d-axis of the synchronous frame is aligned with the grid voltage vector, so that the d-axis

grid voltage is equal to the magnitude of grid voltage and meanwhile q-axis voltage is equal to zero. Due to the inverter's PWM four-quadrant operation, the BESS is capable of adjusting the magnitude and direction of real power and reactive power respectively according to the system operation requirement. The inverter control is implemented in the grid voltage oriented d-q reference frame where the direct-axis current component i_d is in charge of the real power regulation while the quadrature-axis current component i_q is responsible for the reactive power regulation. Note that the power flow direction can be determined by setting the sign of P and Q reference values: positive (deliver power to grid) or negative (absorb power from grid), respectively [79], [88]-[89].

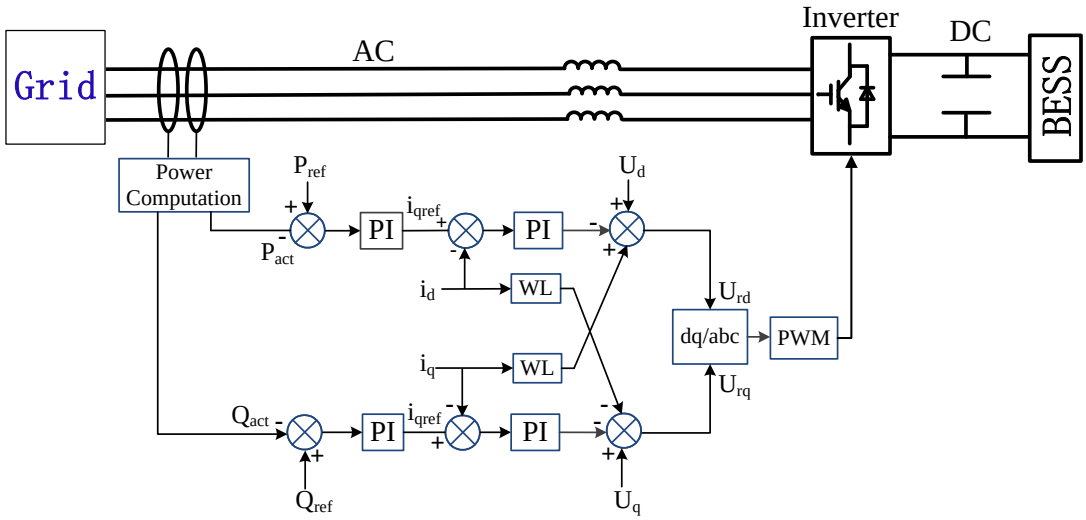

Figure 6.7 Control structure of BESS's inverter

6.2.3 Frequency Support Control of BESS for Inertial Recovery of PMSG-WTG

In order to eliminate the SFD as a result of the PMSG-WTG's deloaded operation, a novel frequency support control strategy is designed for BESS with the purpose of assisting the inertial recovery of PMSG-WTG and reducing its power output to previous

level (zero) when the frequency reaches the post-disturbance steady state [79]. The specific control strategy is illustrated in Figure 6.8.

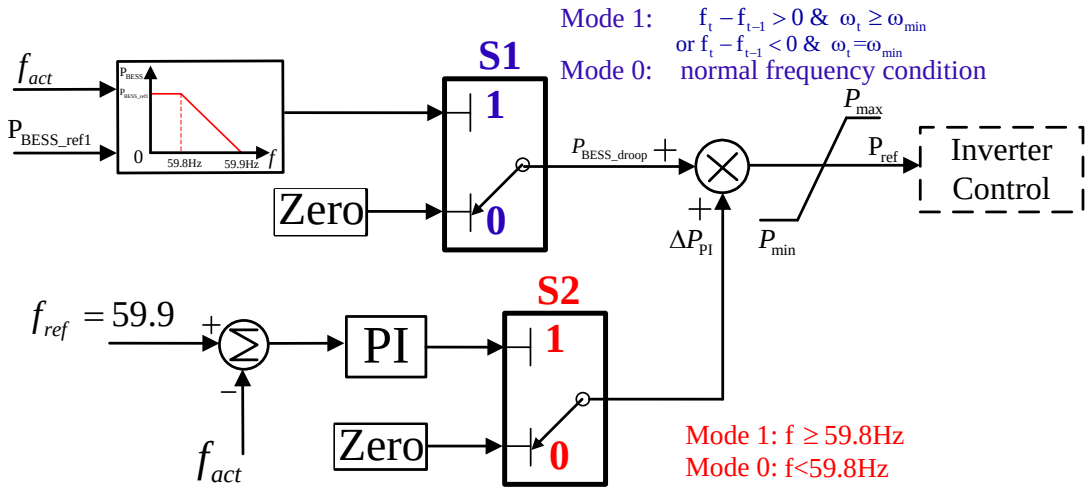

Figure 6.8 Control block of BESS participating in the coordinated frequency control

S1 normally remains in the mode 0. Provided the PMSG-WTG starts to operate in the deloaded condition, S1 is switched to mode 1 with the initial power output P_{BESS_ref1} as given by the following equation:

$$P_{BESS\_ref1} = P_{ele\_t} - P_{ele} \tag{6.25}$$

where, P_{ele_t} refers to the active power output at the moment "t" prior to PMSG-WTG's deloaded operation. P_{ele} represents the real-time active power output of PMSG-WTG throughout the inertial recovery period. P_{BESS_ref1} is set to compensate for the power imbalance when the rotor speed and kinetic energy of wind turbine recover to the pre-disturbance condition. However, this amount of injected power may be excessively larger than the power deficit demanded by the system, it more likely results in a overshoot in the steady frequency. To avoid this impact, the power output ought to be gradually and timely descended to a certain level that allows the frequency to stay in the acceptable frequency range, at least above the threshold for enabling the inertial response

of PMSG-WTG (e.g. 59.9Hz). A simple droop method is applied to adjust the power output according to the frequency measured in real time if the rising frequency exceeds a certain threshold (59.8Hz). In this case, S2 is switched to mode 1 to fulfill this function in Figure 6.8. The power reference P_{BESS_droop} can be accordingly expressed as

$$P_{BESS\_droop} = -P_{BESS\_59.8} \times \frac{(f-59.8)}{59.9-59.8} + P_{BESS\_59.8} \tag{6.26}$$

where, $P_{BESS\_59.8}$ is the BESS power output recorded at the frequency of 59.8Hz, f is frequency measured in real time. To mitigate the impact due to the reduction in P_{BESS_ref2}, an additional control loop is introduced by PI controller so as to maintain the system frequency eventually stable at the 59.9Hz. Thus, the general power reference of BESS can be described as

$$P_{BESS\_ref} = \begin{cases} P_{BESS\_ref1} = P_{ele\_t} - P_{ele}, & f < 59.8Hz \\ P_{BESS\_ref2} = P_{BESS\_droop} + \Delta P_{PI}, & 58.8Hz \le f \le 59.9Hz \\ P_{BESS\_ref3} = P_{BESS\_59.9} + \Delta P_{PI}, & f = 59.9Hz \end{cases} \tag{6.27}$$

where, $P_{BESS\_59.9}$ is the power output of BESS at the moment when the steady frequency reaches 59.9Hz. ΔP_{PI} refers to the power reference generated from PI controller. Another function of PI controller is to reduce the BESS's power output toward zero when other conventional generators raise their power outputs respectively by allocating P_{BESS_ref3} in terms of the available reserve margin of each generator. Using this method, the system frequency can remain around the 59.9 Hz until the proposed coordinated frequency regulation is completed. During the BESS energy recovery process, the total power increased by all the conventional generators should be equal to

the power output of BESS at the moment when frequency is stable at 59.9Hz. The relevant equations can be expressed as follows:

$$P_{BESS\_ref3} = \sum_{i=1}^{n} \Delta P_{AGC\_Gi} \tag{6.28}$$

$$\Delta P_{AGC\_Gi} = \frac{P_{Gi\_re}}{\sum_{i=1}^{n} P_{Gi\_re}} \times P_{BESS\_ref3} \tag{6.29}$$

where, ΔP_{AGC_Gi} is the incremental power for the i^{th} generator, n is the total number of the conventional generators involved in the BESS energy recovery by increasing their own power outputs, P_{Gi_re} is the available reserve margin of the i^{th} generator.

6.3 Coordinated Control Strategy of BESS and PMSG-WTG

As discussed before, the application of TLC inertial control enables PMSG-WTG to maximize its inertial response in order to enhance the temporary frequency support. As a result, the frequency nadir is dramatically raised and also ROCOF is reduced compared to the case without auxiliary frequency control. However, severe SFD will follow as a result of the deloaded power margin ΔP_{de} before the rotor-accelerating process of wind turbine proceeds. Thus, a coordinated control strategy is developed for BESS, PMSG-WTG and other synchronous generators equipped with a certain spinning reserve in a bid to improve the overall system frequency regulation capability by eliminating the SFD and accelerating the frequency recovery. Meanwhile, it can ensure that BESS can smoothly withdraw from the temporary frequency support that can be taken over by other conventional generators through AGC when the frequency reaches the post-disturbance steady condition.

The flow chart of detailed overall coordinated control strategy for PMSG-WTG, BESS and other selected conventional generators is illustrated in Figure 6.9. It is worth noting that the proposed control strategy mainly concentrates on how to effectively coordinate BESS and PMSG-WTG to address the under-frequency and SFD issues, since the over-frequency event can be easily solved by reducing the wind power output through the pitch angle control or rotor speed control. The proposed control strategy mainly include three phases:

Stage 1 - PMSG-WTG Inertial Response: By using frequency detection system, once system frequency drops below 59.9Hz and sustained time exceeds 50ms of time delay and meanwhile rotor speed remains above 0.5 p.u.(allowable minimum rotor speed), PMSG-WTG is allowed to provide the inertial response based on TLC method.

Stage 2 - BESS Frequency Support: When rotor speed reaches 0.5 p.u. and frequency remains in the declining stage or frequency arrives at the frequency nadir and rotor speed is above 0.5 p.u., the deloaded operation of wind turbine will come into effect. At this moment, in order to compensate for the power deficit due to the deloaded margin and eliminate the resultant SFD issue, BESS will immediately provide the active power P_{BESS_ref1}. During this stage, the system frequency tends to keep rising all the time until reaching the post-disturbance steady state. To prevent the transient overshoot at the steady state, one simple preventive measure mentioned above is employed to stabilize the frequency around 59Hz by gradually reducing the BESS's power output if system frequency goes higher than 59.8Hz. Note that the PMSG-WTG can continue to restore its rotor speed to the pre-disturbance level without inducing the potential SFD problem.

Stage 3 - BESS Energy Recovery: Once the system frequency is able to become stabilized at a specified value for a period of time delay, a coordinated control scheme for BESS and other conventional generators will play a role in enabling other synchronous generators equipped with a certain headroom to take over the active power supplied by BESS while maintaining the frequency stable at the post-disturbance value. In this way, BESS can gradually reduce its power output and its operation time participating in the temporary frequency regulation is shorten. At the same time, other conventional generators can take sufficient time to proportionally increase the additional power output of ΔP_{AGC} using AGC system, which is in charge of changing the load reference set points of selected generating units upon the command. The allocation of ΔP_{AGC} is in proportion to the reserve power margin of each synchronous generator available for this control function. Generally, the larger reserve the generator has, the bigger participation factor it is given, the more active power the corresponding generator will generate. The entire coordinated frequency regulation process is accomplished when active power output of BESS is reduced to zero and its SOC restores to the previous level of 50% by charging the power from grid.

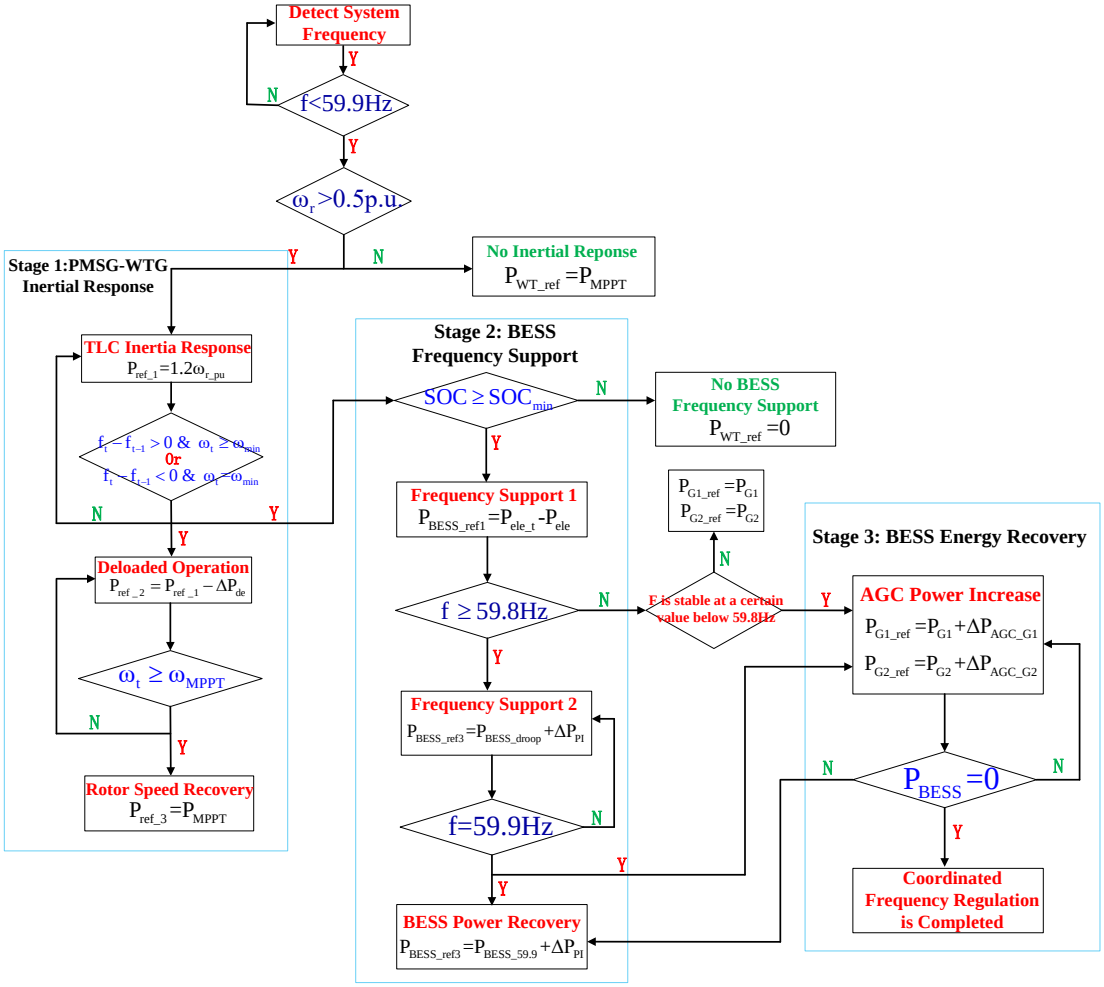

Figure 6.9 Flow chart of coordinated control scheme for PMSG-WTG, BESS and other conventional generators

6.4 Test System with Integration of CART2-PMSG and BESS

A small power system model is established using the Matlab/Simulink platform. As depicted in Figure 6.10, a 60Hz simple power system consists of an aggregated CART2-PMSG based wind farm, three synchronous generators, a small-scale BESS and one constant power load. The 3MW wind farm consisting of 5 single CART2 wind turbines is connected to the point of common coupling (PCC) via a 575/35kV step-up transformer. The three synchronous generators are based on the thermal power plant with IEEE standard steam turbine governor and type 1 excitation system [47]. The inertial

time constant for the 10-MVA SG1, 5.2-MVA SG2, and 0.9MVA SG3 are set as 5s, 4.2s and 3.5s respectively while droop coefficient for all generators is uniformly set as 5%. The baseline operating points for SG1 and SG2 are about 0.76 p.u. of their rated capacities to ensure a certain power headroom for performing the primary frequency regulation. And the initial operating point of SG3 is set as 1 p.u., namely operating at the rated condition. The wind power penetration level of this small grid system is approximately 10.4% when CART2-PMSG operates at the given wind speed of 10m/s. The capacity of BESS is 1MW/h and rated power output is 1MW as shown in Table 1.

In order to evaluate the effectiveness of the TLC method, the SG3 is tripped off the grid at t=30s, resulting in a severe frequency decline due to the transient power imbalance and reduced system inertia. Thus, differences in the frequency regulation performance can be noticeably observed through the following four scenarios: no auxiliary frequency control, TLC without BESS involved, as well as the proposed coordinated frequency control.

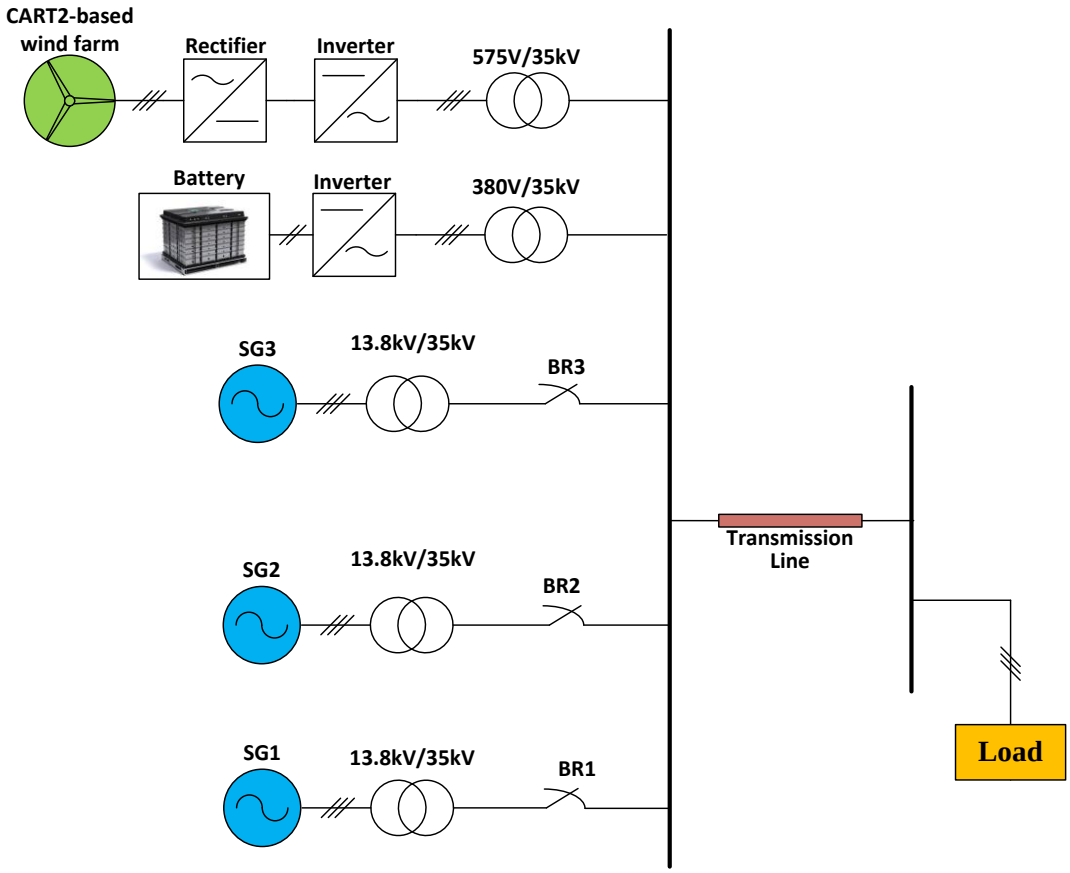

Figure 6.10 Basic configuration of a small-scale power grid system

6.5 Simulation Results

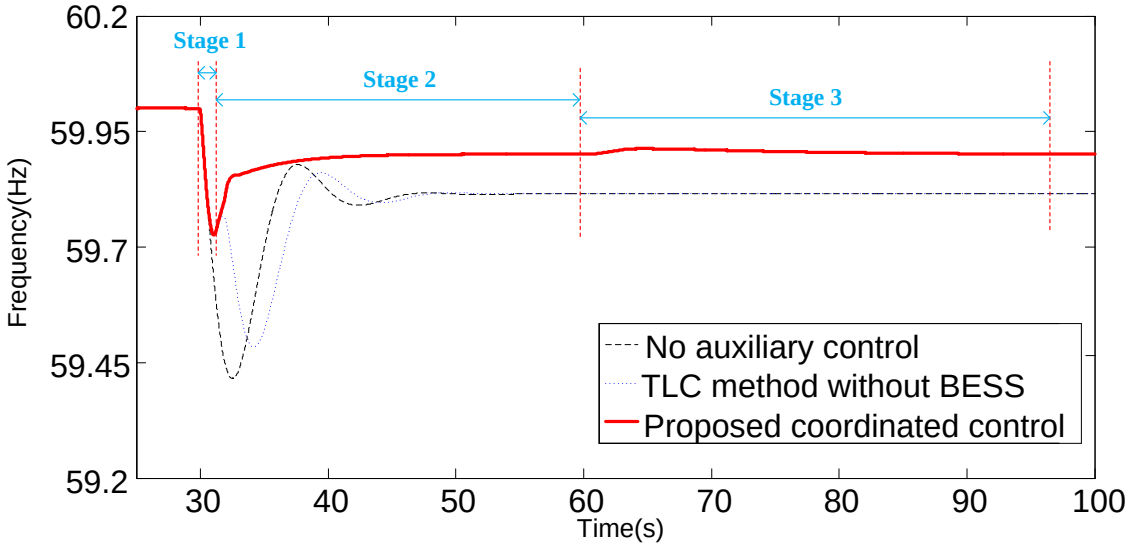

(a) System frequency

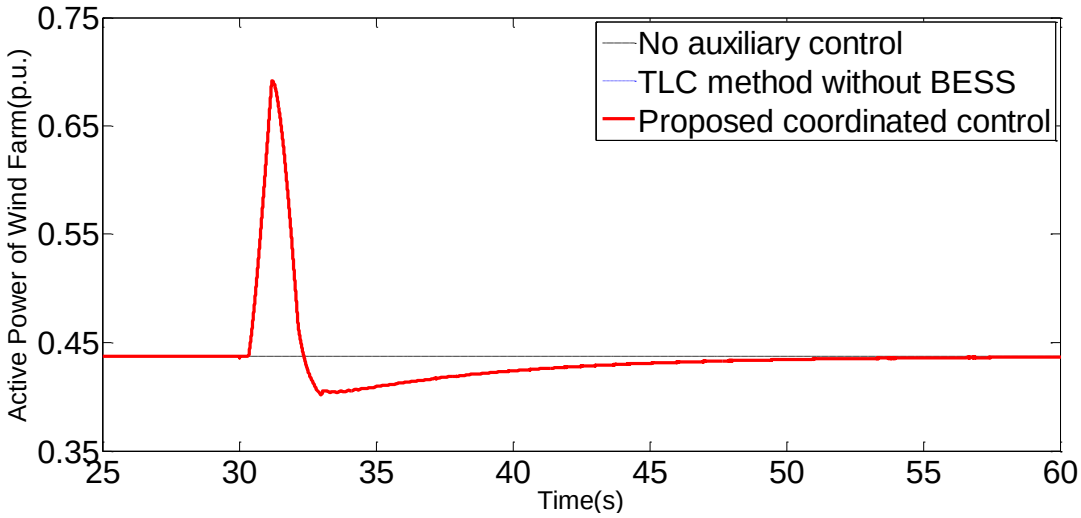

(b) Active power output of CART2-PMSG-based wind farm

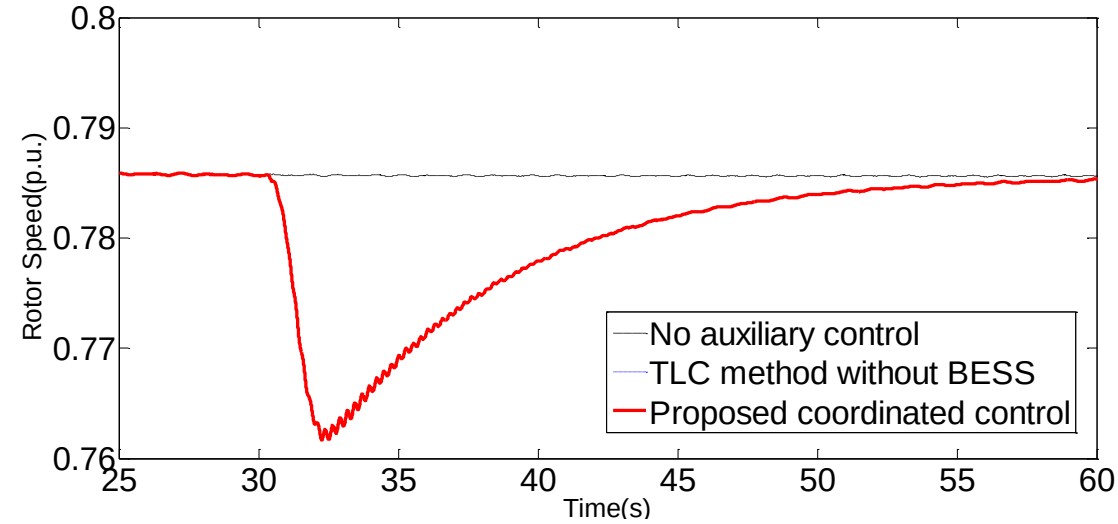

(c) Rotor speed

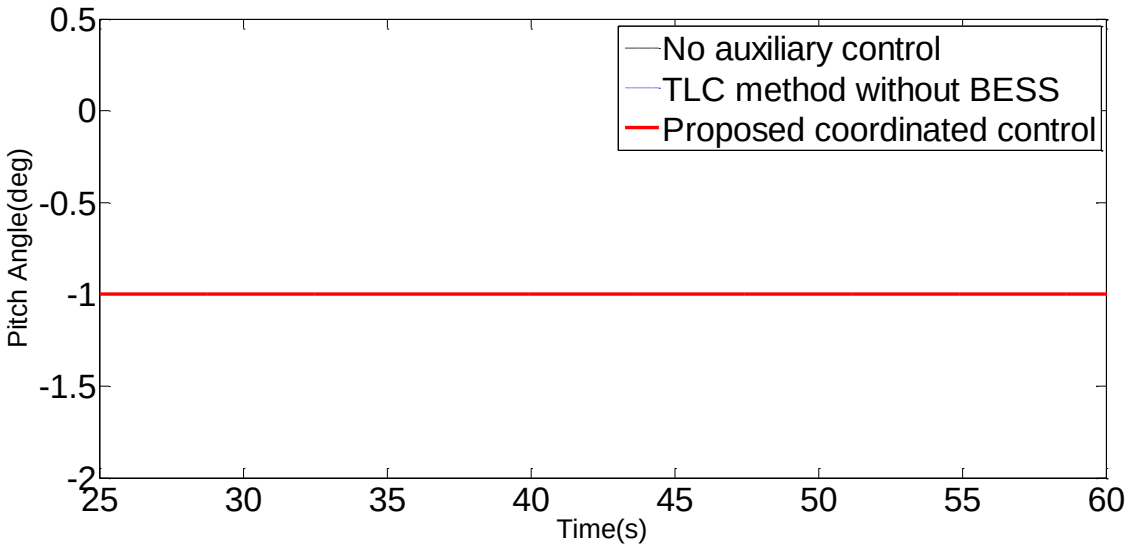

(d) Pitch angle

Figure 6.11 Simulation results of electrical system of CART2-PMSG

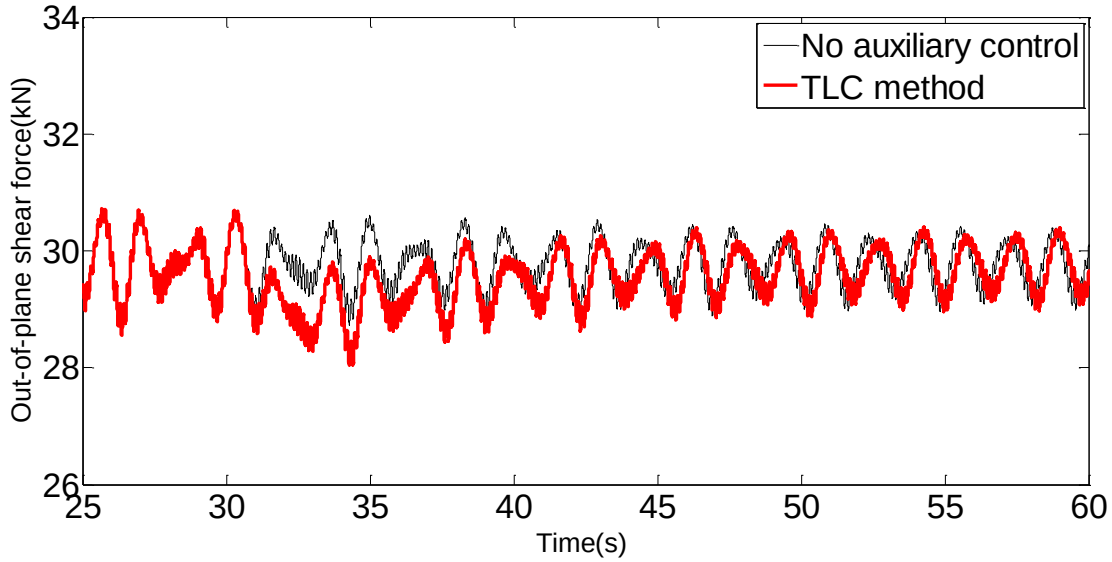

(a) Blade 1 out-of-plane shear force

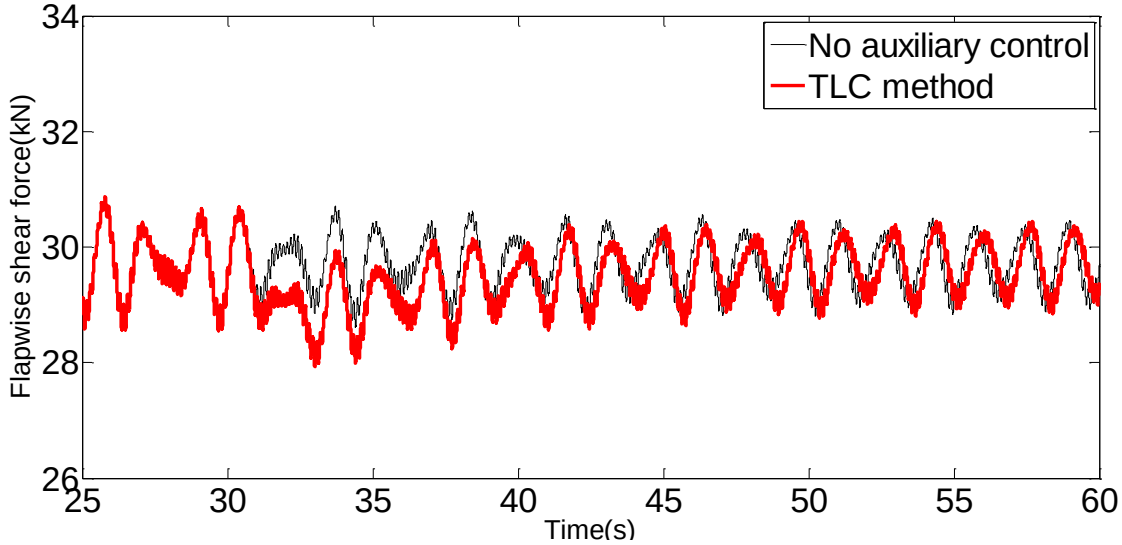

(b) Blade 1 flap-wise shear force

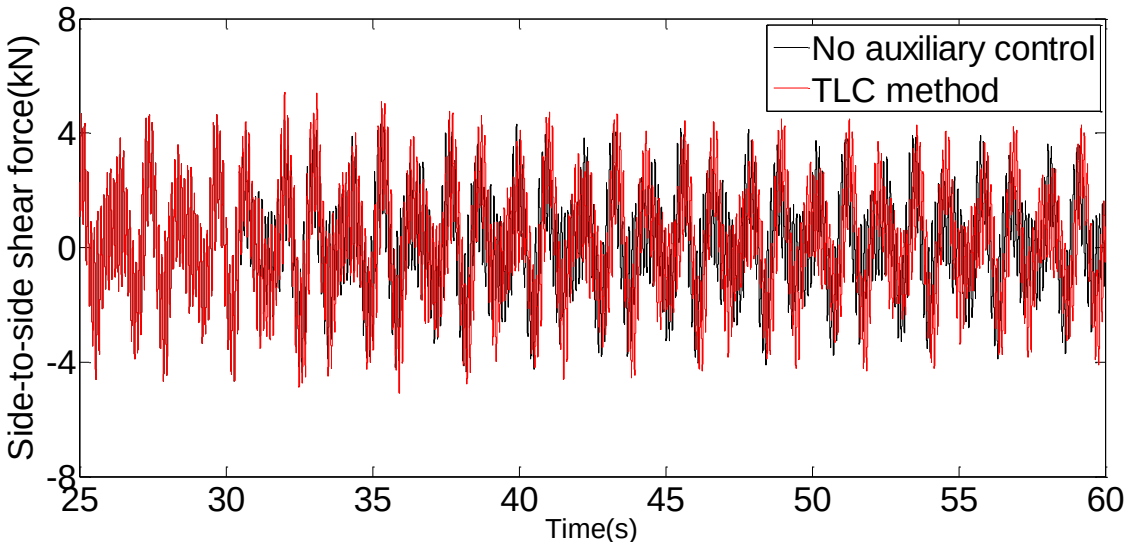

(c) Tower base side-to-side shear force

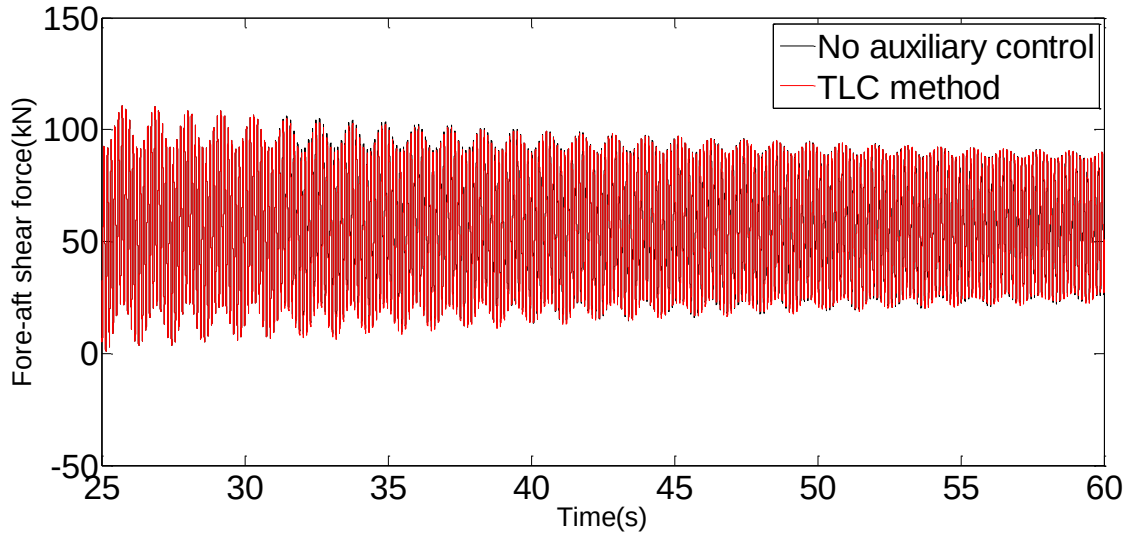

(d) Tower base fore-aft shear force

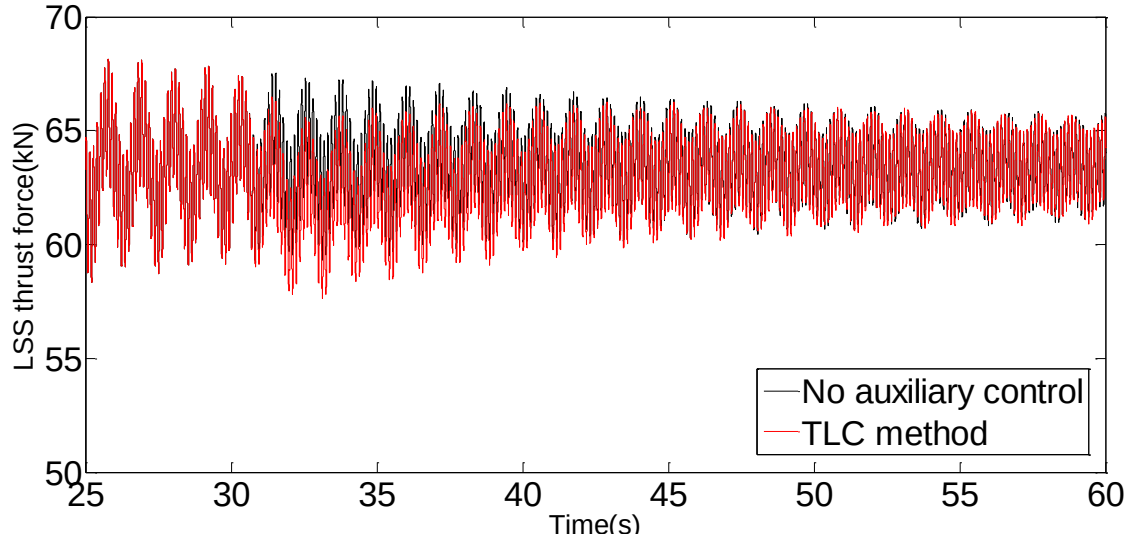

(e) Low speed shaft thrust force/rotor thrust force

Figure 6.12 Simulation results of mechanical stresses of CART2-PMSG

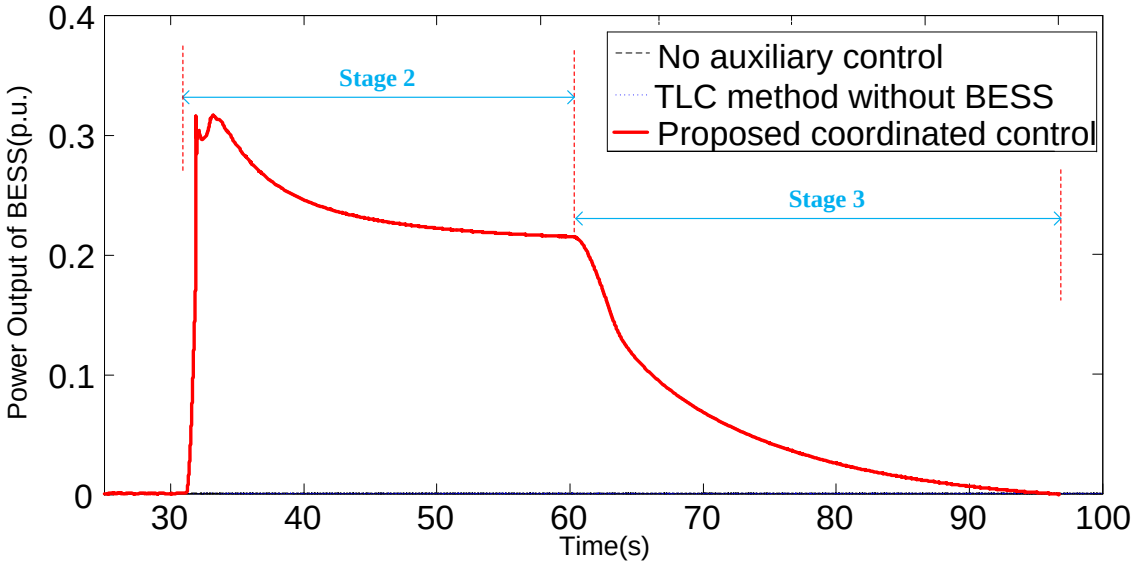

(a) Active power output of BESS

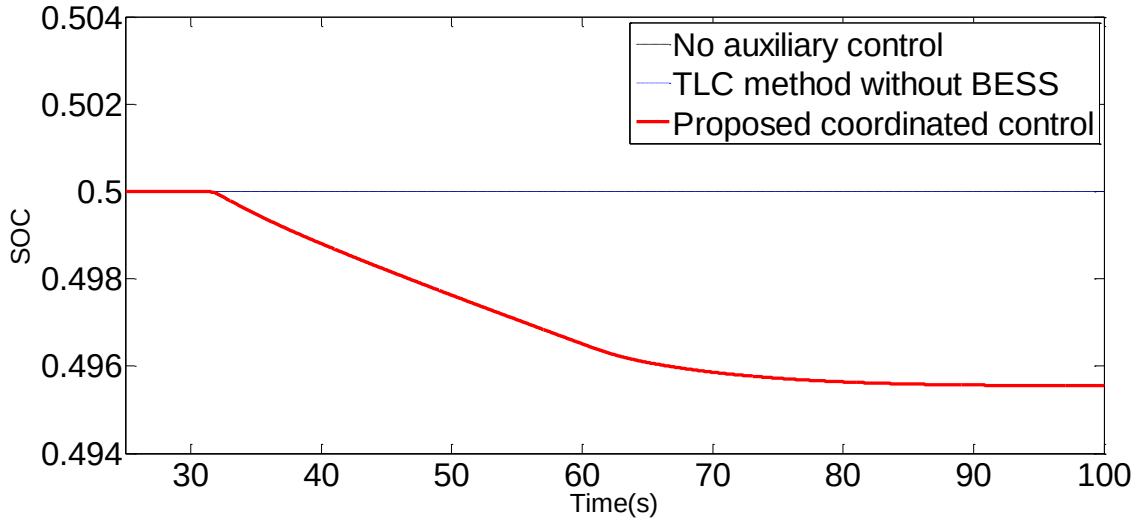

(b) SOC of BESS

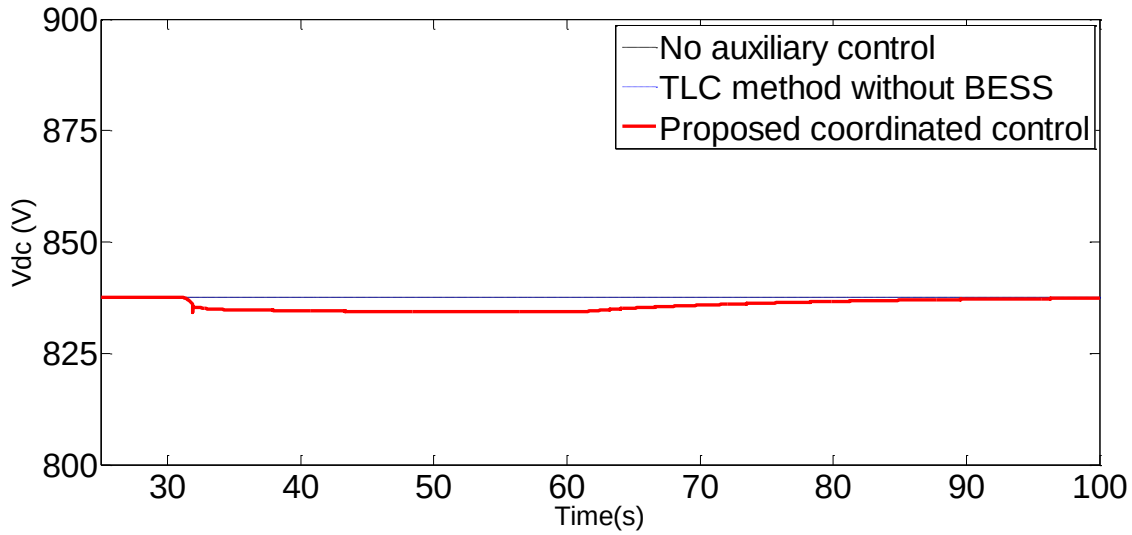

(c) DC link voltage of BESS

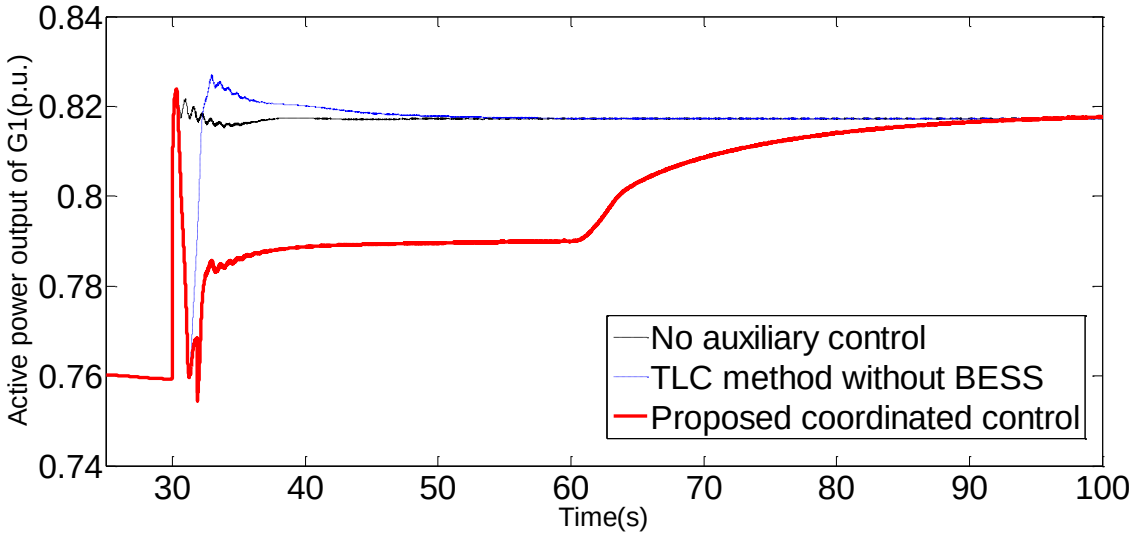

(d) Power output of G1

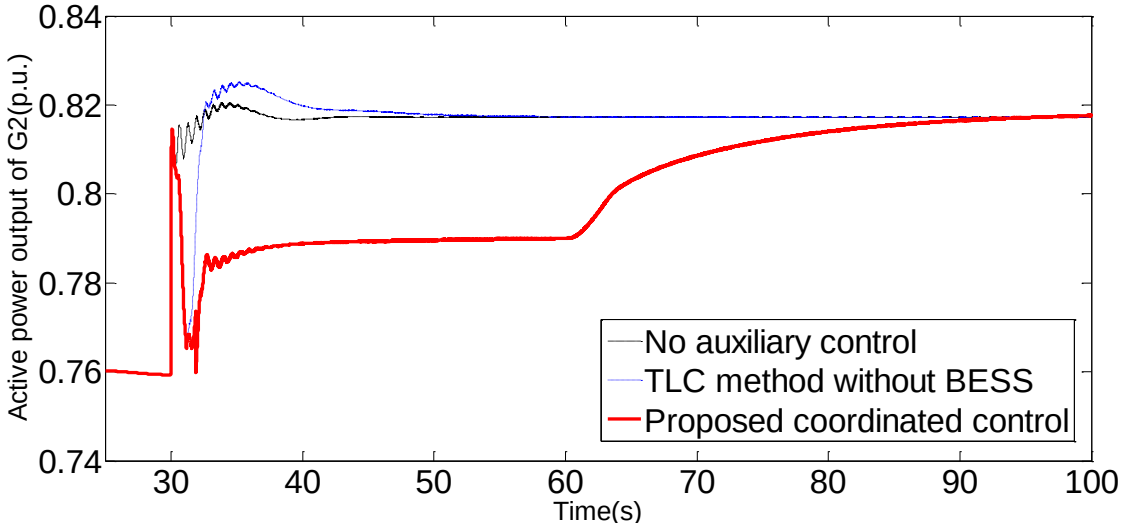

(e) Power output of G2

Figure 6.13 Simulation results of BESS and other conventional generators

6.6 Comparison and Discussion

In Figure 6.11 (a)-(d), dynamics and frequency regulation performance of CART2-PMSG are compared between the proposed coordinated frequency control and other two cases consisting of no auxiliary frequency control and TLC without BESS. In Figure 6.12 (a)-(e), the effects of TLC on the essential mechanical components such as blade, shaft and tower are presented by comparing with the baseline case. Figure 6.13 (a)-(e) shows the dynamic characteristics of BESS and other conventional generators when various frequency control methods are applied separately.

As shown in Figure 6.11(a) and Table 6.2, the proposed coordinated control combining the WTG's TLC and BESS's restoration support demonstrates the optimal performance in allowing the CART2-PMSG to participate in the temporary frequency regulation. It not only can reduce the ROCOF, but also boost the frequency nadir and reduce the steady frequency deviation. In Figure 6.11(c), the rotor speed restoration of PMSG-WTG can be smoothly completed at 60s without affecting the frequency recovery at all. On the contrary, the frequency nadir in the other two cases falls below 59.5Hz (the minimum permissible frequency), so that UFLS relay is automatically activated to rebalance generation and load by shedding a certain amount of loads. Furthermore, the duration that frequency returns to the post-disturbance steady state by using the proposed coordinated scheme is much shorter and meanwhile a smaller overshoot appears during the rotor speed recovery process. In addition, TSL is implemented when PMSG-WTG operates in the MPPT mode without deloaded margin, unlike CFR scheme discussed in Chapter 4.

Table 6.2 Comparisons of the frequency response in different scenarios

Methods	ROCOF （Hz/s）	Frequency nadir （Hz）	Post-disturbance stable frequency (Hz)	Settling time （s）	The overshoot during the frequency recovery (Hz)
No auxiliary control	-0.34	59.42	59.81	48.37	59.86
TLC without BESS	-0.26	59.48	59.81	48.37	59.88
The proposed coordinated control	**-0.26**	**59.73**	**59.9**	**38.42**	**59.85**

According to Figure 6.12 (a)-(e), there are no significant impacts on the tower, drive train and blade as a result of increased electrical power when the proposed TLC is performed. Actually, shear forces associated with tower and blades as well as thrust forces related to drive train tend to be slightly smaller during the inertial response. This is mainly because the descending rotor speed gives rise to the reduced TSR and resultant less force [85]. Once the rotor speed starts to restore to the pre-disturbance condition, forces will gradually increases up to the original values in case of constant wind speed. Therefore, the practical implementation of the proposed TLC scheme should not do any damage to the mechanical components between the blades and the generator and thus wind turbine's lifespan will not be greatly impacted.

Based on results in Figure 6.13, BESS is capable of providing fast and sustained power support during the Stage 2 of BESS Frequency Support in order to eliminate the

possible SFD issue caused by the temporary power imbalance. Meanwhile, the power output of BESS is gradually reduced down to zero during the stage 3 in coordination with other two conventional generators increasing the corresponding active power. During this stage, the frequency can be well maintained around 59.9Hz. In this way, BESS can be available to offer the similar frequency support when the severe frequency fault occurs for the second time. The SOC indicates that only a small amount of storage energy is utilized in order for the coordinated frequency control. There is a small decline in the DC-link voltage of BESS followed by a rapid rise in the active power output throughout the Stage 2 and it finally returns to the original level in the Stage 3. Due to the initial response of PMSG-WTG and frequency support of BESS, other conventional generators with slow ramp rate gain additional time in response to the frequency change by increasing their power outputs based on their own reserve margins. As a result, the total amount of spinning reserve required for emergent frequency response can be minimized and burden placed on the other conventional generators associated with the inertial response and primary frequency regulation is further eased as well.

6.6 Conclusion

In this work, a novel inertial control method based on the torque limit curve is presented for the purpose of maximizing the inertial response of PMSG-WTG without need to reserve the wind power. To demonstrate its effectiveness, an integrated CART2-PMSG wind farm model equipped with the proposed TLC is built in MATLAB/Simulink, and its frequency regulation performance is evaluated in the event of a single generator loss. To resolve the SFD problem during the inertia restoration, a coordinated frequency

control scheme between BESS and PMSG-WTG is designed to enhance the frequency regulation performance by fully taking advantage of BESS's fast response to the system power deficit when TLC remains in effect. Simulation results prove that the proposed coordinated frequency control can dramatically improve the overall system frequency response and minimize the usage of BESS for frequency regulation to a certain extent. On the other hand, the application of proposed inertial control into the PMSG-WTG hardly cause any potential damage to the wind turbine’s mechanical components when it runs at a constant wind speed.

Chapter 7 Conclusion and Future Work

7.1 Conclusion

Today, the total inertia and droop response of power systems tends to be deteriorated with the increasing wind power penetrations. A wind turbine generator's rotor speed cannot inherently respond to a variation in system frequency due to its application of the power electronics in Type 3 and Type 4 VSWT. However, the available equivalent inertial constant of a VSWT is no less than that of conventional generators. It implies that there is a great potential for VSWTs to participate in system frequency regulation by implementing the artificial inertial control and frequency regulation control. Various strategies have been developed by academia and industry to harness this hidden inertia and emulate the primary frequency regulation based on the wind power reserve.

To enhance the frequency regulation capacity of PMSG-WTG, a mathematical electromagnetic dynamic model of the studied CART2-PMSG including the mechanical and electrical wind turbine dynamics is first developed to serve as a baseline for dynamic analysis as well as auxiliary frequency controller design. The proper system configuration and associated control schemes, consisting of rotor speed-based control and active power-based control, can ensure the simulation results are valid respectively when evaluating the PMSG-WTG's frequency regulation performance ahead of real CART2 test.

First of all, this research project concentrated on the design and development of a novel comprehensive frequency regulation (CFR) into CART2-PMSG model based on rotor speed control. It comprises the constant inertia power response and dynamic variable droop control, which are carried out during two sequential stages of frequency event: in the short term, constant inertial power controller emulates the inertial response aiming to improve the transient frequency characteristics; in the long term, based on the available reserve margin, variable droop control allows PMSG-WTG to participate in the enhanced primary frequency regulation along with other synchronous generators. More importantly, this control scheme needs to be achieved through the coordinated control of both rotor speed and pitch angle in accordance with various wind speed modes. To verify the effectiveness of CFR control and its impact on the mechanical loads, a series of simulation cases are carried out in Matlab/Simulink considering different wind speed conditions. It is concluded that the presented CFR control is capable of reducing the initial ROCOF, raising the frequency nadir as well as minimizing the steady-state frequency deviation. What is more important, the implementation of CFR does not do large damage to major mechanical components of wind turbine and affect wind turbine's safe operation.

Secondly, an improved inertial control method based on the MPPT characteristic is presented for the purpose of enhancing the frequency regulation capability of active power control-based PMSG-WTGs while ensuring stable operation during inertial control.

Simulation results demonstrate that the improved inertial control enables the PMSG-WTG to arrest the ROCOF and improve the frequency nadir even in the low wind power penetration condition, whereas the proper deloaded value can avoid an SFD throughout the rotor speed recovery process. Moreover, the application of the improved inertial control into the PMSG-WTG cannot cause any potential damage to the wind turbine's mechanical components when it is operating at a certain wind speed.

Lastly, another novel inertial control method based on the torque limit curve is proposed in an effort to maximize the potential inertial response of PMSG-WTG operating in MPPT mode. To resolve the SFD issue during the inertia restoration, a coordinated frequency control scheme between BESS and PMSG-WTG is designed to enhance the frequency regulation performance when TLC remains in effect. Simulation results prove that the proposed frequency control can dramatically improve the overall system frequency response and minimize the usage of BESS for frequency regulation to a certain extent by coordinating with other conventional generators via AGC system. On the other hand, the application of proposed inertial control into the PMSG-WTG hardly cause any potential damage to the wind turbine's mechanical and structural components when it runs at a constant wind speed.

7.2 Future Work

Future work is intended to implement all these three proposed frequency regulation control methods into the real CART2 machine at the NWTC to validate the actual impact on the extreme loads and fatigue loads of a wind turbine when executing the corresponding frequency response.

Regarding the first CFR control, the impacts of several key factors on the system frequency regulation performance and potential risks on the mechanical stresses need to be further investigated, such as wind speed measurement accuracy, power rate limiter, inertial gain and inertial duration, droop coefficient and governor deadband, and power reserve margin. More efforts will be put into the design of adaptive and robust controller for inertial response and droop control in order to optimize the frequency regulation performance of individual PMSG-WTGs according to different wind speed conditions.

For the second improved inertial control, the maximum value of ΔP corresponding to different wind speeds need to be further studied in terms of various security constrains, so that the PMSG-WTG is capable of fulfilling the optimum frequency support and meanwhile maintain the basic safe operation in case of severe frequency disturbance. The quantitative correlation between the ΔP and specific frequency metrics can be regarded as an interesting topic for the future research.

As to the third TLC method, the inertial response of PMSG-WTG can be further improved by taking into account both MPPT and torque limit curves under different wind speed conditions so as to enhance the frequency support and mitigate the potential SFD without dependence on the BESS. If the TLC method is still employed, the appropriate size of BESS should be identified through a certain optimization algorithm so that a tradeoff can be achieved between the desired frequency performance and the minimized power and energy capacity of BESS.

Last but not the least, the presented frequency regulation approaches can be applicable not only for the transmission grid in this work, but also adopted for the microgrid. Since the standalone microgrid system is more sensitive and vulnerable to

dynamic active power imbalance due to the low inertia resulting from high penetration of power electronics-interfaced renewable resources plus their time-varying power generation. With the developed CFR, MPPT-based inertial response and coordinated frequency regulation between PMSG-WTG and BESS, the system inertial response and frequency stability can be significantly improved to a certain extent.

References

[1] Liu, Y, Gracia, J, King, T and Liu, Y. "Frequency regulation and oscillation damping contriubtions of variable-speed wind generators in the U.S. eastern interconnection (EI)," *IEEE Trans. Sustain. Energy*, vol. 6, no. 3, pp. 951-958, July 2015.

[2] I. A. Gowaid, A. El-Zawawi, and M. El-Gammal, "Improved inertia and frequency support from grid-connected DFIG wind farms," IEEE Power Systems Conference and Exposition, pp.1-9, 2011.

[3] Z. Wu, W. Gao, J. Wang, and S. Gu, "A coordinated primary frequency regulation from Permanent Magnet Synchronous Wind Turbine Generation," IEEE Power Electronics and Machines in Wind Applications, pp.1-6, 2012.

[4] Y.-Z. Sun, Z.-S. Zhang, G.-j. Li, and J. Lin, "Review on frequency control of power systems with wind power penetration," International Conference on Power System Technology, pp.1-8, 2010.

[5] Y. Xue and N. Tai, "Review of contribution to frequency control through variable speed wind turbine," Renewable Energy, vol.36, no.6, pp.1671-1677, 2011.

[6] Janaka Ekanayake, Nick Jenkins, “Comparison of the response of doubly fed and fixed-speed induction generator wind turbines to changes in network frequency,” IEEE Trans. Energy Conversion, Vol.19, no.4, pp.800-802, Dec. 2006.

[7] Brisebois J and Aubut N, “Wind farm inertia emulation to fulfill Hydro-Québec's specific need,” 2011 IEEE Power and Energy Society General Meeting, Montreal, Canada, pp.1-7, July.2011.

[8] Ping-Kwan Keung, Pei Li, Hadi Banakar and Boon Teck Ooi, “Kinetic energy of wind-turbine generators for system frequency support,” IEEE Trans. Energy Systems, Vol.24, no.1, pp.270-287, Feb. 2009.

[9] Le-Ren Chang-Chien, Chih-Min Hung and Yao-Ching Yin, “Dynamic reserve allocation for system contingency by DFIG wind farms,” IEEE Trans. Power Syst., vol 23, no.2, pp.729-736, May. 2008.

[10] Johan Morren, Sjoerd W.H.de Haan, “Contribution of DG units to primary frequency control,” International Conference on Future Power Systems, pp.1-6, 2005.

[11] R.G. de Almeida and J. A. P. Lopes, ”Primary frequency control participation provided by doubly fed induction wind generators,” in Proc. 15rh Power Systems Computation Conf., Liege, Belgium, pp. 22-26, Aug. 2005.

[12] R.G. de Almeida, R.G. Lopes, J.A.P, “Participation of doubly fed induction wind generators in system frequency regulation,” IEEE Trans. Power Syst., vol.22, no.3, pp.944-950, Aug. 2007.

[13] R.G. de Almeida, Edgardo D.Castronuovo and J. A. P. Lopes, “Optimum generation control in wind parks when carrying out system operator request,” IEEE Trans. Power Systems, Vol.21, no.2, May. 2006.

[14] G.Ramtharan and N.Jenkin, “Frequency support from doubly fed induction generator wind turbines,” IET Renew Power Gener, vol.1, no.1,pp.1, Mar. 2007.

[15] James F. Conroy, Rick Watson, “Frequency response capability of full converter

wind turbine generators in comparison to conventional generation," IEEE Trans. Power Systems,vol.23, no.2, pp.649-656, May.2008.

[16] Z.-S.Zhang, Y.-Z. Sun J.Lin and G.J.Li, "Coordinated frequency regulation by doubly fed induction generator-based wind power plants," IET Renew. Power Gen., vol.6, no.1, pp.38-47, Jan. 2012.

[17] A. Buckspan, J. Aho, P. Fleming, Y. Jeong, and L. Pao, "Combining droop curve concepts with control systems for wind turbine active power control," IEEE Power Electronics and Machines in Wind Applications, pp.1-8, 2012.

[18] R. Springer. "Active power control from wind power," Available: http://www.nrel.gov/electricity/transmission/pdfs/springer.pdf.

[19] Z. Wu, W. Gao, D. Yang, and Y. Shi, "Comprehensive modeling and analysis of Permanent Magnet Synchronous Generator-Wind Turbine system with enhanced Low Voltage Ride Through Capability," IEEE Energy Conversion Congress and Exposition, 2012.

[20] S.-K. Kim and E.-S. Kim, "PSCAD/EMTDC-Based modeling and analysis of a gearless variable speed wind turbine," IEEE Trans. Energy Convers., vol. 22, no.2, pp. 421-430, 2007.

[21] N. W. Miller, J. J. Sanchez-Gasca, W. W. Price, and R. W. Delmerico, "Dynamic modeling of GE 1.5 and 3.6 MW wind turbine-generators for stability simulations," IEEE Power Engineering Society General Meeting, 2003.

[22] L. li, L. Xiaoyu, W. Shiqian, S. Tian, and L. Haojiong, "The active power-frequency control strategy of DFIG based on subsection control," Electric Power, 2012.

[23] T.Ackermann., Wind Power in Power Systems Second Edition. UK: John Wiley and Sons Ltd, 2012.

[24] Y. Jun, L. Yong, and Z. Kai, "Coordinated control strategy of back to back PWM converter for permanent magnet direct-driven wind turbine," Automation of Electric Power Systems, vol. 32, no.20, pp. 88-92, 2008.

[25] L.-R. Chang-Chien and Y.-C. Yin, "Strategies for operating wind power in a similar manner of conventional power plant," IEEE Trans. Energy Convers, 2009.

[26] J. Morren, S. W. H. de Haan, W. L. Kling, and J. A. Ferreira, "Wind turbines emulating inertia and supporting primary frequency control," IEEE Trans. Power Syst., vol. 21, no.1, pp. 433-434, 2006.

[27] North American Electric Reliability Corporation, "Frequency response initiative report,"2012. Available:http://www.nerc.com/docs/pc/FRI_Report_10-30-12_Master_w-appendices.pdf

[28] Z. Cao, X. Wang, and J. Tan, "Control strategy of large-scale DFIG-based wind farm for power grid frequency regulation," 31st Chinese Control Conference, pp.6835-6840, 2012.

[29] Rui You, Braulio Barahona, Jianyun Chai and *et al*, "Frequency support capability of variable speed wind turbine based on electromagnetic coupler," Renewable Energy, vol.74, pp.681-688, 2015.

[30] S. Sharma, S.-H. Huang, and N. D. R. Sarma, "System inertial frequency response estimation and impact of renewable resources in ERCOT interconnection," in Proc. IEEE Power Eng. Soc. General Meeting, 2011.

[31] G. C. Tarnowski, P. C. Kjar, P. E. Sorensen, and J. Ostergaard, "Variable speed wind turbines capability for temporary over-production," IEEE Power & Energy Society General Meeting, pp.1-7, 2009.

[32] M. Li and J. D. McCalley, "Influence of renewable integration on frequency dynamics," in Proc. IEEE Power Eng. Soc. General Meeting, pp.1-7, 2012.

[33] A. Žertek, G. Verbič, and M. Pantoš, "Participation of DFIG wind turbines in frequency control ancillary service by optimized rotational kinetic energy," 7th International Conference on the European Energy Market, pp.1-6, 2010.

[34] N.W.Miller and K.Clark, "Impact of frequency responsive wind plant controls on grid performance,"9th International Workshop on Large-scale Integration of Wind Power and Transmission Networks for Offshore Wind Farms, Québec, Canada, 2010.

[35] P.-K. Keung, P. Li, H. Banakar, and B. T. Ooi, "Kinetic energy of wind-turbine generators for system frequency support," IEEE Transactions on Power Systems, vol. 24, no.1,pp. 279-287, 2009.

[36] M. Kayikci and J. V. Milanović, "Dynamic contribution of DFIG-Based wind plants to system frequency disturbances," IEEE Transactions on Power Systems, vol. 24, no.2, pp. 859-867, 2009.

[37] M. Kayikci and J. V. Milanovic, "Assessing transient response of DFIG-based wind plants—the influence of model simplifications and parameters," IEEE Transactions on Power Systems, vol. 23, no.2, pp. 545-554, 2008.

[38] S. Wachtel and A. Beekmann, "Contribution of wind energy converters with inertia emulation to frequency control and frequency stability in power systems," 8th international workshop on large-scale integration of wind power into power systems as well as on transmission networks for offshore wind farms, 2009.

[39] N. R. Ullah, T. Thiringer, and D. Karlsson, "Temporary primary frequency control support by variable speed wind turbines— Potential and Applications," IEEE Trans. Power Syst., vol. 23, no.2, pp. 601-612, 2008.

[40] I. D. Margaris, S. A. Papathanassiou, N. D. Hatziargyriou, A. D. Hansen, and P. Sorensen, "Frequency control in autonomous power pystems with high wind power penetration," IEEE Trans. Sustain. Energy, vol. 3,no.2, pp. 189-199, 2012.

[41] A. Vaidya, B. H. Chowdhury, and M. Chamana, "Enabling wind power plants with frequency and voltage regulation capability by forced curtailment," North American Power Symposium, pp.1-6, 2012.

[42] X. Zhu, Y. Wang, L. Xu, X. Zhang, and H. Li, "Virtual inertia control of DFIG-based wind turbines for dynamic grid frequency support," IET Conference on Renewable Power Generation, pp.1-6, 2011.

[43] L. Ruttledge, D. Flynn, "Emulated inertial response from wind turbines: gain scheduling and resource coordiantion, " IEEE Trans. Power Syst., vol. pp, no.99, pp. 1-9, 2015.

[44] National grid. "Frequency response technical sub-Group report," Available: http://www.nationalgrid.com/NR/rdonlyres/2AFD4C05-E169-4636-BF02-EDC67F80F9C2/50090/FRTSGGroupReport_Final.pdf.

[45] Y. Wang, G. Delille, H. Bayem, X. Guillaud, and B. Francois, "High wind power penetration in isolated power systems—assessment of wind inertial and primary frequency responses," IEEE Trans. Power Syst, vol. 28, no.3, pp. 2412-2420, 2013.

[46] J. Aho, A. Buckspan, J. Laks, P. Fleming, Y. Jeong, F. Dunne, ., "A tutorial of wind turbine control for supporting grid frequency through active power control," American Control Conference, 2012.

[47] P.Kundur, *Power System Stability and Control*: McGraw-Hill, 1994.

[48] L. Wu and D. G. Infield, "Towards an assessment of power system frequency support from wind plant—modeling aggregate inertial response," IEEE Trans. Power Syst, vol. 28, no.3, pp. 2283-2291, 2013.

[49] H. Wang, Z. Chen, and Q. Jiang, "Optimal control method for wind farm to support temporary primary frequency control with minimised wind energy cost," IET Renew Power Gener, vol.9, no.4, pp.350-359, 2015.

[50] L. Ruttledge, D.Flynn, "Co-ordination of frequency responsive wind plant in future power system," 2nd IET Renewalbe power generation conference, Beijing, pp1-4, 2013.

[51] C. Su and Z. Chen, "Influence of wind plant ancillary frequency control on system small signal stability," in Proc. IEEE Power Eng. Soc. General Meeting, pp1-8, 2012.

[52] Y. Liu, Y. Liu, J. R. Gracia, and T. J. King, "Variable-speed wind generation control for frequency regulation in the Eastern Interconnection (EI)," IEEE PES T&D Conference and Exposition, 2014.

[53] L.-R. Chang-Chien, W.-T. Lin, and Y.-C. Yin, "Enhancing frequency response control by DFIGs in the high wind penetrated power systems," IEEE Trans. Power Syst, vol. 26, no.2, pp. 710-718, 2011.

[54] A. Teninge, C. Jecu, D. Roye, S. Bacha, J. Duval, and R. Belhomme, "Contribution to frequency control through wind turbine inertial energy storage," IET Renew. Power Gener., vol. 3, no.3, pp. 358-370, 2009.

[55] Yi Yang, Jianhui Meng, Xiangyu Zhang and *et al*, "Control of PMSG-based wind turbines for sytem inertial response and power oscilallation damping," IEEE Trans. Sustain. Energy, vol.6, no.2, pp. 565-574, 2015.

[56] H. T. Ma and B. H. Chowdhury, "Working towards frequency regulation with wind plants: Combined control approaches," IET Renew. Power Gener., vol. 4, no.4, pp. 308-316, 2010.

[57] J. Morren, S. W. H. de Haan, and J. A. Ferreira, "Contribution of DG units to primary frequency control," International Conference on Future Power Systems, pp.1-6, 2005.

[58] I. Erlich and M. Wilch, "Primary frequency control by wind turbines," in Proc. IEEE Power Eng. Soc. General Meeting, pp.1-8, 2010.

[59] A. Zertek, G. Verbic, and M. Pantos, "A novel strategy for variable-speed wind turbines' participation in primary frequency control," IEEE Trans. Sustain. Energy, vol. 3, no.4, pp. 791-799, 2012.

[60] A. Žertek, G. Verbič, and M. Pantoš, "Optimised control approach for frequency-control contribution of variable speed wind turbines," IET Renew. Power Gener., vol. 6, no.1, pp. 17-23, 2012.

[61] M.Dernbach and D.Bagusche, "Frequency control in Québec with DFIG wind turbine," 9th International Workshop on Large-scale Integration of Wind Power and Transmission Networks for Offshore Wind Farms, Québec, Canada, 2010.

[62] NREL"Active power controls from wind power: bridging the gaps," 2014, Available: http://www.nrel.gov/docs/fy14osti/60574.pdf

[63] G. C. Tarnowski, P. C. Kjær, S. Dalsgaard, and A. Nyborg, "Regulation and frequency response service capability of modern wind power plants," in Proc. IEEE Power Eng. Soc. General Meeting, pp.1-8, 2010.

[64] E. Ela, V. Gevorgian, A. Tuohy, B. Kirby, M. Milligan, and M. O'Malley, "Market designs for the primary frequency response ancillary service-part I: motivation and design," IEEE Trans. Power Syst, vol. 29, no.1, pp. 421-431, 2014.

[65] M. Jalali and K. Bhattacharya, "Frequency regulation and AGC in isolated systems with DFIG-based wind turbines," in Proc. IEEE Power Eng. Soc. General Meeting, pp.1-5, 2013.

[66] K. V. Vidyanandan and N. Senroy, "Primary frequency regulation by deloaded wind turbines using variable droop," IEEE Trans. Power Syst, vol. 28, no.2, pp. 837-846, 2013.

[67] E. Muljadi, V. Gevorgian, M. Singh, and S. Santoso, "Understanding inertial and frequency response of wind power plants," IEEE Power Electronics and Machines in Wind Applications, pp.1-8, 2012.

[68] R. Nelson. "Active power control in Siemens wind turbines,". Available: www.nrel.gov/electricity/transmission/pdfs/nelson.pdf

[69] K. De Vos, S. De Rijcke, and J. Driesen, "Asymmetric reserve power delivered by large wind power plants," Innovative Smart Grid Technologies, pp.1-8, 2010.

[70] M. Wang-Hansen, R. Josefsson, and H. Mehmedovic, "Frequency controlling wind power modeling of control strategies," IEEE Trans. Sustain. Energy, vol. 4, no.4, pp. 954- 959, 2013.

[71] R. Doherty, A. Mullane, G. Nolan, D. J. Burke, A. Bryson, and M. O'Malley, "An assessment of the impact of wind generation on system frequency control," IEEE Trans. Power Syst, vol. 25, no.1, pp. 452-460, 2010.

[72] Abdul Basit, Anca Daniela Hansen and *et al*, "Wind power integration into the automatic generation control of power system with large-scale wind power," The Journal of Engineering, pp.1-8, 2014.

[73] J. Aho, L. Pao, and A. Buckspan, "A novel active power control system for wind turbines capable of AGC and Primary Response," AIAA/ASME Wind Symposium, Grapevine, pp.1-10. 2013.

[74] P. SØrensen, A. D. Hansen, F. lov, F. Blaabjery, and M. H. Donovan. (2005). "Wind farm models and control strategies," Available:http://orbit.dtu.dk/fedora/objects/orbit:90474/datastreams/file_7711074/content

[75] X. Feng, "Dynamic balancing for low inertia power systems," Proc. IEEE Power Eng. Soc. General Meeting, pp.1-5, 2013.

[76] H. Wang, Z. Chen, and Q. Jiang, "Control method for variable speed wind turbines to support temporary primary frequency control," IEEE PES T&D Conference and Exposition, pp.1-5, 2014.

[77] L. Ruttledge and D. Flynn, "System-wide inertial response from fixed speed and variable speed wind turbines,"in Proc. IEEE Power Eng. Soc. General Meeting, pp.1-7, 2011.

[78] M. Wang-Hansen, R. Josefsson, and H. Mehmedovic, "Frequency controlling wind power modelling of control strategies," IEEE Trans. Sustain. Energy, vol. 4, no. 4, pp. 954-959, 2013.

[79] Lu Miao, Jinyu Wen, Hailian Xie and *et al*, "Coordinated control strategy of wind turbine generator and energy storage equipment for frequency support," IEEE Trans Ind. Appl., Vol.51, no.4, pp. 2732-2741, July 2015.

[80] A. D. Wright and L. J. Fingersh, “Advanced control design for wind turbines—Part I: Control design, implementation, and initial tests,” National Renewable Energy Laboratory, Golden, CO, Tech. Rep., NREL/TP-500-42437, March, 2008.

[81] J.M. Jonkman and M. L. Buhl Jr., “FAST user’s guide,” National Renewable Energy Laboratory, Golden, CO, Tech. Rep., NRL-EL-500-38230, August, 2005.

[82] M.Singh, E.Muljadi, J. Jonkman., “Simulation for wind turbine generators-with FAST and MATLAB-simulink modules,” National Renewable Energy Laboratory, Golden, CO, Tech. Rep., NREL/TP-5D00-59195, April, 2014.

[83] Bin Wu, Yongqiang Lang, Navid Zargari and Samir Kouro, P*ower convrsion and control of wind energy systems*. John Wiley & Sons, Ltd., 2011.

[84] Wenzhong Gao, Ziping Wu, Jianhui Wang and Shusheng Gu, “A review of inertia and frequency control technologies for variable speed wind turbines”, Control and Decision Conference (CCDC), pp.2527-2533, May, 2013.

[85] P. A. Fleming, J. Aho, A. Buckspan *et al*., “Effects of power reserve control on wind turbine structural loading,” Wind Energy, Vol.19, no. 3, pp.453-469, 2015.

[86] Moses Kang, Jinsik Lee, Kyeon Hur and *et al*, "Stepwise inertial control of a doubly-fed induction generator to prevent a second frequency dip," J Electr Eng Technology, pp.2221-2227, 2015.

[87] MathWorks, Battery-Implement generic battery model http://www.mathworks.com/help/physmod/sps/powersys/ref/battery.html?s_tid=gn_loc_drop

[88] Cheng Yunzhi, Tabrizi M, Sahni M, *et al*. "Dynamic available AGC based approach for enhancing utility scale energy storage performance," *IEEE Trans. Smart Grid*, 2014, vol.5, no.2, pp. 1070-1078, 2014.

[89] Hiroyuki Amano, Yuji Ohshiro, Tomonori Kawakami, "Utilization of battery energy storage system for load frequency control toward large-scale renewable energy penetration," IEEE PES Innovative Smart Grid Technologies, pp.1-7.Oct 2012.